HSD10 REGULATES CANCER CELL GROWTH AND RESISTANCE TO CELL DEATH

By

Emily Ann Carlson

Submitted to the graduate degree program in Pharmacology and Toxicology and the Graduate Faculty of the University of Kansas in partial fulfillment of the requirements for the degree of Doctor of Philosophy.

_____
Chairperson Dr. Shirley ShiDu Yan

_____
Dr. Rick Dobrowsky

_____
Dr. Nancy Muma

_____
Dr. Honglian Shi

_____
Dr. Liang Xu

Date Defended:

April 29, 2016

The Thesis Committee for Emily Ann Carlson

certifies that this is the approved version of the following thesis:

HSD10 REGULATES CANCER CELL GROWTH AND RESISTANCE TO CELL DEATH

Chairperson Dr. Shirley ShiDu Yan

Date Approved:

May 5, 2016

Abstract

Dysfunction or deregulation of certain cellular processes is commonly used to distinguish known illnesses into separate and unique disease states. Although each cancer type is individually distinct, most cancers initially occur due to genomic mutations of oncogenes and tumor suppressor genes, leading to enhancement or disruption of specific cellular processes, including mitochondrial-mediated events. As an organelle necessary for both cell survival and cell death, the mitochondrion is involved in a variety of diseases, including cancer. Specific alterations to mitochondrial DNA in cancer can result in enhanced proliferation and avoidance of cell death pathways. Thus, alterations to mitochondria function often increase the likelihood of tumor progression.

In this dissertation, the role of a mitochondrial enzyme, 17β-hydroxysteroid dehydrogenase type 10 (HSD10), was examined in relation to cancer progression. In rat adrenal gland tumor cells, upregulation of HSD10 correlated with increased cell growth rate and tumor growth in mice, enhanced energy metabolism, and protection against oxidative stress-induced cell death. Downregulation of HSD10 in the rat adrenal gland tumor cells resulted in decreased cell growth rate, reduced mitochondrial bioenergetics, and increased vulnerability to cell death induction under both baseline and oxidative stress conditions. Reductions in cell growth rate and energy metabolism were also observed upon HSD10 knockdown in T47D human breast cancer cells, which supports the role of HSD10 in cancer across two different cancer types and species. Furthermore, overexpression of HSD10 did not transform MCF10A breast cells, providing evidence that HSD10 may not be a tumor-initiating factor. Together, the data suggest that upregulation of HSD10 promotes cell growth and resistance to stress-induced cell death specifically in cancer cells.

Acknowledgements

I am thankful to all of the people who contributed to the completion of this dissertation and because of whom the past five years have been filled with motivation and passion for furthering my scientific research and overall knowledge. Firstly, I would like to thank my graduate advisor Dr. Shirley ShiDu Yan for her guidance, constant support and encouragement, and providing me with the resources necessary to complete this dissertation. Similarly, I am grateful to Dr. Liang Xu for the opportunity to expand upon my cancer biology knowledge, and learn and refine experimental techniques important in the field of cancer research.

I owe my gratitude to Dr. Rebecca T. Marquez, without whom much of the animal tumor-related work of this research would not have been possible. Her professional and personal guidance was greatly appreciated, as was her patience and willingness to instruct me in all things cancer. Furthermore, I would like to thank all past, present, visiting laboratory members who helped teach me the skills needed for this study: Dr. Heng Du, Dr. Lan Guo, Dr. Xueqi Gan, Dr. Shengbin Huang, Dr. Gang Hu, Dr. Valasani Koteswara Rao, Dr. Guangyue Li, Dr. Fang Du, Dr. Yongfu Wang, Dr. Eva Borger, Adam H. Al Douri, and Qing Yu.

I am thankful to Dr. Rick Dobrowsky, Dr. Nancy Muma, and Dr. Honglian Shi for serving on my committee and for providing me with valuable suggestions, criticisms, and guidance. I would also like to thank the faculty of the Department of Pharmacology and Toxicology for their role in my education and development as a scientist. Likewise, I am thankful to all of the graduate students I had the opportunity to meet along the way.

The support of my friends has helped me remain sane and overcome setbacks throughout these years. I greatly value their friendship and appreciate their belief in me. Most importantly, I would like to thank my family for their love, concern, support, and advice.

Table of Contents

INTRODUCTION

Overview of Cancer and Mitochondria

In 2012, 8.2 million patients died of cancer, which was estimated to account for 15% of all deaths worldwide (1). The 2012 statistical report by the World Health Organization specified that approximately 32.6 million people were living with cancer worldwide, with 14.1 million new cancer cases diagnosed that year. Deaths from cancer worldwide are projected to continue rising, with an estimated 13.1 million deaths in 2030. Although overall cancer death rates have declined by 20% since climaxing in 1991 (2), this group of diseases is still of major importance regarding treatment and prevention. As cancer cells are continuously replicating, treatment regimens often fail to completely rid a patient of malignant cells, resulting in repopulation of the tumor (3). Thus, ongoing research is needed to stay ahead of this complicated disease.

Cancer is composed of a vast group of diseases characterized by unchecked cellular proliferation and metastasis of abnormal cells throughout the body. The development of cancer is initiated by three known factors. First, genomic mutations constitutively activate oncogenes to promote uncontrolled cell growth (**Schematic 1.1** (4)). Second, genetic modifications deactivate tumor suppressor genes so that they fail to inhibit the robust cell growth (**Schematic 1.2** (5)). Third, stability genes necessary for genomic repair are inactivated, allowing for higher rates of mutations in the cellular genome (**Schematic 1.3** (6)). All three genetic mutations allow normal cells to progress to cancer. Once cells become cancerous they exhibit large metabolic imbalances (7) and increased resistance to cell death (8), two processes regulated by mitochondria. As these organelles are vital players in the regulation of cellular function, it is plausible that they are involved in cancer development and progression (9).

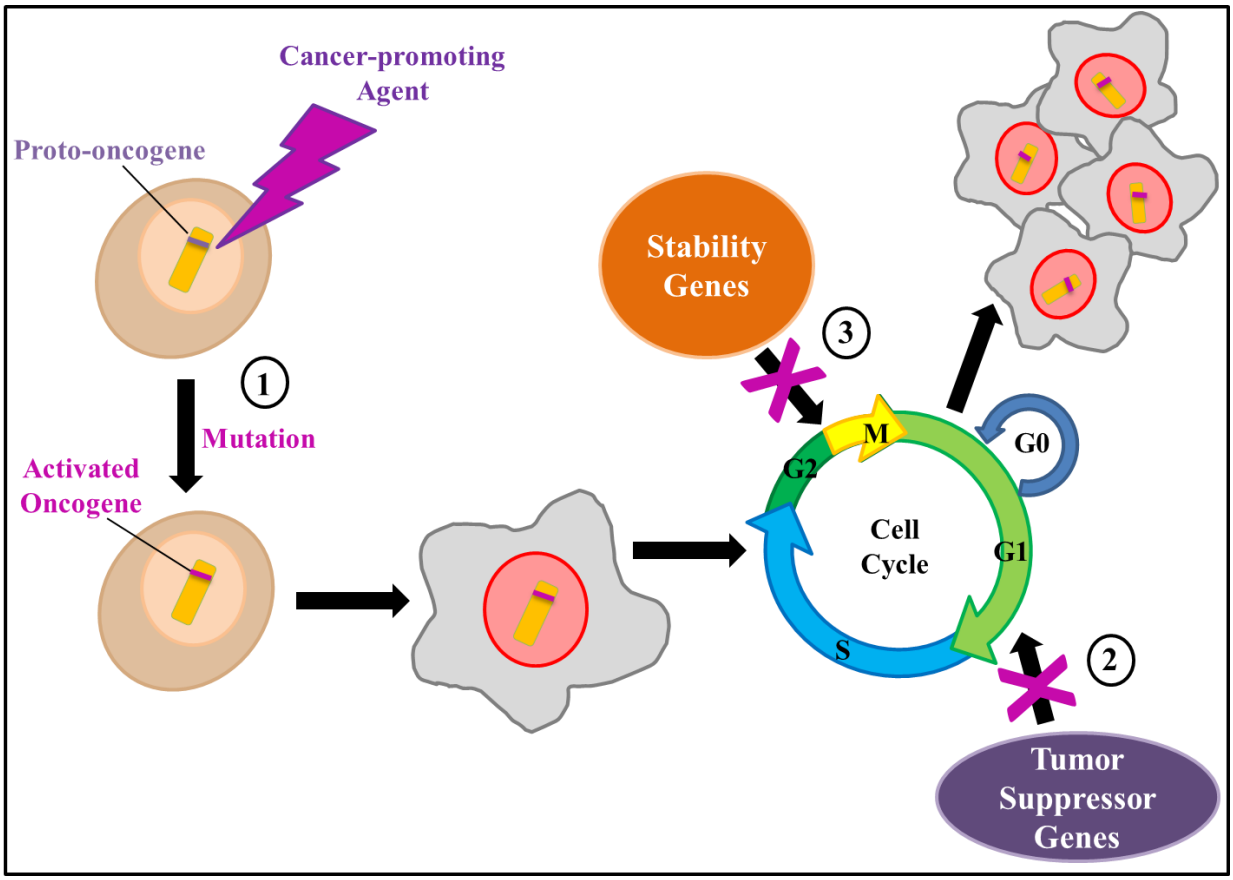

Schematic 1: Tumorigenesis. Three genetic mutation types drive the conversion of normal cells to cancer cells. **1)** Genomic mutations constitutively activate oncogenes to stimulate uninhibited cell growth. **2)** Next, genetic alterations disable tumor suppressor genes so that they do not inhibit the robust cell growth. **3)** Stability genes required for genomic repair are then deactivated, which allows for greater rates of mutations in the cell genome.

Mitochondria are double-membrane-bound organelles composed of an outer membrane (OM) and an inner membrane (IM), which is further constructed into compartments: the intermembrane space, the cristae interior, and the matrix (10). Mitochondria are central players in cellular function with roles in sustaining cell survival, maintaining energy metabolism, balancing reactive oxygen species (ROS), and mediating cell death pathways. Given their extensive role in cells, mitochondrial function has been examined in many diseases, including cancer (11-13). Studying the functions of mitochondria in malignant cells, in comparison with

healthy cells, may help elucidate the modified mechanisms and molecular components involved in specific types of cancer.

Otto Warburg was one of the first investigators to implicate mitochondria in cancer. His phenomenon, termed the Warburg effect, demonstrates that tumor cells exhibit increased glycolytic adenosine triphosphate (ATP) production and reduced oxidative phosphorylation (OXPHOS) (14). Since then, many aspects of the mitochondrion have undergone thorough investigation to shed light on the alterations promoting this aggressive disease.

Altered Mitochondrial DNA in Cancer

Mitochondria contain a DNA molecule (mtDNA) that encodes genes essential for normal mitochondrial function. Human mtDNA contains 37 genes that code for 13 polypeptides involved in respiration and OXPHOS, and two ribosomal RNAs in addition to 22 transfer RNAs important for protein synthesis (15). Furthermore, mtDNA has a noncoding region with a displacement loop for control of mtDNA replication and transcription (16). As mtDNA regulates vital processes, modifications to its genomic material have a profound impact on healthy cells.

Numerous studies have reported the effects of mtDNA mutations in tumors. To begin, mtDNA copy number has been examined in diverse cancer types, indicating that changes in mtDNA content may be regulated in a tumor-specific manner (17, 18). Moreover, studies have shown that mutations in both the coding (19, 20) and non-coding (21-23) mtDNA regions are associated with cancer growth. Interestingly, these alterations strongly correlate with patient outcome (24), as displacement loop mutations typically correlate with lower survival rates (25). Thus, the severity of mtDNA alterations in cancer cells and patient endurance seem to depend on both mtDNA content deviations and mutation locations.

Modified Energy Metabolism in Cancer

In healthy cells, ATP manufacturing is dependent upon oxygen consumption, the tricarboxylic acid (TCA) cycle, and the electron transport chain (ETC). Dehydrogenases of the TCA cycle are stimulated by mitochondrial calcium (Ca^{2+}) intake (**Schematic 2.1**), which propels the reduction of nicotinamide adenine dinucleotide (oxidized NAD^+ to reduced NADH) (26). In addition, succinate dehydrogenase, also known as complex II (succinate-ubiquinone oxidoreductase) of the ETC, catalyzes the oxidation of succinate to fumarate in the TCA cycle (27). ETC complex I (NADH-ubiquinone oxidoreductase) accepts electrons from NADH (28), while complex II receives electrons from succinate. Next, the electrons from complexes I and II transfer to complex III (ubiquinol-cytochrome c oxidoreductase) and are incorporated into cytochrome c (cyto c) for delivery to complex IV (cytochrome c oxidase) (28). This last complex reduces oxygen to water and plays a critical role in ATP synthesis (29). Protons are generated throughout the ETC process and used by ATP synthase (often referred to as complex V) in the OXPHOS pathway to synthesize ATP from adenosine diphosphate (ADP) and inorganic phosphate (30). Once produced, ATP propels many activities in the cell, including signal transduction, active transport, and DNA synthesis. Consequently, changes in energy production due to mtDNA mutations can affect these processes.

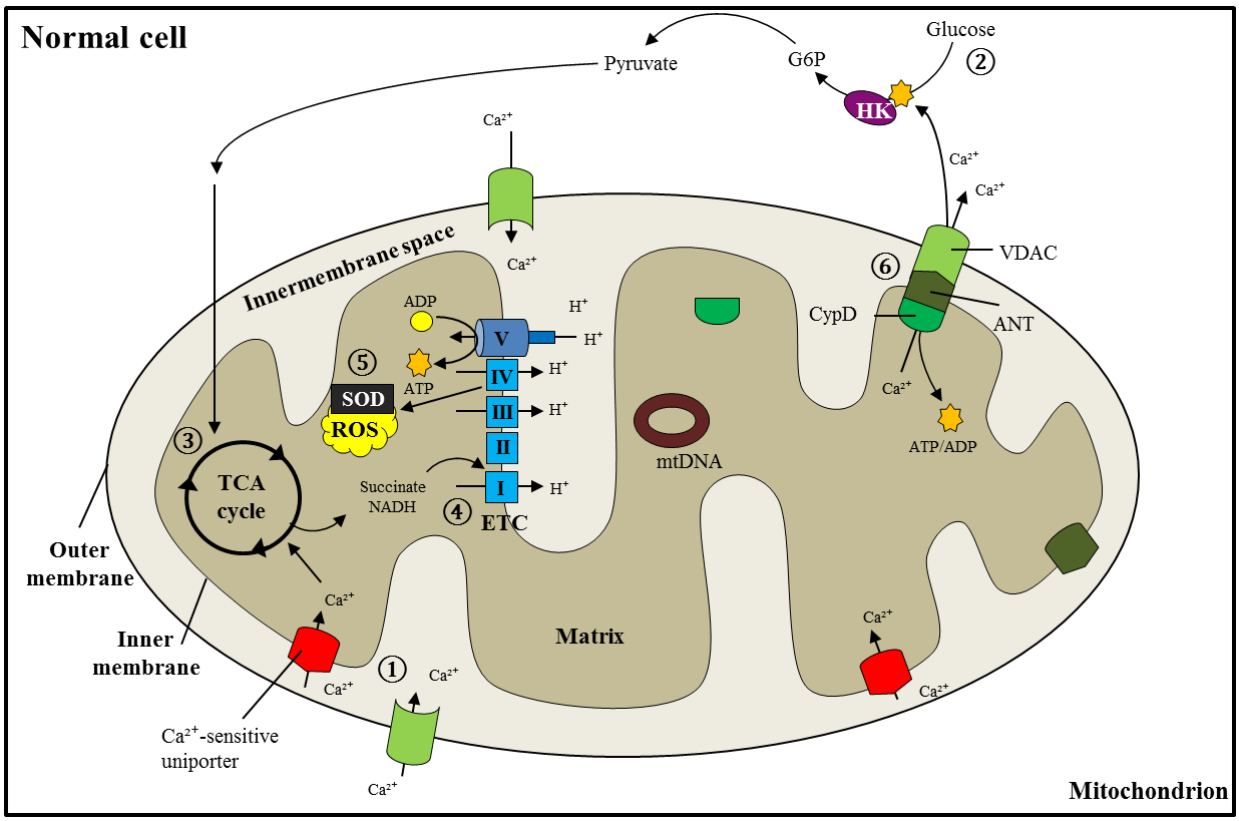

Schematic 2: Mitochondrial function in normal cells. Under regular oxygen conditions, healthy cells primarily rely on mitochondrial OXPHOS for ATP production. **1)** Ca^{2+} ions are taken up into a mitochondrion through voltage dependent anion channels (VDAC) and Ca^{2+}-sensitive uniporter channels, and stimulate ATP generation. **2)** Glucose is converted into pyruvate during glycolysis, **3)** which is imported into the mitochondrion for entry into the TCA cycle. **4)** Reduced succinate and NADH molecules are used in the ETC to power ATP generation. **5)** ROS created along the ETC are balanced by anti-oxidants, such as superoxide dismutase (SOD). **6)** Excess Ca^{2+} ions are expelled from the mitochondrion through the mitochondrial permeability transition pore (MPTP) comprised of VDAC, adenine nucleotide translocase (ANT), and cyclophilin D (CypD). Adapted from Carlson, E.A. et al. (2013) *Drug Discov Today Ther Strateg* (31).

Warburg initially discovered that tumor cells display increased glucose uptake, enhanced glycolytic ATP generation, and diminished OXPHOS (7). Essentially, instead of utilizing pyruvate molecules in the TCA cycle to power the OXPHOS pathway for generation of ATP as is done by normal cells (**Schematic 2.2-2.4**), cancer cells convert pyruvate into lactic acid for energy generation (**Schematic 3.1**). A possible explanation for Warburg's findings involves ATP

synthase malfunctioning as hyperglycemia in hepatocarcinoma cells reduced ATP synthase dimer stability (32). Also, Isidoro et al. found that expression of the β-catalytic subunit of ATP synthase is decreased in cancer cells (33), further implicating the involvement of complex V.

Although the Warburg effect is widely recognized, several groups have challenged it by revealing that mitochondria in tumors are able to operate OXPHOS at lower capacities along with glycolysis (34). In fact, malignant cells can switch from a glycolytic state to OXPHOS under glucose-limiting conditions to adjust to changes in the cellular environment (35). Utilizing both respiration systems under diverse settings is important for tumor survival. For instance, glucose deprivation elevates OXPHOS in breast tumor cells while control cells remain unaffected (36). Conversely, hypoxia improves respiration in control cells whereas it is impaired in breast cancer cells (37), signaling for tumor cells to switch to glycolysis. Therefore, cancer cells can direct the energy metabolism systems according to their specific needs under a variety of conditions. This likely aids in cancer cell growth and resistance to cell death.

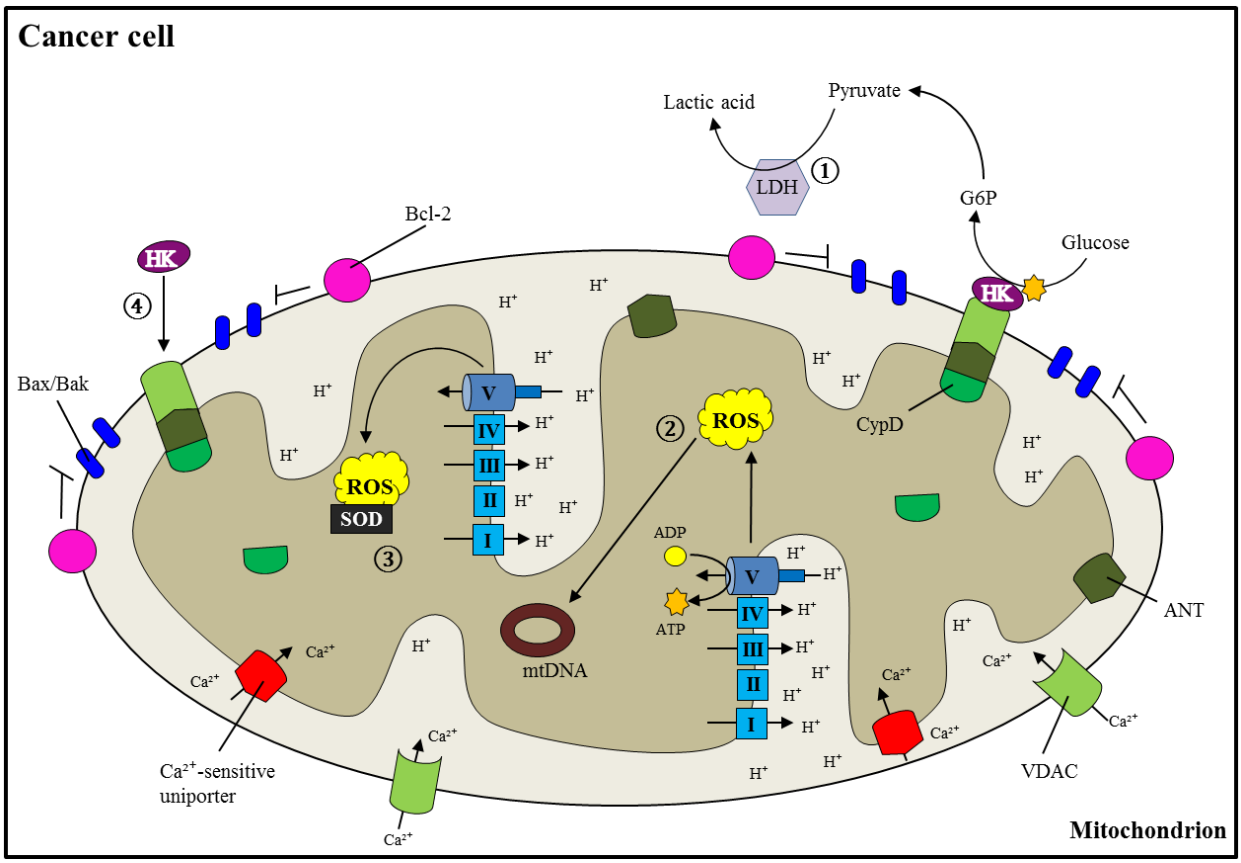

Schematic 3: Altered mitochondrial processes during cancer. In cancer cells there is a shift from OXPHOS to glycolytic ATP production, **1)** producing large amounts of lactic acid via lactate dehydrogenase (LDH). **2)** High levels of ROS induce carcinogenic mutations in mtDNA, but are **3)** balanced by activated antioxidants. **4)** Hexokinase (HK) inhibits opening of the MPTP, and as a result blocks cell death induction. Thus, the increased carcinogenicity and decreased cell death promotes cancer cell growth. Adapted from Carlson, E.A. and Yan, S.S. (2014) *ICST* (38).

Balanced Oxidative Stress in Cancer

Under homeostatic conditions, enhanced ATP production via increasing ETC activity propels the reduction of oxygen to water. Consequently, this contributes to greater leakage of free electrons from the respiratory complexes, resulting in the formation of superoxides, free radicals, and peroxides jointly known as ROS (39). As a compensatory mechanism, ROS scavenging enzymes are activated to eradicate harmful oxidants (40). Healthy cells tightly regulate the balance between oxidants and anti-oxidants to prevent destructive consequences

(**Schematic 2.5**). However, deficiencies in ETC complex activities are associated with depleted energy and heightened ROS production (41). Chiefly, reduced complex I, II, and IV respiratory capacities lead to increased risk of dysfunction (42). With low levels of ROS scavengers, harmful oxidants accumulate within the cell and cause damage, such as mtDNA mutations (43). Thus, unrestrained oxidative stress can propel cancer initiation and metastasis (44).

Elevated oxidative stress has been observed in many different tumors, with persistently high ROS levels seen in malignant cells (**Schematic 3.2**) compared with paired controls (45). Accordingly, cells are able to use mitochondrial ROS as a mechanism to increase their chance of cancer development through a kind of pro-cancer feedback loop. Also, extra-mitochondrial ROS production can affect cancer behavior, correlating with enhanced tumor growth and invasiveness (46, 47). Thus, cancer cells are able to utilize enhanced intra- and extra-mitochondrial ROS generation to increase tumor developmental and metastatic abilities.

However, elevated ROS levels can cause substantial damage to normal and cancerous cells alike. As a result, tumor cells are capable of rebalancing ROS production and elimination by activating antioxidants (**Schematic 3.3**) for restoration of an optimal redox state necessary for continuous proliferation (48). For example, it was found that increasing ROS caused inhibition of glycolytic enzyme pyruvate kinase M2, which in turn activated the antioxidant systems required for detoxifying ROS in cancer cells (49). Therefore, tumor cells regulate ROS levels not only for initial development, but for long-term management of cancer progression as well.

Reduced MPTP Formation in Cancer

A nonselective mitochondrial Ca^{2+}-activated pore was initially discovered to take in and extrude ions during membrane permeability oscillations (50). Currently called the MPTP

(**Schematic 2.6**), it is often connected with cell death elicited by stress and Ca^{2+} overload (51). Under stress conditions in healthy cells, the MPTP forms in the IM where its induction can lead to mitochondrial swelling, loss of transmembrane potential ($\Delta\Psi$), release of apoptotic mediators, and eventual cell death (52). However, MPTP-mediated cell death is suppressed in tumor cells, rendering them resistant to therapies (53). Many factors participate in protecting cancer cells from MPTP-regulated membrane disruption and cell death induction, a few of which are presently discussed.

CypD is a prolyl isomerase located within the mitochondrial matrix and has been established as a modulatory component of the MPTP (54-56). Upon Ca^{2+} overload or oxidative stress in healthy cells, CypD translocation from the matrix to the IM activates the MPTP, inducing cell death (57). Interestingly, cancer cells overexpress CypD, which leads to the suppression of cell death by interacting with anti-apoptotic Bcl-2 (58). CypD-mediated inhibition of cell death also correlates with mitochondrial-bound HK molecules, as depicted in **Schematic 3.4**. Inactivation of CypD results in the release of bound HK-II and enhances pro-apoptotic Bax/Bak-mediated apoptosis (59). Additionally, heat shock protein interactions with CypD inhibit normal CypD-dependent MPTP opening and cell death in some tumors (60). Thus, CypD seems to be involved in promoting cancer growth, and exhibits a variety of molecular interactions which aid in this.

The translocator protein (TSPO; initially known as the peripheral benzodiazepine receptor) is another recognized component, first linked to the MPTP due to its ligand interactions (61). Moreover, the OM has been shown to have a regulatory role in MPTP formation, primarily through TSPO (62). As with CypD, TSPO is elevated in many types of cancer and in particular breast cancer (63). Intriguingly, increased levels of this protein are associated with enhanced

breast cancer invasiveness (64, 65), and correlate with shortened disease-free survival in lymph node-negative patients (66). It has been postulated that high TSPO levels may render malignant cells more resistant to MPTP formation and cell death, comparable to CypD. This is plausible, though additional research is required to determine the particular function of TSPO in cancer.

Along with CypD and TSPO, two other channels were strongly suggested as constituents of the MPTP (67), but have since been shown to not be necessary for MPTP formation.

Mitochondria take up small molecules and ions through VDACs on the OM (68). VDAC was originally hypothesized to play a role in MPTP configuration (69), however recent data suggests otherwise (70, 71). In cancer cells, VDACs are significantly upregulated; as expected, downregulation of VDAC directly affects proliferation (72, 73). HK expression is also linked with VDAC quantities as overexpression of HK-I and -II induces VDAC closure and prevents MPTP opening in cancer cells (74). This HK-mediated closure of VDAC may allow for CypD-induced MPTP inhibition (**Schematic 3.4**), thus enhancing tumor cells' proliferative abilities.

ANT was another proposed component of the MPTP (75), as it functions to catalyze the exchange of mitochondrial ATP for cytosolic ADP through the IM (76). Nevertheless, studies demonstrated it is not essential for MPTP induction (77). Of the four ANT isoforms, increased levels of ANT-1 and -3 promote cancer cell death (78, 79), while high amounts of ANT-2 and -4 contribute to malignant cell resistance (80, 81). Furthermore, ANT-2 seems to be critical for importation of glycolytic ATP in cancer cells (82). Interestingly, overexpression of CypD inhibits ANT-1-mediated apoptosis in tumor cells (83). Hence, the ANT isoforms oppositely participate in cancer, with CypD interactions vital in controlling cancer cell survival. Collectively, this suggests that interactions occur between MPTP components and other molecules for cancer cell survival; further investigation is needed for in-depth assessment.

Manipulated Cell Death Pathways in Cancer

Two alternative pathways can initiate apoptosis within cells. The extrinsic route is triggered by death receptors on the cell surface (84), while the intrinsic path originates in mitochondria (85) (**Schematic 4.1**). Induction of apoptosis signaling stimulates initiator caspases (86), which activate executioner caspases for cleavage of death substrates (87). In mitochondria, anti-apoptotic Bcl-2 and Bcl-xL release tBid upon its activation by caspases (88). Pro-apoptotic Bax and Bak form multi-domain molecules after stimulation from tBid, propelling the release of cyto c and other factors from the MPTP (89). The apoptotic factors perpetuate the process, causing the organized collapse and shrinkage of the cell. Finally, the cell body is engulfed by nearby cells for removal (90). Also known as programmed cell death as it can be purposefully initiated, apoptosis is a cell death pathway that can be activated specifically by the mitochondrion.

Most often, cancer cells display increased inhibition of apoptosis due to mutations that either disrupt pro-apoptotic proteins (91, 92) or elevate anti-apoptotic proteins (93). On the contrary, Smith et al. found that enhanced levels of pro-apoptotic Bad promote prostate cancer growth (94). This discrepancy illustrates that cancer cells tightly regulate all apoptotic protein levels according to their proliferative needs. Additionally, in the event of apoptosis initiation, some cancer cells can reverse the process and survive (8). Clearly, tumors manipulate many aspects of apoptosis to avoid cell death, which can render cancer therapies ineffective. As this is a major problem in cancer medicine, many groups are searching for treatments that target apoptosis. For instance, small molecule mimetics that inactivate anti-apoptotic proteins (95), concurrent inhibition of nuclear factor κB activity (96), and overexpression of tumor-suppressor protein p53 (97) are a few exploratory mechanisms by which apoptosis can be induced in tumor

cells. Simultaneously targeting cancer cell-specific apoptotic inhibitory pathways while administering anticancer agents may help to eliminate the resistance seen in tumors.

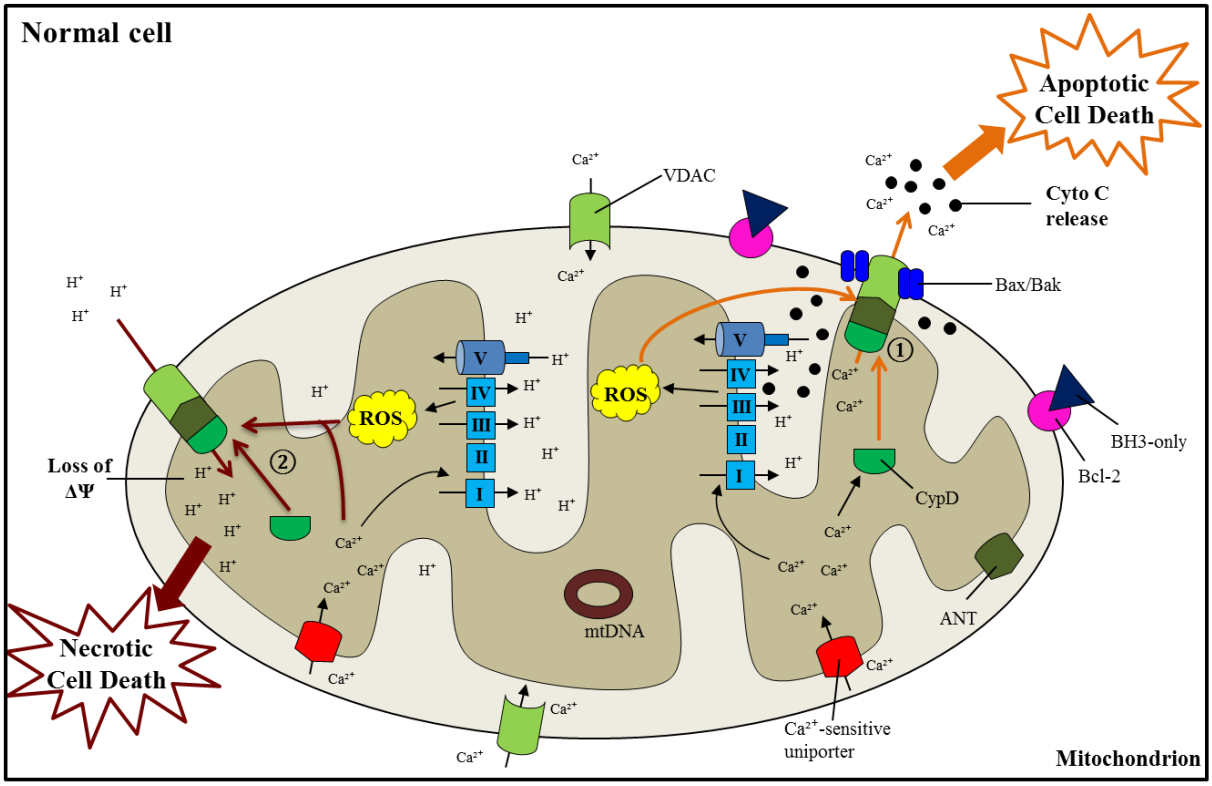

Schematic 4: Mitochondrial-mediated cell death pathways in normal cells. In the event of cellular injury, a mitochondrion can signal cell death pathways for destruction of the damaged material or whole cell. **1) Apoptosis** is initiated due to excessive Ca^{2+} and/or ROS levels. Bcl-2 is inhibited by BH3-only proteins, allowing Bax and Bak to interact, inducing MPTP opening for Ca^{2+} and cyto c release into the cytosol. These apoptotic factors further propel the process until the cell collapses in an organized manner. **2) Necrosis** results from ATP depletion and enhanced Ca^{2+} and ROS accrual. This leads to the loss of ΔΨ and eventual unplanned rupture of the cell. Adapted from Carlson, E.A. et al. (2013) *Drug Discov Today Ther Strateg* (31).

In the event of cellular injury, an unplanned cell death pathway called necrosis can be launched (**Schematic 4.2**). Activation of death receptor adaptors leads to their translocation to the IM (98, 99). This disrupts the ANT-mediated ATP/ADP exchange, resulting in ATP depletion and ROS accumulation (100). Excessive levels of ROS and Ca^{2+} promote mitochondrial uncoupling, swelling, and disruption of ΔΨ via MPTP opening (101, 102).

Imbalances activate degradative enzymes that propagate the damage until the plasma membrane ruptures (103), leaking the intracellular contents in an unorganized manner.

Studies have shown that necrotic cell death is impaired in cancer cells, although the particular mechanisms are still being examined. For instance, Nakagawa et al. found that inhibiting CypD protects malignant cells from necrosis (104). Also, although leucine zipper/EF hand-containing transmembrane-1 (LETM1) induces necrosis in normal cells, LETM1 overexpression is common in many forms of cancer, leading to inhibition of necrotic cell death (105). Due to inconsistent outcomes with apoptosis-mediated treatments, several groups are focused on developing cancer therapies targeting necrosis. For example, enhanced expression of nuclear IM protein lamin B1 (106) and activation of DNA damage response pathways (107, 108) are two investigative components that induce necrosis upon anticancer agent administration. Potentially, the induction of necrosis may provide an alternative tool for treating cancer cells resistant to apoptosis-inducing methods.

17β-Hydroxysteroid Dehydrogenase Type 10 (HSD10)

HSD10 is a mitochondrial enzyme that catalyzes the oxidation of a wide variety of substrates and is important in diverse disease states. Our group originally identified HSD10 as a single chain polypeptide capable of binding amyloid-β (Aβ) peptide (109), connecting it with Alzheimer's disease (110). **Table 1** lists all of the alternative names used for HSD10 in the literature.

Alternate Names for HSD10	
Abbreviation	Full Name
ABAD	Aβ-binding alcohol dehydrogenase (110)
ERAB	Endoplasmic reticulum-associated Aβ-peptide binding protein (109)
HSD10	17β-hydroxysteroid dehydrogenase type 10 (111)
HADH2	L-3-hydroxyacyl-CoA dehydrogenase type II (112)
MHBD	2-methyl-3-hydroxybutyryl-CoA dehydrogenase (113)
SCHAD	Short chain 3-hydroxyacyl-CoA dehydrogenase (114)
SCHMAD	Short chain L-3-hydroxy-2-methylacyl-CoA dehydrogenase (115)

Table 1: Alternative names for HSD10

As shown in **Schematic 5A**, the HSD10 gene is located on the short arm of the X-chromosome (Xp11.2), spans approximately 3 kb, and is comprised of six exons (116). Exons 1-3 form the NADH-binding domain at the N-terminus, while exons 4-6 at the C-terminus function to bind substrates and catalyze enzymatic reactions (**Schematic 5B**) (117). The HSD10 protein product consists of 261 amino acids, and is expressed ubiquitously in all tissues, but is most prominent in the liver, heart, and brain (109, 118). On the subcellular level, HSD10 is located in the mitochondrial matrix (119). Computational analysis of the HSD10 amino acid sequence revealed a mitochondrial localization signal at the N-terminus of the protein, ERLVGQ (120), for specific targeting of HSD10 to mitochondria. Eleven amino acids at the N-terminus form a positively charged amphiphilic α helix which aids in the mitochondrial import of HSD10 (111).

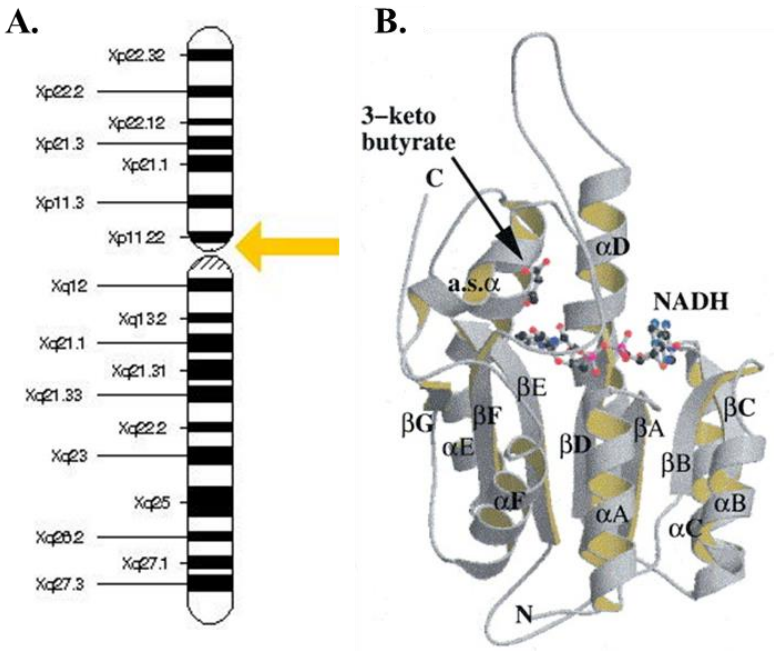

Schematic 5: HSD10 gene location and product structure. A. The HSD10 gene is located on the short arm of the X chromosome at position 11.2, specifically from base pair 53,431,257 to base pair 53,434,375; Adapted from NIH Genetics Home Reference (121). **B.** Computerized structure of HSD10 with N- and C-terminals labeled; Adapted from Powell, A.J. (2000) *J Mol Biol* (122).

HSD10 belongs to the short-chain dehydrogenase/reductase superfamily, namely the 17β-hydroxysteroid dehydrogenases (HSD17B). These alcohol oxidoreductases catalyze the dehydrogenation of 17-hydroxysteroids (123). Interestingly, HSD10 is the only HSD17B family member located in mitochondria. It can further catalyze NADH-dependent redox reactions of many different substrates, including β-hydroxybutyrate (BHB), fatty acids, linear alcohols, branched short chain acyl-CoAs, amino acid catabolites, and steroids (112, 124, 125).

In healthy cells, HSD10 is a crucial component in the maintenance of cellular homeostasis, and overexpression of HSD10 has been shown to provide a protective effect in cells undergoing nutritional stress (126). As depicted in **Schematic 6**, the ability of HSD10 to metabolize vital substrates leads to an increase in energy production. Furthermore, sequestration of CypD by HSD10 likely aids in cellular protection by inhibiting cell death pathway initiation.

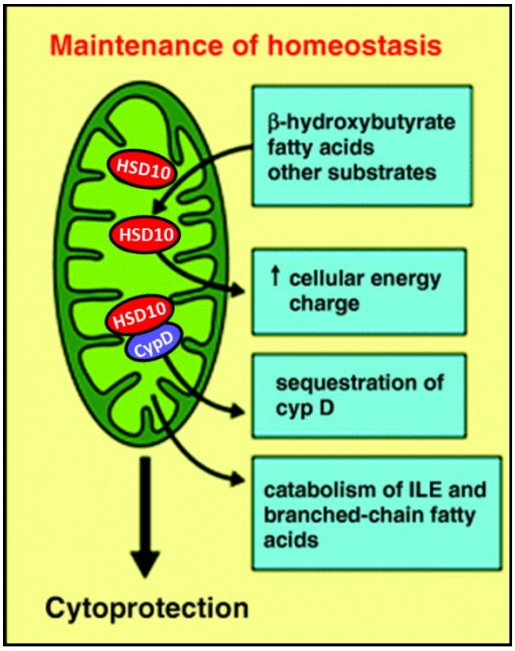

Schematic 6: HSD10 plays a vital role in the maintenance of cellular homeostasis. In healthy cells, HSD10 catalyzes the reactions of a variety of substrates, such as BHB and fatty acids, to propel mitochondrial respiration and increase ATP output. HSD10 also functions to break down isoleucine (ILE) and process branched-chain fatty acids. Additionally, HSD10 reduces cell death induction by binding and retaining CypD in the matrix. Adapted from Yan, S.D. and Stern, D.M. (2005) *Int J Exp Pathol* (127).

It should be noted that the names ABAD and ERAB (**Table 1**) have recently gone under debate as new evidence suggests that this enzyme does not exhibit generalized alcohol dehydrogenase activity, and that it is not localized in the endoplasmic reticulum, respectively (128). However, it remains well established that HSD10 is present in mitochondria and has the ability to bind Aβ. Fundamentally, in view of the absence of an Aβ-rich environment in cancer cells, this dissertation will recognize the enzyme by its most common name: HSD10.

Implication of HSD10 in Disease

As HSD10 holds a significant role in healthy cell function, it is logical that HSD10 is important in disease progression. Indeed, alterations in HSD10 have been implicated in a variety of disease states.

A very rare congenital neurodegenerative disease called HSD10 deficiency is caused by missense mutations in the HSD10 gene (129, 130) which impairs isoleucine degradation. The condition is X-linked, and predominately affects males. Of the seven known mutations which cause HSD10 deficiency, three have been investigated thus far. The R130C mutation causes a progressive neurodegenerative disease course beginning from 1 or 2 years after birth, and can lead to patient death within a few years. Symptoms include a progressive loss of motor and mental skills, and patients often develop epilepsy that is difficult to treat (131-133). The D86G mutation is associated with very severe neurological abnormalities, little psychomotor development, and extremely poor patient prognosis (134). Patients with the Q165H mutation display normal cognitive and motor development (134). At present, there are no available treatments for HSD10 deficiency. Additionally, a silent mutation in the HSD10 gene which affects splicing efficiency has been linked to mental retardation, choreoathetosis, and abnormal behavior (135, 136).

Reductions in HSD10 levels in dopaminergic neurons have been observed in Parkinson's disease (PD) patients (137), which is a neurodegenerative disease accompanied by the loss of dopaminergic neurons in the substantia nigra pars compacta. Using a PD mouse model, it was discovered that simultaneous overexpression of HSD10 has a protective effect on neurons, including improved mitochondrial respiration, ATP production, and MPTP inhibition (137). These PD studies suggest that HSD10 overexpression may be beneficial as a treatment method.

HSD10 has been most prominently studied in Alzheimer's disease (AD), which is characterized by dementia due in part to progressive nerve cell death in the human brain. Irregular Aβ production and its accumulation in Aβ plaques is a vital component in the pathogenesis of AD, although its role is not yet fully understood. The binding interaction between HSD10 and Aβ leads to disruption of HSD10 enzyme activity as the cofactor binding site is blocked (138, 139). HSD10-Aβ interaction has been observed in neuronal mitochondria in AD patients as well as in double transgenic amyloid precursor protein (APP)/HSD10 overexpression mice (110). Furthermore, AD-affected brain regions in patients exhibit elevated HSD10 levels (140). Interestingly, co-transfection of HSD10 and Aβ in cultured neurons results in increased apoptosis, which cannot be seen with HSD10 or Aβ treatment alone (141). Moreover, ETC complex IV activity is reduced in AD patients, leading to impaired energy metabolism (41). In transgenic APP/HSD10 mice it was shown that complex IV activity is diminished, ROS production is enhanced, cell viability is reduced, and rodent learning ability is decreased in comparison with transgenic APP mice (110, 142). Opposite of PD, these AD studies indicate that knockdown of HSD10 may be useful as a therapeutic strategy.

Involvement of HSD10 in Cancer

Several HSD17B family members have been implicated in breast (143-145), endometrial (146), and colorectal (147) cancers, suggesting that this group of proteins is important in the pathogenesis of many different types of cancer. Recently, HSD10 was specifically shown to be elevated in certain forms of prostate carcinomas and osteosarcomas (118, 148), indicative of a potential role in cancer. Furthermore, HSD10 may promote tumorigenesis and aggressiveness, as elevated HSD10 levels were observed in prostate-to-bone metastases in comparison to non-malignant prostate and primary prostate tumor tissue (149).

Additionally, a preliminary study performed by collaborator Dr. Hanina Hibshoosh revealed that human breast cancer tissue has higher quantities of HSD10, as shown by immunohistochemistry using Fast Red dye in **Figure A**. Since the adjacent normal breast tissue had minimal HSD10 staining, it is inferred that HSD10 overexpression is involved in breast cancer progression as well.

Figure A: Preliminary data of HSD10 in human breast cancer tissue. A biopsy taken from a breast cancer patient was obtained and the tissue was stained for HSD10 protein using Fast Red Immunohistochemistry. Normal breast morphology is depicted on the left; cancerous tissue is shown on the right with enhanced staining of HSD10. Work by Dr. Hanina Hibshoosh.

While HSD10 remains underexplored in all cancer types, the published data in bone and prostate cancers, in addition to the preliminary data in breast cancer tissue, strongly suggest that HSD10 may be utilized in cancer cells for protection against cell death induction and enhancement of unrestricted growth.

Interaction Partners of HSD10

As previously described, HSD10 can bind Aβ *in vitro* and *in vivo* in brains of AD patients, which leads to inhibition of many HSD10 enzymatic functions. Also detailed is the physical interaction between HSD10 and CypD in the mitochondrial matrix (127), which may prevent CypD translocation to the IM and ultimately block formation of the MPTP.

Additionally, HSD10 has been shown to bind to estrogen receptor α (ERα) in the mitochondria of rat cardiomyocytes (150), effectively blocking the metabolism of estradiol. As HSD10 converts potent 17β-estradiol (E2) to less potent estrogens such as estrone, it has been postulated that ERα regulates estrogen levels by mediating HSD10 activity.

Furthermore, two potential interaction partners have been identified using a yeast-2-hybrid screen: PolyC binding protein 1 and ubiquitously expressed transcript (151). Further investigation is needed to identify the function of such interactions with HSD10.

Purpose of this Dissertation

HSD10 has been vastly studied in a variety of disease states, yet the role it plays in cancer development and resistance to anticancer treatments remains to be determined. This study should contribute to the understanding of the involvement of HSD10 in the development and growth of several cancer types, in addition to how cancer cells become increasingly resistant to cell death induced by therapeutics.

Several published studies provide preliminary evidence suggesting that HSD10 is important in cancer development and aggressiveness.

1. Certain malignant prostatic epithelial cells exhibited higher levels of HSD10 then non-malignant control prostate cells (118), demonstrating that HSD10 is elevated in some cancer types.
2. HSD10 gene expression was up-regulated in osteosarcoma patients classified as poor responders to chemotherapy (148), indicating a correlation between HSD10 and poor patient prognosis.
3. Elevated HSD10 levels were observed in prostate-to-bone metastases compared to non-malignant prostate and primary prostate tumor tissue (149), suggesting that HSD10 may promote tumorigenesis and aggressiveness.

The aim of this work was to investigate the function of mitochondrial HSD10 in cancer cell growth and resistance to cell death. In order to elucidate whether HSD10 promotes cancer development, the cellular components involved and underlying mechanisms were identified, with particular emphasis placed on the interaction between HSD10 and CypD in cancer cells (**Schematic 7**). Furthermore, it was investigated whether HSD10 is involved in cancer cell resistance to cell death induction.

Taken together, these experiments are designed to help investigate the relatively unknown function of HSD10 in cancer cell growth and resistance to cell death.

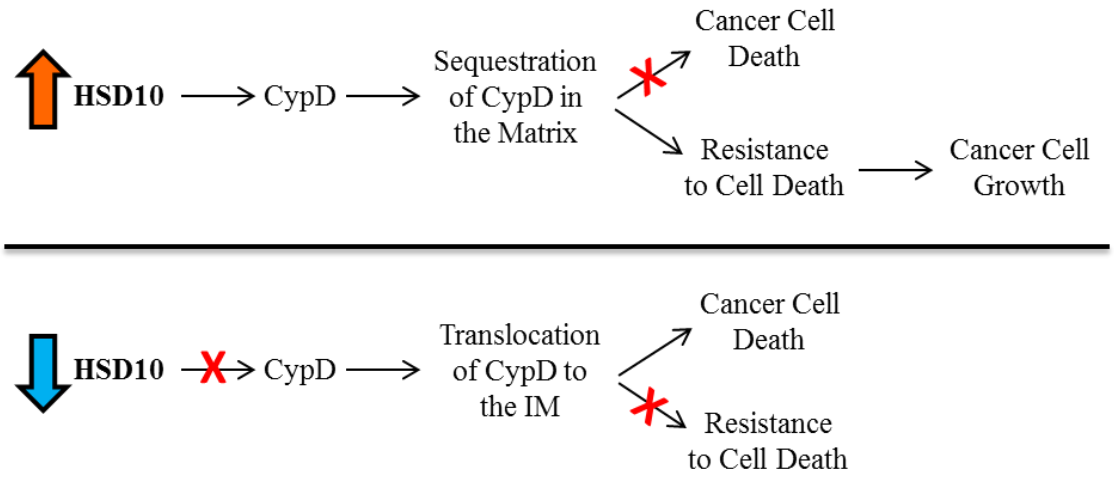

Schematic 7: Dissertation hypothesis for HSD10-mediated cancer cell growth. Top panel, cells overexpressing HSD10 bind to CypD and sequester it in the mitochondrial matrix, thereby avoiding cell death induction; this resistance allows for continued cancer cell proliferation. Bottom panel, cells under-expressing HSD10 cannot bind all of the available CypD; thus unbound CypD translocates to the IM where it induces cell death via MPTP opening. Adapted from Carlson, E.A. et al. (2015) *BMC Cancer* (152).

MATERIALS

All chemicals used are listed in **Table 2**, all solutions created are described in **Table 3**, all equipment is recorded in **Table 4**, all assay kits utilized are listed in **Table 5**, and all enzymes, antibodies, and markers used are indicated in **Table 6**. Additionally, all oligonucleotides used are described in **Tables 7** and **8**, all plasmids utilized are recorded in **Table 9**, all cell lines used are detailed in **Table 10**, and all software used are listed in **Table 11**.

Chemicals

Chemical	Source
2X Quick Ligation Buffer	Roche
5X Colorless GoTaq Reaction Buffer	Promega
10X TaqManRT	Roche
Acetyl CoA	Sigma-Aldrich
Bis-Acrylamide (30%)	BioRad
Ammonium persulfate (APS, 15%)	Sigma-Aldrich
Ampicillin (Amp)	Sigma-Aldrich
Antimycin A	Sigma-Aldrich
Blotto, non-fat dry milk	LabScientific
Bovine serum albumin (BSA)	Sigma-Aldrich
Bromophenol Blue	Sigma-Aldrich
Cholera toxin	Sigma-Aldrich
Chloroform	Thermo Fisher Scientific
Coenzyme Q1	Sigma-Aldrich
Coenzyme Q2	Sigma-Aldrich
Cytochrome c	Sigma-Aldrich
4',6-Diamidino-2-phenylindole (DAPI)	Pierce
2,6-Dichlorophenolindophenol (DCPIP)	Sigma-Aldrich
Dimethyl sulfoxide (DMSO)	Sigma-Aldrich
Dipotassium phosphate (K_2HPO_4)	Thermo Fisher Scientific
Disodium phosphate (Na_2HPO_4)	Sigma-Aldrich
Dithiothreitol (DTT)	Active Motif
dNTP	Roche
n-Dodecyl β-D-maltoside	Sigma Aldrich
Dulbecco's modified eagle's medium (DMEM)	Gibco Invitrogen
DMEM/nutrient mixture F-12 medium (DMEM/F12)	Gibco Invitrogen
Epidermal growth factor (EGF)	Sigma-Aldrich

Chemical	Source
Ethanol absolute (EtOH)	Decon Laboratories
17β-Estradiol pellets (0.36 mg/pellet; 45-day release)	Innovative Research of America
Ethidium bromide	Sigma-Aldrich
Ethylenediaminetetraacetic acid (EDTA)	Sigma-Aldrich
Fetal bovine serum (FBS)	Gibco Invitrogen
Fluoro-gel with Tris buffer	Electron Microscopy Sciences
G418 Supplement	Sigma-Aldrich
GeneAmp dNTP mix with dTTP	Applied Biosystems
Glycerol	Thermo Fisher Scientific
Glycine	Sigma-Aldrich
Hank's buffered saline solution (HBSS)	Gibco Invitrogen
Horse serum	Gibco Invitrogen
Hydrochloric acid (HCl)	Alfa Aesar
Hydrocortisone	Sigma-Aldrich
Hydrogen peroxide (H_2O_2)	Thermo Fisher Scientific
Insulin	Sigma-Aldrich
IRDye 800CW 2-deoxyglucose (2-DG)	Li-Cor Biosciences
Isofluorane	MWI Veterinary Supply
Isopropanol	Alfa Aesar
Kanomycin (Kan)	Sigma-Aldrich
LB Agar	Thermo Fisher Scientific
LB Broth, Lennox	BD Difco
LE Agarose	BioExpress
Lentiviral Packaging Mix	Sigma-Aldrich
Lipofectamine 2000	Invitrogen
Lipofectamine RNAiMAX	Invitrogen
Liquid Nitrogen	Matheson Tri-Gas, Inc.
Magnesium Chloride ($MgCl_2$)	Sigma-Aldrich
D-Mannitol	Sigma-Aldrich
Methanol absolute (MeOH)	Sigma-Aldrich
MitoSOX Red	Invitrogen
MitoTracker Green	Invitrogen
MitoTracker Red	Invitrogen
N, N, N', N'-tetramethylethylenediamine (TEMED)	Thermo Fisher Scientific
β-Nicotinamide adenine dinucleotide (NADH)	Sigma Aldrich
Opti-MEM medium	Gibco Invitrogen
Oxaloacetic acid	Sigma-Aldrich
Paraformaldehyde (PFA)	Sigma-Aldrich
Penicillin/Streptomycin (Pen/Strep)	Gibco Invitrogen
Phenylmethylsulfonyl fluoride (PMSF)	Thermo Fisher Scientific
Potassium chloride (KCl)	Sigma-Aldrich
Potassium cyanide (KCN)	Sigma-Aldrich

Chemical	Source
Potassium dihydrogen phosphate (KH_2PO_4)	Sigma-Aldrich
Protease inhibitor cocktail set	CalBioChem
Protein assay dye reagent	BioRad
Random Hexamers	Roche
Restore Western blot strip buffer	Thermo Fisher Scientific
RNAse inhibitor	Roche
Rotenone	Sigma-Aldrich
Roswell Park Memorial Institute (RPMI) 1640 medium	Gibco Invitrogen
Sodium Chloride (NaCl)	Thermo Fisher Scientific
Sodium dodecyl sulfate (SDS)	Sigma-Aldrich
Solubilization solution	Invitrogen
Succinate	Sigma-Aldrich
Sucrose	Thermo Fisher Scientific
TaqMan universal PCR master mix	Roche
Tert-Butyl hydroperoxide (TBH)	Sigma-Aldrich
Tetramethylrhodamine methyl ester (TMRM)	Molecular Probes
Tris base	Sigma-Aldrich
Triton X-100	Sigma-Aldrich
TRIZOL reagent	Invitrogen
Tryptone	Sigma-Aldrich
Yeast extract	Thermo Fisher Scientific

Table 2: List of chemicals used in this study

Buffers, Solutions, and Cell Culture Media

Solution	Recipe
BSA buffer	5% BSA, TBS
Cell culture media 1 (HEK-293T, MCF7, MDA-MB-231, T47D)	DMEM, 10% FBS, 100X Pen/Strep
Cell culture media 2 (PC-12)	RPMI-1640, 10% horse serum, 5% FBS, 100X Pen/Strep
Cell culture media 3 (MCF10A)	DMEM/F12, 5% horse serum, 100X Pen/Strep, 100 µg/ml EGF, 1 mg/ml Hydrocortisone, 1 mg/ml Cholera toxin, 10 mg/ml Insulin
Citrate Synthase assay buffer	100 mM Tris (pH 7.4), 0.17 mM Oxaloacetic acid, 0.2 mM Acetyl CoA
Co-IP collection buffer	50 mM Tris-HCl (pH 7.4), 150 mM NaCl, 0.2% Triton X-100, 1 mM EDTA, 100X protease inhibitor, 100X PMSF
Co-IP wash buffer	50 mM Tris-HCl (pH 7.4), 150 mM NaCl, 0.2% Triton X-100, 1 mM EDTA

Solution	Recipe
Complex I reaction buffer	5 mM $MgCl_2$, 2 mM KCN, 0.13 mM NADH, 2 µg/ml Antimycin; diluted in K buffer
Complex II reaction solution 1	5 mM $MgCl_2$, 20 mM succinate; diluted in K buffer
Complex II reaction solution 2	2 µg/ml Antimycin, 2 µg/ml Rotenone, 2 mM KCN, 50 µM Dichlorophenlindophenol
Complex III reaction buffer	5 mM $MgCl_2$, 2 mM KCN, 15 µM cytochrome c, 2 µg/ml of Rotenone, 0.6 mM Dodecyl-β-d-maltoside; diluted in K buffer
Complex IV assay buffer	10 mM Tris-HCl (pH 7.0), 120 mM KCl
Complex IV enzyme dilution buffer	10 mM Tris-HCl (pH 7.0), 250 mM sucrose
DNA loading buffer (6X)	40% glycerol, 0.25% Bromophenol Blue
LB-Amp media	1000X Ampicillin in LB broth
LB-Kan media	1000X Kanomycin in LB broth
LB plate	1.5% agar in LB media containing antibiotics
Milk buffer	5% non-fat dry milk, TBS
Mitochondrial isolation buffer	225 mM D-mannitol, 75 mM sucrose, 2 mM K_2HPO_4
Phosphate buffered saline (PBS, 10X)	1.37 M NaCl, 27 mM KCl, 20 mM KH_2PO_4, 100 mM Na_2HPO_4, pH 7.4
Polyacrylamide gel separating buffer	3 M Tris-HCl, pH 8.8
Polyacrylamide gel stacking buffer	0.5 M Tris-HCl, pH 6.8
Potassium buffer (25 mM)	3 M KCl, 1 M Tris-HCl, pH 7.4, 0.5 M EDTA
SDS-PAGE running buffer (10X)	0.25 M Tris, 1.92 M Glycine, 1% SDS, pH 8.0
SDS-PAGE sample buffer (4X)	150 mM Tris-HCl (pH 6.8), 6% SDS, 0.3% Bromophenol Blue, 30% glycerol, 300 mM DTT
Super optimal broth with catabolite repression (SOC) media	2% Tryptone, 0.5% Yeast extract, 10 mM NaCl, 2.5 mM KCl, 10 mM $MgCl_2$
Tris-buffered saline (TBS, 1X)	1 M Tris-HCl (pH 7.4), 5 M NaCl
TE buffer	10 mM Tris-HCl, 1 mM EDTA, pH 8.0
Western blot transfer buffer (10X)	0.25 M Tris, 1.92 M Glycine, 20% MeOH, pH 8.3

Table 3: List of solutions used in this study

Equipment

Equipment	Source
Animal weighing scale	Kent Scientific Corporation
Autoclave	Service-Rite Medical, Inc.
Autoflow IR water-jacketed CO_2 incubator	NuAire
Branson Sonifier 250	Emerson Industrial Automation

Equipment	Source
Caliper	Staples Inc.
Cell culture dishes; 6, 12, 24, and 96 well and 60, 100, 150 mm dish	Corning, Thermo Fisher Scientific
Cell culture flasks; 75 cm^2 and 25 cm^2	Nunc
Confocal microscope	Leica Microsystems
Conical tubes; 15 and 50 ml	Thermo Fisher Scientific
FluorChem HD2 imager	Protein Simple
GeneAmp PCR system 9700	Applied Biosystems
Hemocytometer	VWR
Hypoxia chamber	Coy Laboratories
Ice machine	Hoshizaki America, Inc.
Inverted microscope	Nikon Instruments, Inc.
In-Vivo Multispectral FX PRO imager	Carestream
LMax II 384 Microplate Reader and SoftMax Pro	Molecular Devices
Microcentifuge tubes; 0.5, 1.0, and 2.0 ml	MidSci
NanoDrop 1000 spectrophotometer	Thermo Fisher Scientific
Needles, 22-gauge	Becton Dickinson
Pipettes	AlphaPette, Rainin
Pipette tips	MidSci
Precision Trochar	Innovative Research of America
Purified biological safety cabinet tissue culture hood	Labconco
Sorvall RC 5C plus	Thermo Fisher Scientific
Synergy HT Multi-Mode Microplate Reader	BioTek Instruments
Syringe, 1 ml	Becton Dickinson
Tabletop centrifuge 5417R	Eppendorf
Tabletop centrifuge 5418	Eppendorf
Ultrospec 3100 pro spectrophotometer	Amersham Biosciences
XF96 extracellular flux analyzer	Seahorse Bioscience

Table 4: List of equipment used in this study

Assay Kits

Assay Kit	Source
ATP Bioluminescence Assay Kit HS II	Roche
Bicinchoninic Acid (BCA) Protein Assay	Pierce
cDNA High Capacity Reverse Transcription Kit	Thermo Fisher Scientific
CellTiter 96 Non-Radioactive Cell Proliferation Assay	Promega
In Situ Cell Death Detection Kit, Fluorescein	Roche
Power SYBR Green RT-PCR Reagents Kit	Thermo Fisher Scientific

Assay Kit	Source
Qiaex II Agarose Gel Extraction	Qiagen
Qiagen Plasmid Mini Kit	Qiagen
Qiagen Plasmid Midi Kit	Qiagen
Qiagen Plasmid Maxi Kit	Qiagen
QiaQuick PCR Purification Kit	Qiagen
Super Signal West Pico Chemiluminescent Substrate	Thermo Fisher Scientific

Table 5: List of assay kits used in this study

Enzymes, Antibodies, and Markers

Enzyme, Antibody, or Marker	Source
Alexa Fluor 488 anti-rabbit	Invitrogen
Alexa Fluor 594 anti-mouse	Invitrogen
Anti-β-actin (mouse)	Sigma-Aldrich
Anti-HSD10 (mouse)	Yan laboratory
Anti-HSD10 (rabbit)	Yan laboratory
Anti-COX4/Complex IV Subunit IV (mouse)	Invitrogen
Anti-CypD (mouse)	Abcam
Anti-CypD (rabbit)	Yan laboratory
Anti-Hsp60 (mouse)	Enzo Life Sciences
Anti-NADH dehydrogenase (ubiquinone) 1 alpha subcomplex, 5 (rabbit, complex I)	Thermo Fisher Scientific
Anti-SDHB (rabbit, complex II)	Thermo Fisher Scientific
Anti-SODII (rabbit)	Enzo Life Sciences
Anti-UQCRC2 (rabbit, complex III)	Thermo Fisher Scientific
Multiscribe Reverse Transcriptase	Roche
O'GeneRuler 100bp DNA ladder	Thermo Fisher Scientific
Pierce Protein A/G Sepharose beads	Thermo Fisher Scientific
Quick T4 DNA Ligase	Roche
Trypsin/EDTA	Gibco Invitrogen

Table 6: List of enzymes, antibodies, and markers used in this study

Oligonucleotides

The following oligonucleotides were purchased from Sigma-Aldrich, unless stated otherwise.

Oligonucleotide	Target sequence 5' ⟶ 3'
HSD17B10 MISSION® shRNA bacterial glycerol stock, human TRCN0000318937 Clone ID: SHCLNG-NM_004493.2-352s21c1 HSD10 shRNA 1	ccgggacccataccttggaagacttctcgagaagtcttccaaggtatgggtctttttg
HSD17B10 MISSION® shRNA bacterial glycerol stock, human TRCN0000318935 Clone ID: SHCLNG-NM_004493.2-189s21c1 HSD10 shRNA 2	ccggagttaggaaacaactgcgtttctcgagaaacgcagttgtttcctaacttttttg
HSD17B10 MISSION® shRNA bacterial glycerol stock, human TRCN0000318938 Clone ID: SHCLNG-NM_004493.2-751s21c1 HSD10 shRNA 3	ccggcatcgagaacccattcctcaactcgagttgaggaatgggttctcgatgtttttg
HSD17B10 MISSION® shRNA bacterial glycerol stock, human TRCN0000318872 Clone ID: SHCLNG-NM_004493.2-320s21c1 HSD10 shRNA 4	ccgggctagcaagacgtacaacttactcgagtaagttgtacgtcttgctagcttttg
ON-TARGET*plus* Non-targeting Pool Human, mouse, and rat GE Dharmacon: D-001810-10-05 Control siRNA	(1) ugguuuacaugucgacuaa (2) ugguuuacauguuguguga (3) ugguuuacauguuuucuga (4) ugguuuacauguuuuccua
Peptidylprolyl Isomerase F (PPIF) Silencer Human, siRNA ID: 107808 Thermo Fisher Scientific: AM16708 CypD siRNA	cggctctaagagtgggaggacatccaagaagattgtcatcacagactgtggccagtt

Table 7: shRNA and siRNA oligonucleotides used for HSD10 and CypD knockdown in rat and human cancer cell lines

The following primers were ordered from Sigma-Aldrich.

Primer	Organism	Forward Primer Sequence 5'⟶3'	Reverse Primer Sequence 5'⟶3'
HSD10	Human	ctgtcaactgtgcaggcatc	ttgaaggtgcccatgagatt
GAPDH	Human	atgttcgtcatgggtgtgaa	ggtgctaagcagttggtggt

Table 8: Primer oligonucleotides used for amplification of different RNA transcripts

Plasmids

Clone	Source
CSCW-IRES-GFP	ShiDu Yan
CSCW-HSD10-IRES-GFP	ShiDu Yan
pcDNA3	ShiDu Yan
pcDNA3/(human) wild-type HSD10	ShiDu Yan
MISSION® TRC2 pLKO.5-puro non-mammalian shRNA control plasmid DNA	Sigma-Aldrich

Table 9: Plasmids used for expression of HSD10 in rat and human cancer cell lines

Bacteria

E.coli XL1 chemocompetent.

Cell Lines

Cell Line	Source
Human breast carcinoma (MCF7)	ATCC
Human breast (MCF10A)	Liang Xu
Human breast carcinoma (MDA-MB-231)	Liang Xu
Human breast carcinoma (T47D)	Liang Xu
Human embryonic kidney (HEK-293T)	ATCC
Rat pheochromocytoma (PC-12)	ShiDu Yan

Table 10: List of cell lines used in this study

Animals

Severe combined immunodeficient (SCID) mice were purchased from Jackson Laboratories (Bar Harbor, ME). All animals were housed under pathogen-free conditions according to AAALAC guidelines. All animal-related experiments were performed in full compliance with institutional guidelines and approved by the Animal Care and Use Committee of the University of Kansas.

Software

Software	Source
AlphaView 3.2.2.0	Cell Biosciences
Carestream Molecular Imaging	Carestream
EndNote X6	EndNote
GraphPad QuickCalcs	GraphPad
ImageJ	National Institutes of Health
Microsoft Office	Microsoft
StateView 5.0.1	SAS Institute

Table 11: List of software used in this study

METHODS

The following sections describe the experiments used throughout this dissertation pertaining to molecular biology, protein biochemistry, cell culture, mitochondrial function, animal use, and statistical analysis.

Molecular Biology

Cloning Work

The pcDNA3 plasmid vector (**Fig. B-A, Table 9**) was used for insertion of the full length human HSD10 sequence, as previously described (141). The restriction enzymes Hind III and Xho I were used to cut the vector and insert, and were joined together via the ligation reaction method described in the following section. The resulting plasmid vector was pcDNA3/(human) wild-type HSD10 (**Fig. B-B, Table 9**). The pcDNA3 vectors were used for stable transfection of the PC-12 cells.

The CSCW-IRES-GFP plasmid vector (**Fig. B-C, Table 9**) was used for insertion of the full length human HSD10 sequence. The restriction enzymes Xba I and Xho I were used to cut the vector and insert, and were ligated together. The resultant plasmid vector was CSCW-(human) wild-type HSD10-IRES-GFP (**Fig. B-D, Table 9**). The CSCW vectors were used for lentiviral transfection of the MCF10A, MCF7, and MDA-MB-231 breast cancer cells.

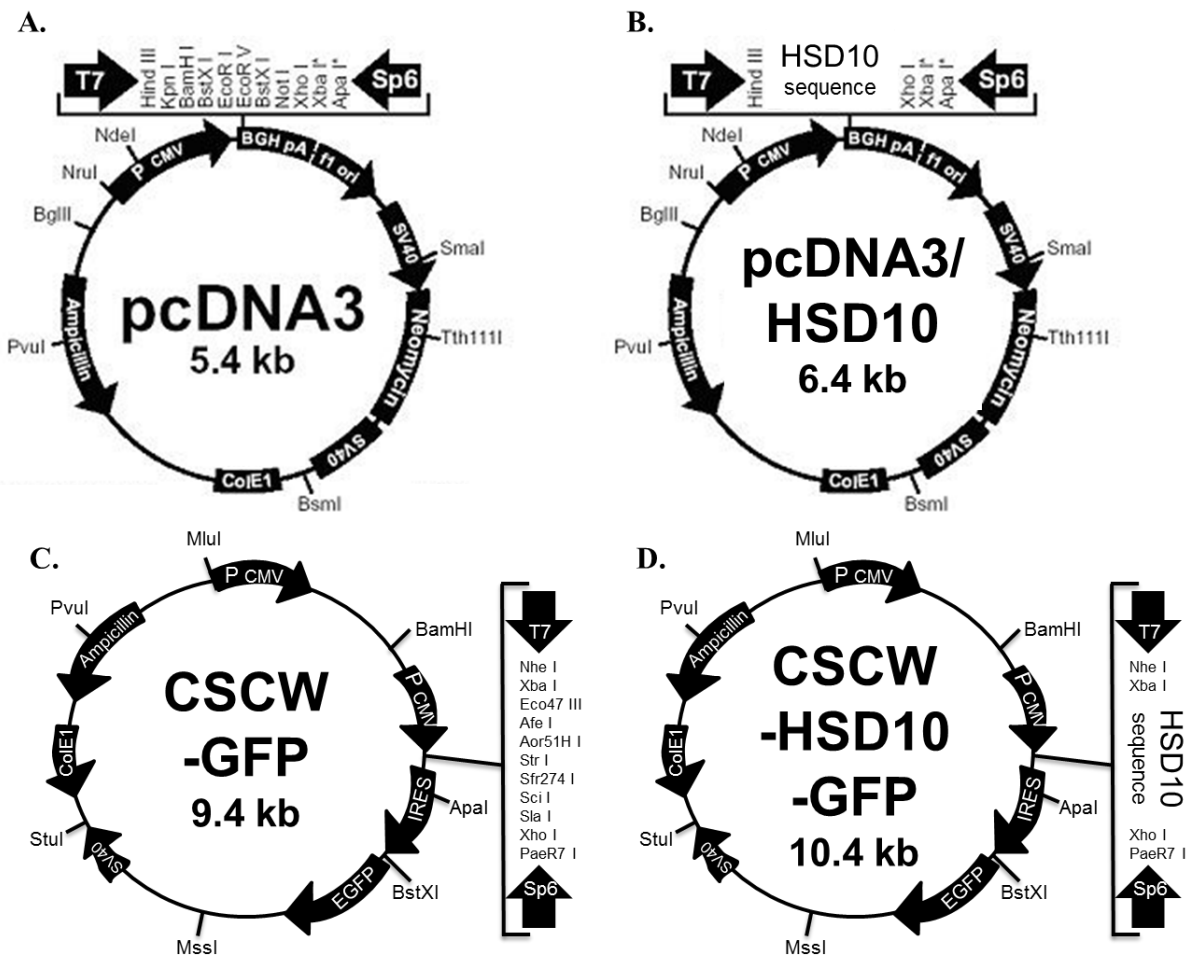

Figure B: Plasmid vector maps used in this study. A. pcDNA3 vector alone was used for the stably transfected control PC-12 EV cell line. **B.** pcDNA3/(human) wild-type HSD10 vector was used for the stably transfected HSD10 overexpression PC-12 HSD10 ov cell line. **C.** CSCW-IRES-GFP vector alone was used for the lentiviral transfected control MCF10A EV, MCF7 EV, and MDA-MB-231 EV cell lines. **D.** CSCW-HSD10-IRES-GFP vector was used for the lentiviral transfected HSD10 overexpression MCF10A HSD10 ov, MCF7 HSD10 ov, and MDA-MB-231 HSD10 ov cell lines. Adapted from pcDNA3 vector map (153).

Ligation Reaction

50 ng of vector was combined with a 3-fold molar excess of insert. The volume was adjusted to 10 µl with H_2O. 10 µl of 2X Quick Ligation Buffer was added, followed by 1 µl of Quick T4 DNA Ligase. After thoroughly mixing the solution, the reaction was incubated at room temperature (RT) for 5 min. The ligation reaction was kept on ice until the transformation step.

Transformation of Bacteria

Transformation of chemically competent *E. coli* was achieved by mixing 1 µl of purified plasmid DNA (0.1 to 1 ng total) or ligation reaction into 25 µl of competent cells. Samples were mixed gently, followed by incubation on ice for 30 min. Bacteria were heat shocked for 30 sec at 42°C, and then immediately transferred to ice. After the addition of 250 µl of RT SOC media, bacteria were incubated at 37°C for 1 hour with shaking. Successively, 50 µl of bacterial culture media was spread on a pre-warmed LB agar plate containing the proper antibiotics, and cultured overnight at 37°C.

Isolation of DNA (mini, midi, and maxiprep)

One of the resulting bacterial colonies was picked and cultured in 5 ml LB broth containing the proper antibiotics overnight at 37°C with shaking. Plasmid DNA was isolated from bacterial with the appropriate kit (**Table 5**) according to the manufacturer's instructions. Determination of the appropriate kit to use was based on the target amount of isolated plasmid DNA: 20 µg for Mini Kit, 100 µg for Midi Kit, and 500 µg for Maxi Kit.

Isolation of RNA

Total RNA from cancer cells was isolated using 1 ml TRIZOL reagent. Subsequently, 200 µl of chloroform was added and samples were mixed thoroughly by vigorous shaking. Centrifugation for 15 min at 12,000 x g at 4°C separated the upper aqueous phase, which was transferred to a new tube. RNA was precipitated by the addition of 500 µl isopropanol and incubation at RT for 10 min, followed by centrifugation for 10 min at 12,000 x g at 4°C. The pellet was resuspended in 1 ml of 70% EtOH and centrifuged for 5 min at 7,600 x g at 4°C. The

resultant pellet was dried in a chemical fume hood for 5-10 min, and then resuspended in a suitable volume of water or TE buffer. The concentration of RNA solutions was measured using a NanoDrop 1000 spectrophotometer (**Table 4**).

cDNA Synthesis (reverse transcription)

RT-PCR (reverse transcription Polymerase Chain Reaction) was performed to convert total RNA to single-strand cDNA using the cDNA High Capacity Reverse Transcription Kit (**Table 5**). The RT-PCR reaction was set up in the following 20 µl PCR reaction and the subsequent PCR program was used, according to the manufacturer's instructions.

Materials	Volume for One Reaction
10X RT Buffer	2 µl
25X dNTP Mix (100 mM)	0.8 µl
10X RT Random Primers	2 µl
MultiScribe Reverse Transcriptase	1 µl
RNase Inhibitor	1 µl
Nuclease-free H_2O	3.2 µl
RNA sample (1 µg)	10 µl
Total	20 µl

Table 12: RT-PCR reaction for the reverse transcription of total RNA

Temperature	Time	Cycle
25°C	10 min	1X
37°C	120 min	1X
85°C	5 min	1X
4°C	∞	

Table 13: PCR program used for the reverse transcription of total RNA

Quantitative Real-Time PCR

To quantify gene expression, qRT-PCR (quantitative real-time PCR) was performed on a PCR cycler using the Power SYBR Green RT-PCR Reagents Kit (**Table 5**). The qRT-PCR reaction was set up in the following 50 µl PCR reaction and the subsequent PCR program was used, according to the manufacturer's instructions. The human HSD10 primers used are listed in **Table 8**.

Materials	Volume for One Reaction
Power SYBR Green PCR Master Mix (2X)	25 µl
Forward Primer (5 µM)	2 µl
Reverse Primer (5 µM)	2 µl
cDNA	4 µl
H_2O	17 µl
Total	50 µl

Table 14: qRT-PCR reaction for the quantification of total RNA

Temperature	Time	Cycle
95°C	10 min	1X
95°C	15 sec	40X
60°C	1 min	40X
4°C	∞	

Table 15: PCR program used for the quantitative amplification of total RNA

CT values measured via qRT-PCR were normalized to GAPDH in human (**Table 8**). Relative expression levels were calculated using a standard curve.

Protein Biochemistry

Protein Extraction from Cultured Cells

Adherent cells were washed twice with PBS and then detached in PBS using a scrapper. Samples were centrifuged for 5 min at 300 x g at 4°C. The resultant pellet was resuspended in PBS containing 100X protease inhibitor cocktail, followed by sonication. Protein concentration was measured using the BCA method.

SDS-PAGE

Continuous SDS-PAGE (polyacrylamide-gel electrophoresis) was performed. Protein extracts were boiled with 1 X SDS sample buffer for 10 min at 100°C, followed by separation on a 12% separating gel topped with 4% stacking gel alongside stained protein molecular weight standards. Gels were run in an electrophoretic chamber at a constant voltage of 100 V until the loading dye reached the chamber bottom. A 12% separating gel topped with 4% stacking gel was prepared as follows for a standard size SDS gel:

Material	1 separating gel	1 stacking gel
H_2O (RT)	2.1 ml	1.0 ml
30% bis-acrylamide (4°C)	1.8 ml	220 µl
Separating buffer (4°C)	560 µl	----
Stacking buffer 4°C)	----	440 µl
10% SDS (RT)	45 µl	18 µl
15% APS (4°C)	23 µl	9 µl
TEMED (4°C)	3 µl	2 µl

Table 16: Separating and stacking gel protocol for SDS-PAGE

Immunoblotting

Proteins that were separated via SDS-PAGE were transferred to a 0.45 µm nitrocellulose membrane (Thermo Fisher Scientific) by wet transfer at constant voltage (110 V, 80 min) in Western blot transfer buffer. The membrane was blocked in 5% milk buffer for 1 hour at RT. Antibody incubation times were overnight at 4°C for primary, and 1 hour at RT for secondary antibodies with three washing steps in TBS at RT before and after both incubation steps.

Specific protein bands were visualized by chemiluminescence using Super Signal West Pico Chemiluminescent Substrate (**Table 5**) and a FluorChem HD2 image system (**Table 4**).

Co-Immunoprecipitation of Protein Complexes

This pull-down method was used to isolate HSD10 together with potential binding partners from HSD10-transfected cancer cells, specifically CypD.

For extract collection, cells were washed twice with PBS and then detached in Co-IP collection buffer using scrappers. Samples were lysed by freezing in liquid nitrogen followed by thawing in a 37°C water bath. This freeze-thaw method was repeated for a total of 10 cycles, followed by brief sonication and 30 min of lysis on ice. Subsequently, samples were centrifuged for 5 min at 8000 x g at 4°C. The resulting supernatant protein concentration was measured using the BCA method. Samples with 500 µg protein extracts within 500 µl Co-IP buffer were incubated overnight with pull-down antibodies while rotating at 4°C.

The following morning, samples were incubated with 30 µl of Protein A/G Sepharose beads for 2-3 hours on a rotator at 4°C. Subsequently, the beads were washed three times with Co-IP wash buffer, and finally resuspended in 1X SDS-PAGE sample buffer. Following incubation of the samples in boiling water for 10 min, the supernatant was used for SDS-PAGE.

Cell Culture Methods

Cultivation of Cell Lines

All adherent cell lines (**Table 10**) used in this study were grown at 37°C in a humidified 5% CO_2 incubator in either DMEM supplemented with 10% FBS and 100X Pen/Strep (HEK-293T, MCF7, MDA-MB-231, T47D), RPMI-1640 medium supplemented with 10% horse serum, 5% FBS, and 100X Pen/Strep (PC-12), or DMEM/F12 supplemented with 5% horse serum, 100 μg/ml EGF, 1 mg/ml Hydrocortisone, 1 mg/ml Cholera toxin, 10 mg/ml Insulin, and 100X Pen/Strep (MCF10A). At 80-90% confluence, cells were subcultured using trypsin/EDTA and a split ratio of 1:10 for HEK-293T and PC-12 cells, 1:7 for MCF10A, MDA-MB-231, and T47D cells, and 1:3 for MCF7 was used.

Overexpression of HSD10 in Cultured Cells

Stable transfection of HSD10 was previously performed in PC-12 cells (127). In brief, cells (10^5 cells) were transfected with pcDNA3/(human) wild-type HSD10 or pcDNA3 alone (vector) (**Table 9**), using Lipofectamine 2000 (141). 48 hours after transfection, cells were plated at 1:10-1:20 dilution in 100-mm dishes supplemented with 1 mg/ml G418. After 1-2 weeks, single clones were isolated, and cells were separated with trypsin, subjected to limiting dilution, and replated in medium containing 1 mg/ml G418 for 2-4 weeks. After, cells were maintained in the appropriate media supplemented with 1 mg/ml G418 in a humidified 37°C, 5% CO_2 environment. PC-12 pcDNA3-10 (**Fig. B, Lane 1**) was chosen as the control cell line. PC-12 HSD10-52 displayed the greatest abundance of HSD10 (**Fig. B, Lane 4**) and was selected as the HSD10-overexpressing cell line used in **Chapters 1** and **3** of this dissertation.

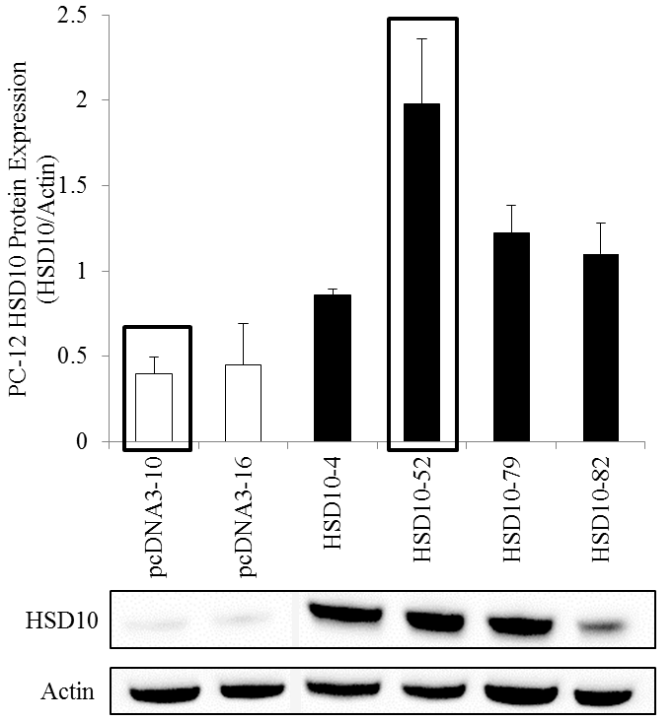

Figure C: Selection of the PC-12 HSD10 overexpression cell lines. Stably transfected PC-12 cell lines were examined for protein expression using the rabbit anti-HSD10 antibody (1:3000) via immunoblotting. Actin (mouse anti-Actin antibody, 1:8000) was used as the loading control and HSD10 expression was normalized to actin. Lanes: 1) pcDNA3-10, 2) pcDNA3-16, 3) HSD10-4, 4) HSD10-52, 5) HSD10-79, 6) HSD10-82.

Due to time constraints, lentiviral transfection was performed in MCF7, MCF10A, and MDA-MB-231 cells for the experiments detailed in **Chapter 2**. HEK 293T cells (2.5×10^5 cells/well of a 6-well plate) were transfected with CSCW-HSD10-IRES-GFP (green fluorescent protein) or CSCW-IRES-GFP (**Table 9**) using Lipofectamine 2000 and Lentiviral Packaging Mix. Cell media was harvested at 36 and 72 hours post-transfection. MCF7, MCF10A, and MDA-MB-231 cells (10^5 cells/well of a 12-well plate) were infected with HSD10 overexpression and control media over 10 days with continual passaging. After, the cells were maintained in the appropriate media in a humidified 37°C, 5% CO_2 incubator, with viral media added to cell cultures twice weekly.

Knockdown of HSD10 in Cultured Cells

HEK-293T cells (2.5 x 10^5 cells/well of a 6-well plate) were transfected with HSD10 shRNA (**Table 7**) or non-mammalian control shRNA (**Table 9**) using Lipofectamine 2000 and Lentiviral Packaging Mix. Cell media was harvested at 36 and 72 hours post-transfection. HSD10 shRNA 3 demonstrated the largest reduction in HSD10 (**Fig. C, Lane 4**), and was selected as the HSD10 shRNA construct used for all of the HSD10 knockdown studies in this dissertation, along with the non-target control shRNA (**Fig. C, Lane 1**). PC-12 and T47D cells (10^5 cells/well of a 12-well plate) were infected with HSD10 shRNA 3 and control shRNA media over 10 days with continual passaging, and then were maintained in the appropriate media in a humidified 37°C, 5% CO_2 incubator, with viral media added to cell cultures twice a week.

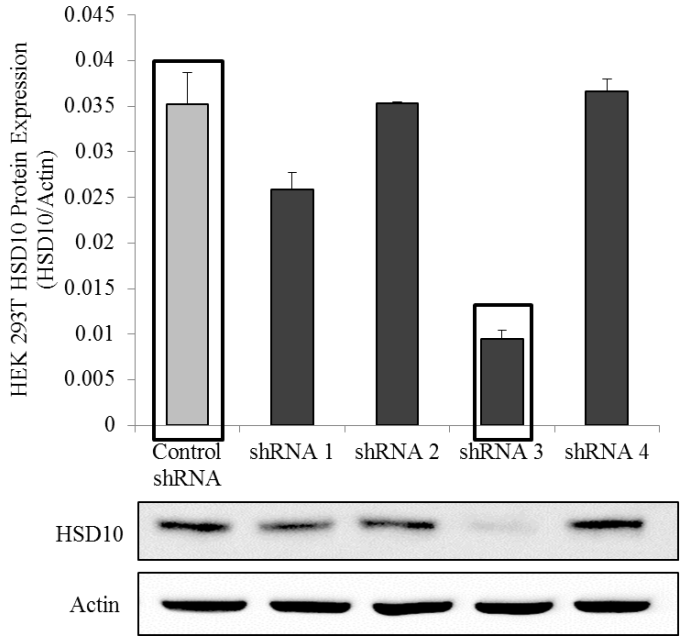

Figure D: Selection of the HSD10 shRNA construct. HEK 293T cells were transfected with four HSD10 shRNA constructs (Sigma-Aldrich) and harvested for detection of protein expression using the rabbit anti-HSD10 antibody (1:3000) via immunoblotting. Actin (mouse anti-Actin antibody, 1:8000) was used as the loading control and HSD10 expression was normalized to actin. Lanes: 1) non-target control shRNA, 2) HSD10 shRNA 1, 3) HSD10 shRNA 2, 4) HSD10 shRNA 3, 5) HSD10 shRNA 4.

Knockdown of CypD in PC-12 HSD10 ov Cultured Cells

PC-12 HSD10 overexpression (HSD10 ov) cells (2.5×10^5 cells/well of a 6-well plate) were transiently transfected with CypD siRNA (**Table 7**) or ON-TARGET*plus* non-targeting pool control siRNA (**Table 7**) using Lipofectamine RNAiMAX. Cells were harvested for experimental use 48 hours post-transfection.

Immunofluorescence Staining of Cultured Cells

Cells (2×10^4 cells/well) were grown in 8-well chamber slides until 70% confluent, and then incubated with 100 nM Mito Tracker Red for 30 min, followed by fixation in 4% paraformaldehyde and 0.1% Triton X-100 for 30 min. Fixed cells were incubated with rabbit anti-HSD10 (1:300) at 4°C overnight. Secondary antibody (Alexa Fluor 488 anti-rabbit, 1:2000) was applied to the cells followed by confocal microscopy (**Table 4**). The intensity of fluorescence (ex: 581 nm, em: 644 nm for Mito Tracker Red; ex: 499 nm, em: 520 nm for HSD10) was recorded to determine HSD10 expression and mitochondrial localization.

Co-Immunofluorescence Staining of Cultured Cells

Cells (2×10^4 cells/well) were grown in 8-well chamber slides until 70% confluent, and then fixed in 4% paraformaldehyde and 0.1% Triton X-100 for 30 min. Fixed cells were incubated with mouse anti-HSD10 (1:100) and rabbit anti-CypD (1:200), mouse anti-HSD10 (1:100) and rabbit anti-SODII (1:1000), or mouse anti-Hsp60 (1:1000) and rabbit anti-CypD (1:200) overnight, and then incubated with secondary antibodies (Alexa Fluor 488 anti-rabbit and Alexa Fluor 594 anti-mouse; 1:2000). DAPI was applied to the cells for 5 min followed by confocal microscopy. The intensity of fluorescence (ex: 499 nm, em: 520 nm for HSD10; ex:

343 nm, em: 442 nm for CypD; ex: 494 nm, em: 518 nm for SODII; ex: 495 nm, em: 519 nm for Hsp60; ex: 358 nm, em: 461 nm for DAPI) was recorded to determine HSD10 and CypD expression and localization to the mitochondrial markers, SODII and Hsp60.

TUNEL Staining of Cultured Cells

The *In Situ* Cell Death Detection Kit, Fluorescein (**Table 5**) was used as described. Cells (2×10^4 cells/well) were grown in 8-well chamber slides until 70% confluent. Following incubation for 24 hours with 0.75 mM H_2O_2, the cells were fixed in 4% paraformaldehyde for 1 hour. Fixed cells were permeabilisated for 2 min on ice, followed by incubation with 75 µl TUNEL (terminal deoxynucleotidyl transferase dUTP nick end labeling) reaction mixture for 1 hour at 37°C. After washing twice with PBS followed by 5 min of nuclear staining with DAPI, the cells were imaged via confocal microscopy and the intensity of fluorescence (ex: 488 nm, em: 565 nm for TUNEL; ex: 358 nm, em: 461 nm for DAPI) was recorded to determine cells undergoing apoptotic cell death.

Cell Growth Curve Analysis

Cells were plated in 7-10 100-mm dishes at a density of $1\text{-}2.5 \times 10^5$ cells/dish, depending on the cell type. One dish was chosen each consecutive day to be counted. The cells in the dish were detached with trypsin/EDTA, centrifuged, and resuspended in 1 ml of media, followed by counting using a hemocytometer.

Mitochondrial Function Assays

Mitochondrial Membrane Staining of Cultured Cells

Cells (2 x 10^4 cells/well) were grown in 8-well chamber slides until 70% confluent, and then incubated with 150 nM Mito Tracker Green and 100 nM TMRM (non-quench mode) for 30 min, followed by washing twice with HBSS media. Cells were imaged live by confocal microscopy and the intensity of fluorescence (ex: 490 nm, em: 516 nm for Mito Tracker Green; ex: 490 nm, em: 550 nm for TMRM) was recorded to determine the uncollapsed proton gradient.

MTT Reduction

The CellTiter 96 Non-Radioactive Cell Proliferation kit (**Table 5**) was used to measure metabolic activity. Cells (10^4 cells/well) were plated in 96-well plates 48 hours prior to the experiment. For cellular resistance experiments, H_2O_2 (0.1, 0.25, 0.5, 0.75, and 1 mM) and TBH (0.1 and 0.25 mM) were added to cells 24 hours prior to incubation with 15 µl/well of MTT (3-(4,5-dimethylthiazol-2-yl)-2,5-diphenyltetrazolium bromide) dye solution for 4 hours. Successively, 100 µl/well of solubilization solution was added to stop the reaction, and then the plates were incubated for 1 hour. The change in absorbance at 570 nm was recorded using a 96-well Synergy HT Multi-Mode Microplate Reader (**Table 4**). A reference wavelength of 650 nm was taken to reduce background.

ATP Activity

Cellular ATP levels were measured using the Bioluminescence Assay Kit HS II (**Table 5**) following the manufacturer's instructions as previously described (154). Briefly, cells (30 x 10^4 cells/well) were grown in 6-well plates until fully confluent. Cells were washed twice with

ice-cold PBS, followed by the addition of 50 µl/well of ATP Lysis Buffer. Samples were harvested, incubated on ice for 20 minutes, and then centrifuged. Protein content of the supernatant was determined using the BCA method. Proportional amounts of sample were added to a 96-well ATP plate (25 µl/well). The reaction solution was brought to 50 µl/well with the addition of ATP Dilution Buffer. ATP levels were determined using an LMax II 384 Microplate Reader and SoftMax Pro (**Table 4**).

ETC Enzyme Activity

Briefly, cells (10^6 cells/dish) were grown in 150-mm dishes until fully confluent. For measurement of complex IV enzymatic activity in response to oxidative stress, 750 µM of H_2O_2 was added to cells and incubated for 1, 6, 16, and 24 hours before collection. Cells were washed twice with pre-chilled PBS, and then harvested, centrifuged, and suspended in 100 µl of mitochondrial isolation buffer. A working solution of 25 mM K buffer was used for complex I, II, III, and IV assays as described (154). An Ultrospec 3100 pro spectrophotometer (**Table 4**) was used to measure the change in absorbance for all complexes. Background levels were measured in the absence of cell suspensions. All complex enzyme activities are expressed as nanomoles of substrate oxidized per $mg^{-}1$ protein $min^{-}1$ $ml^{-}1$ (nmol/mg protein/min/ml) converted to fold increase.

a. Complex I

Cell lysate (30-50 µg of protein/ml) was added to a cuvette containing 0.5 ml of Complex I reaction buffer. The reaction was started by the addition of Coenzyme Q1 (2 µl of 65 µM solution). At 180 sec, 2 µl of Rotenone (2 µg/ml) was added to the cuvette.

The change in absorbance at 340 nm, resulting from the oxidation of NADH, was measured using a kinetic program with 20 sec intervals and a total of 18 readings.

b. Complex II

Cell suspensions (30-50 µg of protein/ml) were added to a 1.5 ml microcentrifuge tube containing 0.5 ml of Complex II reaction solution 1, and then incubated in a 37°C water bath for 10 minutes. After transferring the cell solution to a cuvette, the reaction was started by the addition of 8 µl of Complex II reaction solution 2. At 180 sec, 2 µl of Coenzyme Q_2 (65 µM) was added to the cuvette. The change in absorbance at 600 nm, resulting from the reduction of DCPIP, was measured using a kinetic program with 20 sec intervals and a total of 18 readings.

c. Complex III

The reaction was started by the addition of 2 µl of Coenzyme Q_2 (65 µM) to a cuvette containing 0.5 ml of Complex III reaction buffer. At 60 sec, a cell suspension (30-500 µg of protein/ml) was added to the cuvette. The change in absorbance at 550 nm, resulting from the reduction of cytochrome c, was measured using a kinetic program with 20 sec intervals and a total of 12 readings.

d. Complex IV

Cell lysate (30 µg of protein/ml) was added to a cuvette containing 0.475 ml of Complex IV assay buffer, and the reaction volume was brought to 0.525 ml with Complex IV enzyme dilution buffer. The reaction was started by the addition of 25 µl of ferrocytochrome c substrate solution (0.22 mM). The change in absorbance at 550 nm, resulting from the oxidation of cytochrome c, was measured using a kinetic program with a 5 sec delay, 10 sec intervals, and a total of 6 readings.

Citrate Synthase Enzyme Activity

Cells in 100-mm dishes were washed twice with cold PBS, and cells were harvested, centrifuged, and suspended in 100 µl of mitochondrial isolation buffer. The reaction was started by the addition of cell lysate (10-30 µg of protein/ml) to a cuvette containing 150 µl of citrate synthase assay buffer. The change in absorbance at 232 nm was measured using a kinetic program with 60 sec intervals and a total of 8 readings.

Animal Work

Maintenance of Mouse Lines

Two-month old SCID mice were purchased from Jackson Laboratories and continuously bred on the Yan breeding protocol to acquire SCID mouse generations for experimental use.

Injection of Cultured Cells into Mice

HSD10-transfected cancer cells were grown in 150-mm dishes until fully confluent, followed by suspension in serum free cell culture medium. Single injections containing 1-5 x 10^6 cells per 100 µl medium were prepared under a sterile tissue culture hood. Cancer cells were injected into the mammary fat pad tissue of female SCID mice using the following protocol. Following anesthesia with 2% isofluorane, the mammary gland area was shaved and sterilized with alcohol. Two injections of HSD10-transfected cancer cells were made using a sterile 22-gauge needle with manual restraint (155), one injection per fifth mammary fat pad area on each side of the mouse.

Imaging and Measurement of Tumor Growth

Tumor-inoculated mice were weighed and tumor size was measured using a caliper twice per week for a total of 30 days. Tumor volume was calculated using the formula: (length x width^2)/2 (156). Mice were imaged with an In-Vivo Multispectral FX PRO imaging system (**Table 4**) on day 30 of the experiment, 24 hours post-injection of 15 nmol 2-DG optical probe (**Table 2**) (157) given via tail vein injection. An excitation filter of 760 nm and emission filter of 830 nm was applied for Near Infrared imaging to visualize tumor growth.

Statistics

Paired t tests were used for statistical comparison of empty vector (EV) with HSD10 ov groups, control shRNA with HSD10 shRNA groups, and control siRNA with CypD siRNA groups. Unpaired t tests were used to analyze all animal data. Concerning the TUNEL staining assays, one-way analysis of variance was used for statistical comparison between groups, with the post-hoc tests Bonferroni/Dunn and Tukey-Kramer performed after. All data was analyzed using the software described in **Table 11**, and results are reported as mean ± SE. $P<0.05$ was considered significant.

RESULTS

Chapter 1: Impact of HSD10 on Altered Pheochromocytoma Cells

The rat adrenal gland cancer cell line, PC-12, was used to examine the role of HSD10 in cancer progression. PC-12 cell growth rate was first observed in the HSD10-transfected cells to determine if HSD10 influences PC-12 cell differentiation in cell culture. Subsequently, the effect of HSD10 on tumor growth was examined using an *in vivo* tumor mouse model. After observing differing growth patterns in PC-12 cells due to overexpression and knockdown of HSD10, mitochondrial functions were assessed to investigate the impact of HSD10 on intracellular function. The role of HSD10 in PC-12 cellular resistance to cell death was also examined. Finally, the interaction between HSD10 and CypD was investigated as a possible mechanism of action for the observed HSD10 overexpression phenotype in PC-12 cells.

1.1. Generation of HSD10-transfected Pheochromocytoma Cell Lines

Following transfection, PC-12 cancer cells expressing either an empty pcDNA3 vector or an HSD10 ov vector (**Table 9**) were subjected to immunoblotting for analysis of protein content. HSD10 protein expression was increased by over 2.5-fold in HSD10 ov cells compared to EV cells (**Fig. 1-1 A**). To thoroughly examine the effect of HSD10 in cancer, lentiviral transfection using a shRNA oligonucleotide (**Table 7**) was used to knockdown HSD10 in PC-12 cells. Immunoblot analysis revealed that HSD10 protein expression was significantly reduced by 80% in HSD10 shRNA-transfected cells in comparison with control shRNA-transfected cells (**Fig. 1-1 B**). These experiments verify that HSD10 overexpression and knockdown in PC-12 cells was successful.

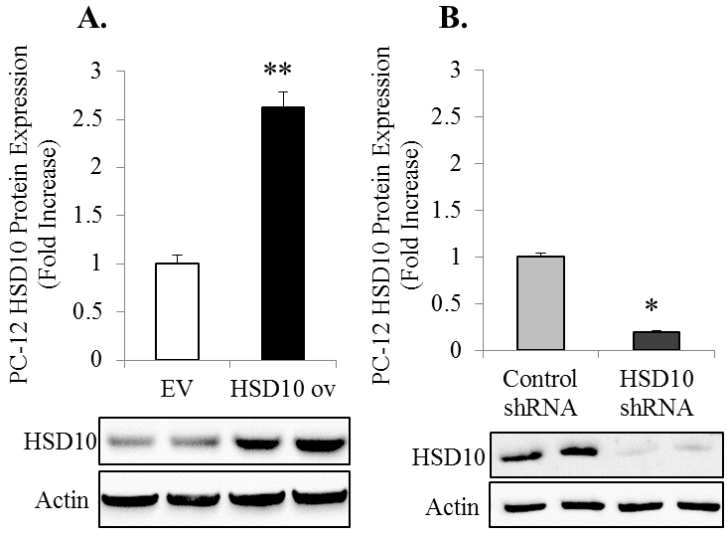

Figure 1-1: Generation of PC-12 HSD10-transfected cells. PC-12 transfected cells were harvested for detection of protein expression using rabbit anti-HSD10 antibody (1:3000, generated in the Yan lab) via immunoblotting. Actin (mouse anti-Actin antibody, 1:8000) was used as the protein loading control and HSD10 expression was normalized to actin. Results are displayed as fold increase relative to EV (**A**) or control shRNA (**B**). **A.** EV and HSD10 ov whole cell lysates were analyzed for HSD10 protein expression (n=4). **B.** Control shRNA and HSD10 shRNA whole cell lysates were analyzed for HSD10 protein expression (n=4). Data presented as mean ± SE. *P<0.05, **P<0.01 versus control group. Adapted from Carlson, E.A. et al. (2015) *BMC Cancer* (152).

1.2. Localization of HSD10 in HSD10-transfected Pheochromocytoma Cells

At the N-terminus, HSD10 contains a mitochondrial targeting sequence (111), which was shown to direct HSD10 to mitochondria in human neuroblastoma cells (141). To further confirm HSD10 transfection success and to investigate whether upregulation and/or downregulation of HSD10 interferes with the enzyme's normal localization pattern, HSD10 in PC-12 cells was co-stained with the mitochondrial dye Mito Tracker Red (**Fig. 1-2**).

The intensity of HSD10 staining was significantly enhanced in HSD10 ov cells in comparison with EV cells (**Fig. 1-2 A-B**). In addition to confirming increased levels of HSD10 in the PC-12 HSD10 ov cells, the immunofluorescence assay established the localization of HSD10 to mitochondria, as depicted in the merged picture of **Figure 1-2 A**. The level of HSD10 knockdown was also confirmed by immunofluorescence staining of HSD10 (**Fig. 1-2 C**), which revealed that the intensity of HSD10 staining was decreased in HSD10 shRNA cells compared to control shRNA cells (**Fig. 1-2 D**).

Thus, HSD10 upregulation does not seem to interfere with the enzyme's normal localization pattern to mitochondria. Similarly, HSD10 downregulation does not appear to disrupt mitochondrial localization; there was less co-staining with Mito Tracker Red, however this is most likely due to the large reduction in HSD10, and not as a result of HSD10 sequence targeting disruption.

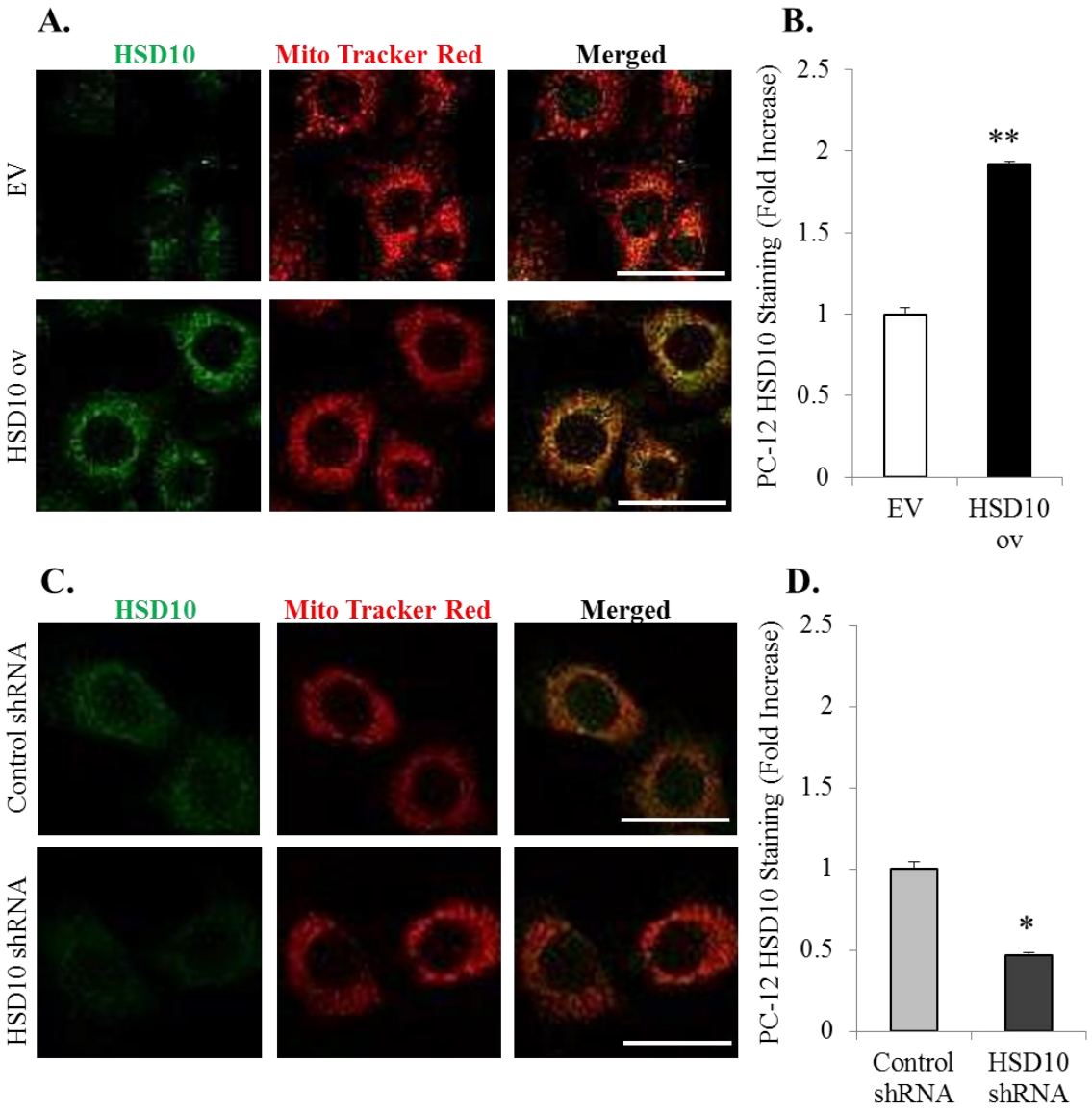

Figure 1-2: Localization of HSD10 in PC-12 HSD10-transfected cells. PC-12 transfected cells were cultivated on chamber slides and proteins were detected using rabbit anti-HSD10 antibody (1:300) and Mito Tracker Red (1:500). After incubation with anti-rabbit Alexa Fluor 488 (1:500), cells were mounted in fluorescence mounting media. Confocal microscopy was used to visualize immuno-fluorescence staining of **A.** HSD10 alone (green), Mito Tracker Red alone (red), and these two antigens co-localized (yellow) in EV and HSD10 ov PC-12 cells (scale bar: 30 μm). **B.** Quantification of HSD10 immunofluorescence staining (depicted in **A**) displayed as fold increase relative to EV (n=5). **C.** Immunofluorescence staining of HSD10 alone (green), Mito Tracker Red alone (red), and merged (yellow) in control shRNA and HSD10 shRNA PC-12 cells (scale bar: 30 μm). **D.** Quantification of HSD10 immunofluorescence staining (depicted in **C**) displayed as fold increase relative to control shRNA (n=5). Data presented as mean ± SE. *P<0.05, **P<0.01 versus control group. Adapted from Carlson, E.A. et al. (2015) *BMC Cancer* (152).

1.3. In Vitro *HSD10-transfected Pheochromocytoma Cell Growth Curve Analysis*

The effect of HSD10 modification on PC-12 cell growth was examined using *in vitro* cell culture. PC-12 HSD10-overexpression and PC-12 HSD10-knockdown cell lines were plated in dishes at a constant density and grown over the course of seven days, with a dish counted each day. As shown in **Figure 1-3 A**, HSD10 ov cells grew at a significantly faster rate compared to EV cells over the seven days. In contrast, knockdown of HSD10 led to a considerable decrease in growth rate compared with control shRNA cells (**Fig. 1-3 B**). Taken together, these results suggest that HSD10 promotes pheochromocytoma cell growth in cell culture and that knockdown of HSD10 has a negative effect on cancer cell growth.

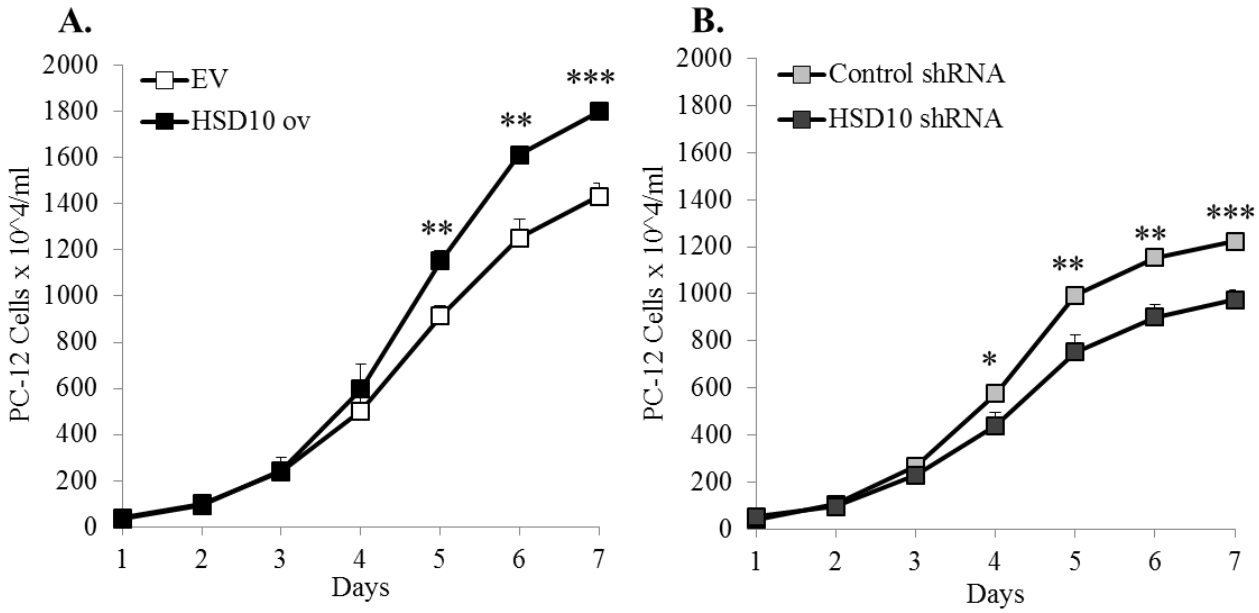

Figure 1-3: Effect of HSD10-modification on *in vitro* PC-12 cell growth. PC-12 transfected cells plated at a constant density were grown and counted over the course of 7 days to determine cell growth rate. **A.** Growth curve of EV (white ■) and HSD10 ov (black ■) cells displayed as cells x 10^4 per ml (n=9). **B.** Growth curve of control shRNA (light gray ■) and HSD10 shRNA (dark gray ■) cells depicted as cells x 10^4 per ml (n=9). Data presented as mean ± SE. *P<0.05, **P<0.01, ***P<0.001 versus control group. Adapted from Carlson, E.A. et al. (2015) *BMC Cancer* (152).

1.4. **In Vivo *HSD10-transfected Pheochromocytoma Tumor Growth Analysis***

After observing an enhancement in PC-12 cell growth rate in HSD10 ov cells compared to EV cells, a xenograft tumor mouse model was used in a study to validate the role of HSD10 on PC-12 cancer cell growth *in vivo*. SCID mice inoculated with HSD10 ov cells exhibited drastically larger tumors compared to mice with EV tumor xenografts which displayed very minimal growth (**Fig. 1-4 A**). Furthermore, HSD10 ov tumors grew at a significantly faster rate over 32 days compared to EV tumors (**Fig. 1-4 B**). These results demonstrate that HSD10 overexpression accelerates tumor development *in vivo*, providing further evidence that HSD10 is an important cancer mediator in adrenal gland cancer.

While there are limited *in vivo* xenograft studies involving PC-12 cells, one group revealed that following implantation of PC-12 cells into the striatum of Sprague-Dawley rats, the number of cells remained unchanged and there was no continued tumor growth (158). This study corroborates the minimal growth observed in the EV tumors (**Fig. 1-4**) and provides further support for the tumor-promoting role of HSD10.

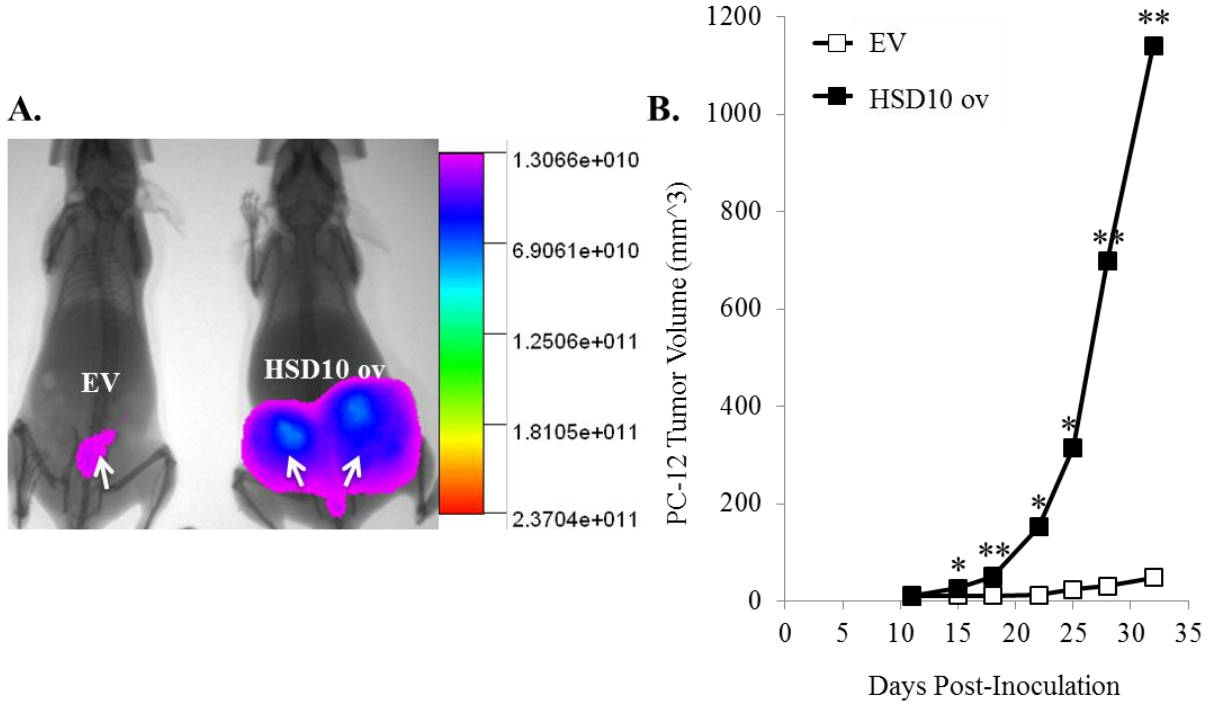

Figure 1-4: HSD10 overexpression enhances *in vivo* PC-12 tumor growth. PC-12 transfected EV and HSD10 ov cells were injected into the mammary fat pad tissue of 10 two-month old female SCID mice. **A.** Day 30 tumor growth in two SCID mice inoculated with EV (left mouse) or HSD10 ov (right mouse) cells was visualized 24 hours post-injection of 15 nmol 2-DG optical dye with an In-Vivo Multispectral FX PRO imager. Arrows point to tumors. **B.** Quantification of tumor growth in all SCID mice injected with EV (n=8; white ■) or HSD10 ov (n=12; black ■) cells grown over a total of 32 days, depicted in tumor volume (mm^3). Data presented as mean. *P<0.001, **P<0.0001 versus control group. Adapted from Carlson, E.A. et al. (2015) *BMC Cancer* (152).

1.5. Effect on Altered Pheochromocytoma Mitochondrial Function

Following the successful studies evaluating HSD10-mediated PC-12 cancer growth, the effect of HSD10 on intracellular mitochondrial function was examined for changes in processes. The enzyme activities of complexes I, II, III, and IV of the ETC were tested first to investigate the impact of HSD10 alteration on mitochondrial respiration.

While the enzyme activities of complexes I, II, and III remained unchanged (**Fig. 1-5 A-C**), complex IV activity was significantly increased in HSD10 ov cells compared with EV cells (**Fig. 1-5 D**), suggesting an enhancement in the ETC system of HSD10-overexpressing PC-12 cells. Conversely, HSD10 shRNA cells displayed significantly decreased ETC complex enzyme activity in all of the complexes measured, in comparison to control shRNA cells (**Fig. 1-5 A-D**). This reduction in all of the complexes indicates that HSD10 is important for PC-12 cancer cell functionality, and would likely have a substantial impact on subsequent mitochondrial processes.

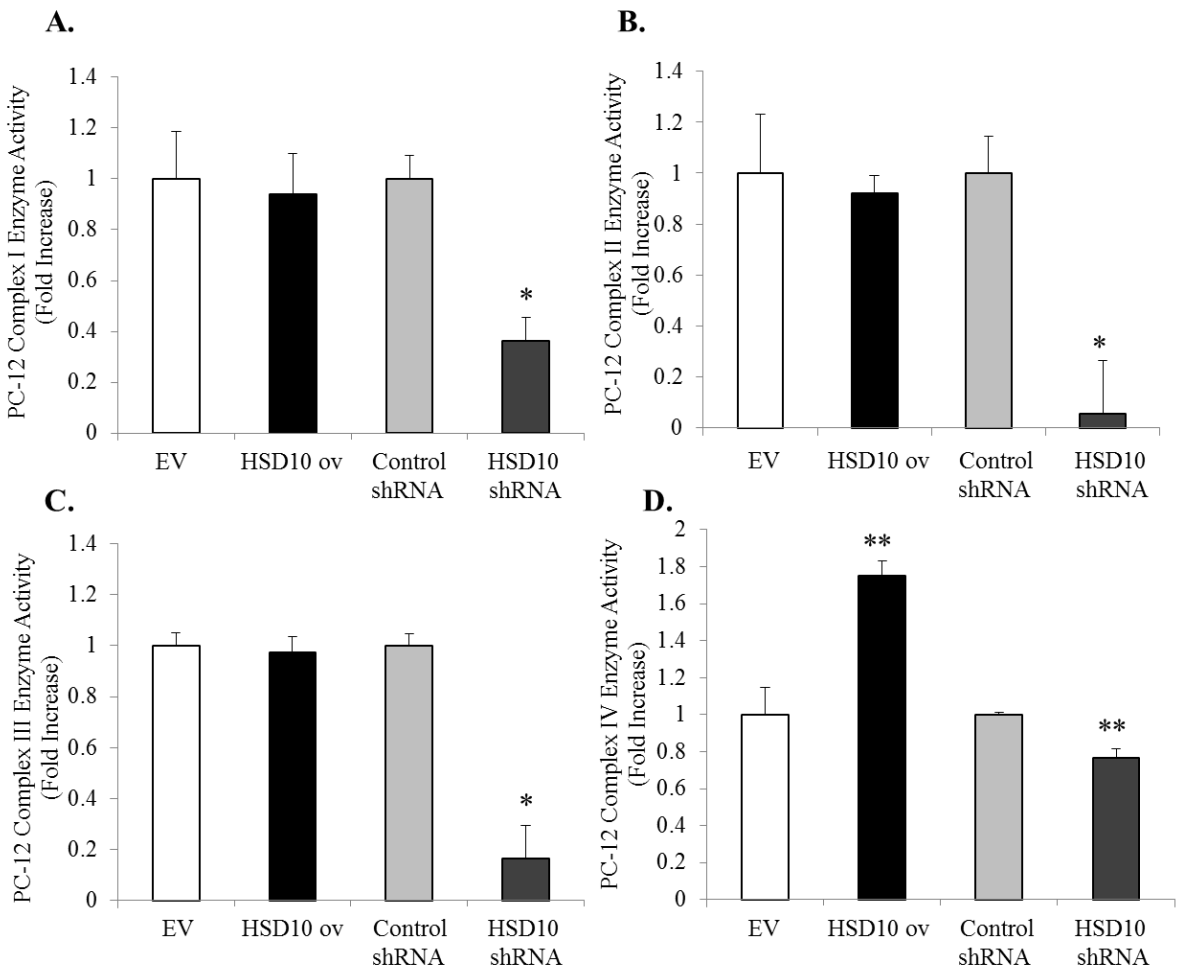

Figure 1-5: Examination of ETC enzyme activities in PC-12 HSD10-transfected cells. PC-12 transfected cells were harvested and tested for ETC complex I (**A**), II (**B**), III (**C**), and IV (**D**) enzyme activities. Results are displayed as fold increase relative to EV for HSD10 ov, and control shRNA for HSD10 shRNA (n=5 for each assay). Data presented as mean ± SE. *P<0.05, **P<0.01 versus EV and control shRNA groups. Adapted from Carlson, E.A. et al. (2015) *BMC Cancer* (152).

The changes seen in the ETC complex enzyme activities for the HSD10-overexpression cell lines were not accompanied by variations in ETC complex protein expression (**Fig. 1-6 A-D**). However, the HSD10-knockdown cells showed a trend toward reduced ETC complex protein expression (**Fig. 1-6 E-H**); although the only statistically significant difference was observed in complex II of the HSD10 shRNA cells (**Fig. 1-6 F**). This implies that loss of HSD10 impacts both ETC complex protein content and enzyme activity.

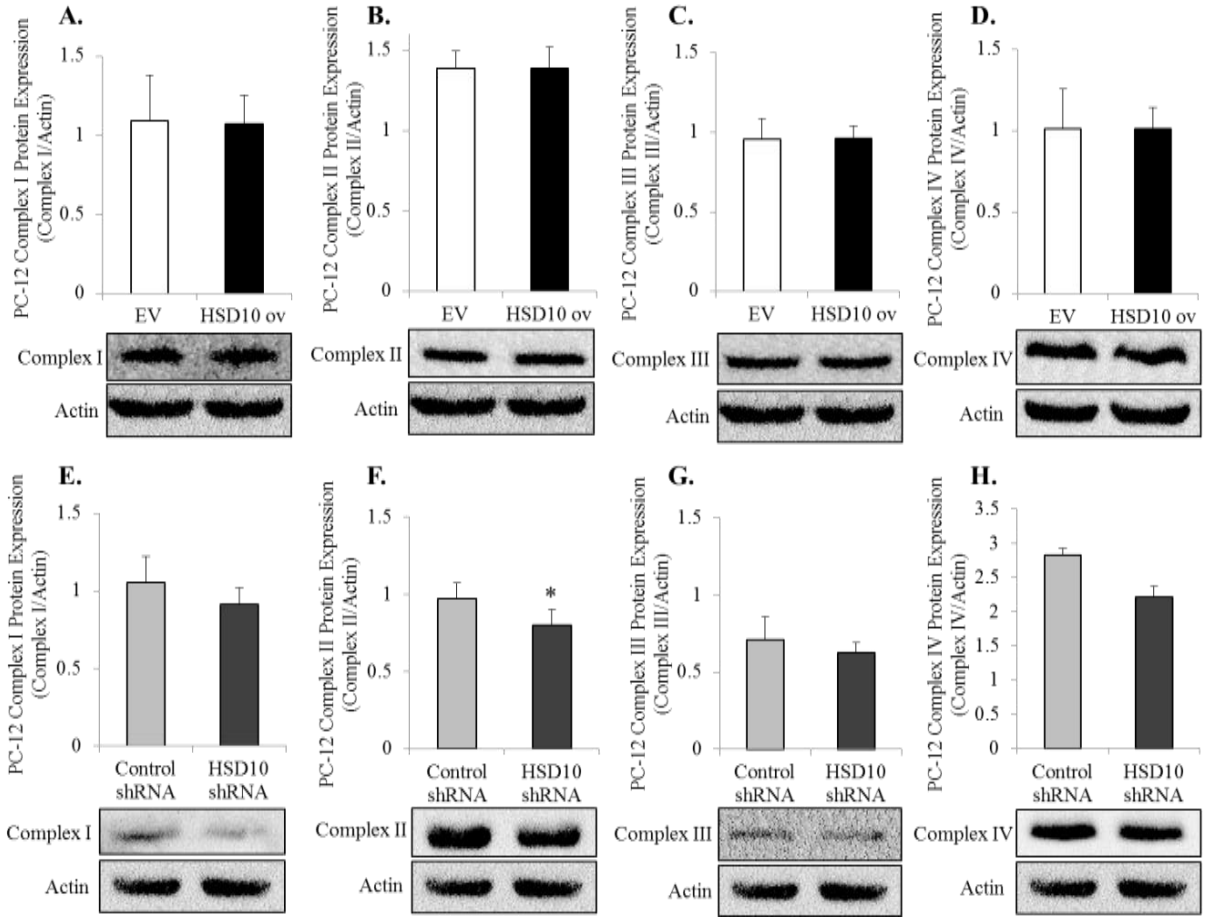

Figure 1-6: Effect of HSD10-modification on PC-12 ETC complex protein expression. PC-12 EV and HSD10 ov cells were harvested for detection of complex I (**A**), II (**B**), III (**C**), and IV (**D**) protein expression via immunoblotting with the appropriate antibodies listed in **Table 6**. PC-12 control shRNA and HSD10 shRNA cells were harvested for detection of complex I (**E**), II (**F**), III (**G**), and IV (**H**) protein expression via immunoblotting with the appropriate antibodies. Actin (mouse anti-Actin antibody, 1:4000) was used as the loading control and each complex protein expression was normalized to actin (n=4 for each group). Data presented as mean ± SE. *P<0.05 versus control shRNA group.

As complex IV enzyme activity was enhanced in PC-12 HSD10 ov cells, the impact of this change on ATP production was assessed. ETC complexes I, III, and IV are proton pumps, which generate the transmembrane proton gradient necessary to drive ATP generation by ATP synthase. Thus, changes in the ETC system would impact mitochondrial ATP generation and any ensuing mitochondrial processes.

In conjunction with the complex IV data observed in **Figure 1-5 D**, the level of ATP was significantly elevated in HSD10 ov cells compared to EV cells (**Fig. 1-7**), demonstrating a possible increase in energy generation in HSD10-overexpressing PC-12 cells. On the other hand, ATP production was diminished in HSD10 shRNA cells compared to control shRNA cells (**Fig. 1-7**), which was expected in view of the decreased activity and protein content observed in all of the ETC complexes in **Figure 1-5 A-D**.

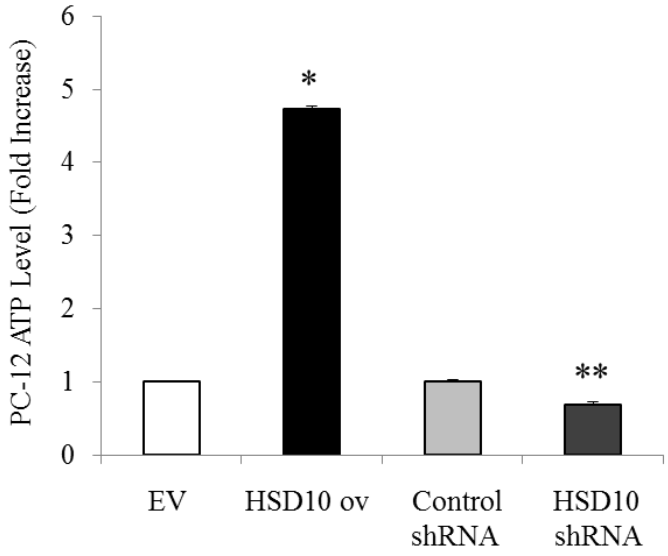

Figure 1-7: Assessment of ATP production in PC-12 HSD10-transfected cells. PC-12 transfected cells were harvested for determination of cellular ATP content. Densitometry of results displayed as fold increase relative to EV for HSD10 ov, and control shRNA for HSD10 shRNA (n=6). Data presented as mean ± SE. *P<0.05, **P<0.01 versus EV and control shRNA groups. Adapted from Carlson, E.A. et al. (2015) *BMC Cancer* (152).

As alterations in several ETC complexes and ATP production were observed in HSD10-modified PC-12 cells, citrate synthase enzyme activity was assessed as a mitochondrial control; it is typically used as a quantitative enzyme marker for the presence of intact mitochondria.

Citrate synthase enzyme activity was similar between HSD10 ov cells and EV cells (**Fig. 1-8**), indicating that, despite an overabundance of HSD10, the PC-12 HSD10-overexpressing

cells were healthy. However, citrate synthase enzyme activity, which serves as a measurement of mitochondrial fitness, was slightly reduced in HSD10 shRNA cells (**Fig. 1-8**). This suggests that HSD10 knockdown disrupts mitochondrial function and structure. Further investigation into how knockdown of HSD10 influences mitochondrial morphology is needed.

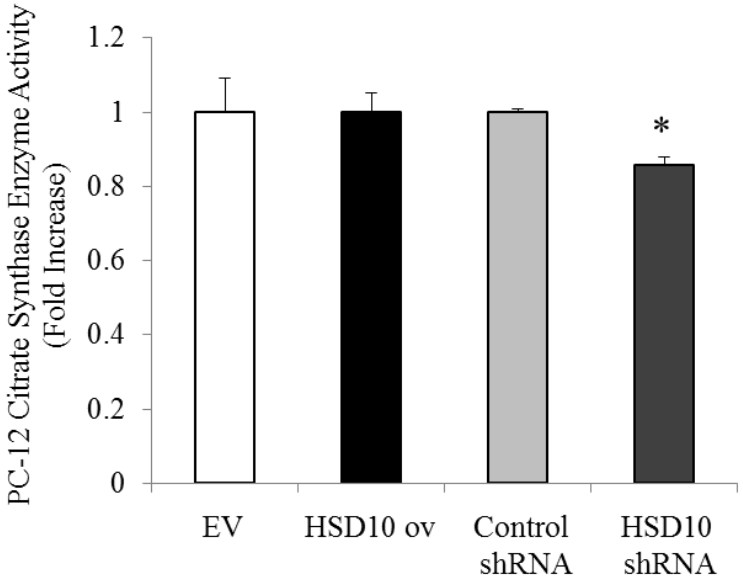

Figure 1-8: Analysis of citrate synthase enzyme activity in PC-12 HSD10-transfected cells. PC-12 transfected cells were harvested and citrate synthase enzyme activity was tested. Densitometry of results displayed as fold increase relative to EV for HSD10 ov, and control shRNA for HSD10 shRNA (n=5). Data presented as mean ± SE. *P<0.01 versus control shRNA group. Adapted from Carlson, E.A. et al. (2015) *BMC Cancer* (152).

ATP is a key driver for many mitochondrial and cellular processes. As ATP levels in the HSD10-transfected PC-12 cells were altered compared to controls, the effect of HSD10 on cell viability was measured using the MTT reduction assay which tests cellular metabolic activity due to NAD(P)H flux.

MTT reduction levels remained similar between HSD10 ov cells and EV cells after 24 hours, indicating comparable cell viability (**Fig. 1-9 A**). Furthermore, the change in MTT

reduction between control shRNA and HSD10 shRNA cells was not statistically significant after 24 hours (**Fig. 1-9 A**), although the slight decrease observed in HSD10 shRNA cells demonstrates a small trend. The MTT reduction data indicate that the changes observed in the ETC complexes and ATP generation is the result of PC-12 cell growth rate.

The effect of HSD10 on mitochondrial function was further assessed via mitochondrial membrane potential using the cell-permeant dye, TMRM. This red dye is readily taken up by active mitochondria and emits a stronger fluorescence in mitochondria with intact organelle membranes (159). Also, TMRM co-localizes with Mito Tracker Green (**Fig. 1-9 B and D**).

HSD10 ov cells displayed enhanced TMRM staining as opposed to the normal levels observed in EV cells (**Fig. 1-9 B-C**). Alternatively, HSD10 shRNA cells displayed a decrease in TMRM staining intensity compared to control shRNA cells (**Fig. 1-9 D-E**). Due to the significant increase in TMRM fluorescence observed in HSD10 ov cells, HSD10 overexpression may promote mitochondrial membrane hyperpolarization. Whereas loss of mitochondrial membrane potential can induce cell death pathways, hyperpolarization mediated in part by HSD10 could lead to protection against induction of cell death. In HSD10 shRNA cells, there is considerably less HSD10 present within mitochondria; hence HSD10 knockdown may induce mitochondrial membrane depolarization, thus increasing the chance of cell death induction.

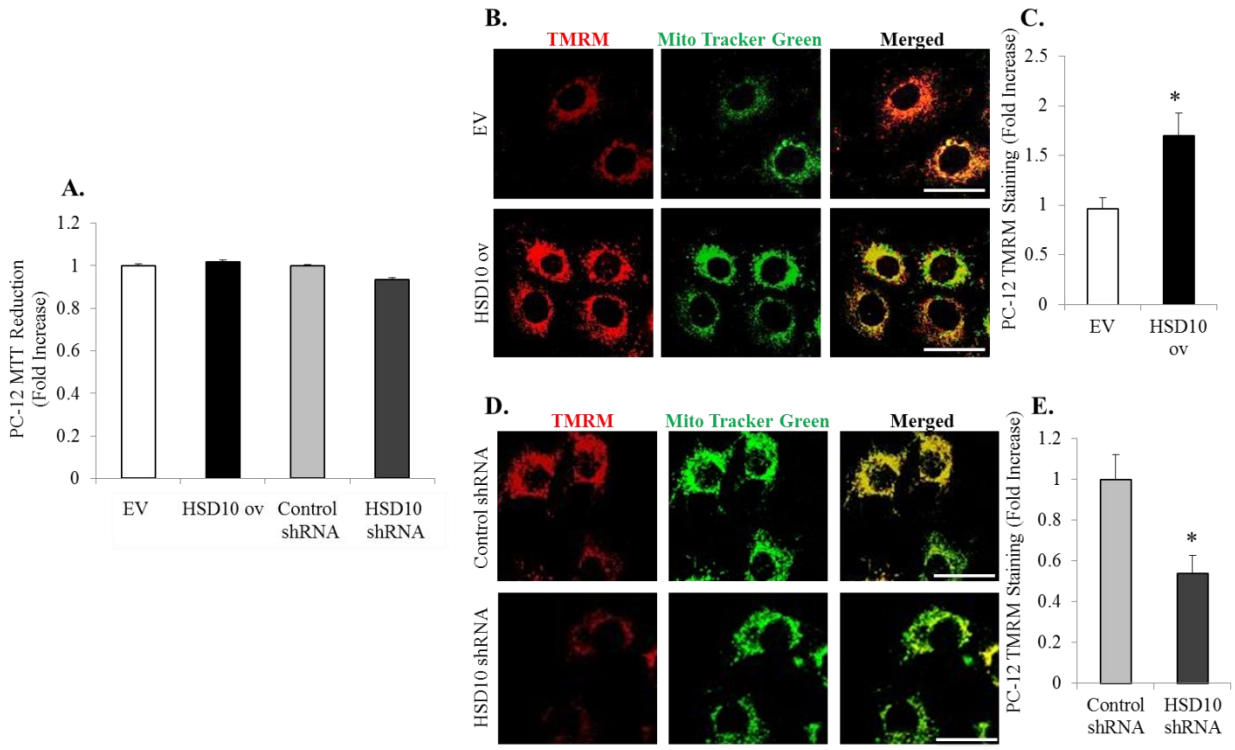

Figure 1-9: Examination of intact mitochondria in PC-12 HSD10-transfected cells. PC-12 transfected cells were cultivated on a 96-well plate for an MTT assay and on chamber slides for observation of mitochondrial membrane potential. Following treatment with MTT dye for 4 hours, cells were assessed for MTT reduction using a multi-plate reader. **A.** Densitometry of MTT reduction displayed as fold increase relative to EV for HSD10 ov, and control shRNA for HSD10 shRNA (n=4). After incubation with TMRM (1:300) and Mito Tracker Green (1:500), cells were imaged live for membrane potential. **B.** Confocal microscopy was used to observe immunofluorescence staining of mitochondrial membrane potential with TMRM alone (red), Mito Tracker Green alone (green), and their co-localization (yellow) in EV and HSD10 ov cells (scale bar: 30 μm). **C.** Quantification of TMRM immunofluorescence staining (depicted in **B**) displayed as fold increase of intensity of fluorescence relative to EV (n=4). **D.** Immunofluorescence staining of TMRM alone (red), Mito Tracker Green alone (green), and merged (yellow) in control shRNA and HSD10 shRNA cells (scale bar: 30 μm). **E.** Quantification of TMRM immunofluorescence staining (depicted in **D**) displayed as fold increase of fluorescence intensity relative to control shRNA (n=4). Data presented as mean ± SE. *P<0.05 versus control group. Adapted from Carlson, E.A. et al. (2015) *BMC Cancer* (152).

1.6. Influence on Altered Pheochromocytoma Cell Resistance

It is a well-known, discouraging fact that many cancers can become resistant to anticancer therapies over time. As this is a major problem for patients, the effect of HSD10 overexpression on cancer cell resistance to oxidative stress was assessed using the PC-12 cells overexpressing HSD10. The cells were treated with various concentrations of H_2O_2 and TBH for 24 hours to stimulate oxidative stress conditions, as cancer cells are typically exposed to higher oxidative stress levels (45). While cell viability steadily decreased for both groups as the chemical dosage increased, HSD10 ov cells demonstrated significantly higher reduction of MTT at 0.75 and 1 mM concentrations of H_2O_2 compared to EV cells (**Fig. 1-10 A**). Treatment of the cells with TBH showed similar results, with HSD10 ov cells reducing considerably more MTT compared to EV cells at the lowest dosage of TBH used (0.1 mM, **Fig. 1-10 B**). Thus, while these two oxidative stressors reduce cell viability in both EV and HSD10 ov cells, PC-12 cells with HSD10 overexpression exhibited more resistance to chemical-induced oxidative stress.

This observed cellular resistance was further examined using complex IV enzyme activity. PC-12 cells were treated with 0.75 mM of H_2O_2 as the amount of MTT reduced by EV cells remained at a higher level compared to the amount seen at 1 mM H_2O_2 (**Fig. 1-10 A**) and the lowest dose of TBH given (**Fig. 1-10 B**). As a starting point, complex IV activity was assessed in cells treated with 0.75 mM of H_2O_2 for 24 hours. However, H_2O_2 treatment showed no difference in enzyme activity between the two PC-12 groups (**Fig. 1-10 C**). Rationalizing that any changes in enzymatic activity would likely be more visible earlier in the chemical treatment, the activity of complex IV was assessed at several time points during the 24 hour period. As speculated, complex IV enzyme activity was significantly increased in HSD10 ov cells compared to EV cells after just one hour of H_2O_2 treatment (**Fig. 1-10 D**). Indeed, this difference in activity

occurred earlier into the treatment period as the difference between HSD10 ov and EV cells at 16 hours of H_2O_2 treatment returned to similar levels (**Fig. 1-10 D**). This data implies that HSD10 overexpression aids cell survival under oxidative stress settings, conceivably by elevating and/or maintaining mitochondrial bioenergetics, such as ETC activity and ATP generation, during this death-inducing condition.

Additionally, complex IV enzyme activity was used to assess cellular resistance in the PC-12 HSD10 knockdown cells treated with 0.75 mM H_2O_2 for the same time points over 24 hours. Interestingly, complex IV enzyme activity was significantly decreased in HSD10 shRNA cells in comparison to control shRNA cells after just one hour of H_2O_2 treatment (**Fig. 1-10 E**). The significant difference observed between HSD10 shRNA and control shRNA cells was sustained for all other time points during the 24 hour treatment period (**Fig. 1-10 E**), indicating that HSD10 knockdown renders cells less functional under both basal and oxidative stress conditions.

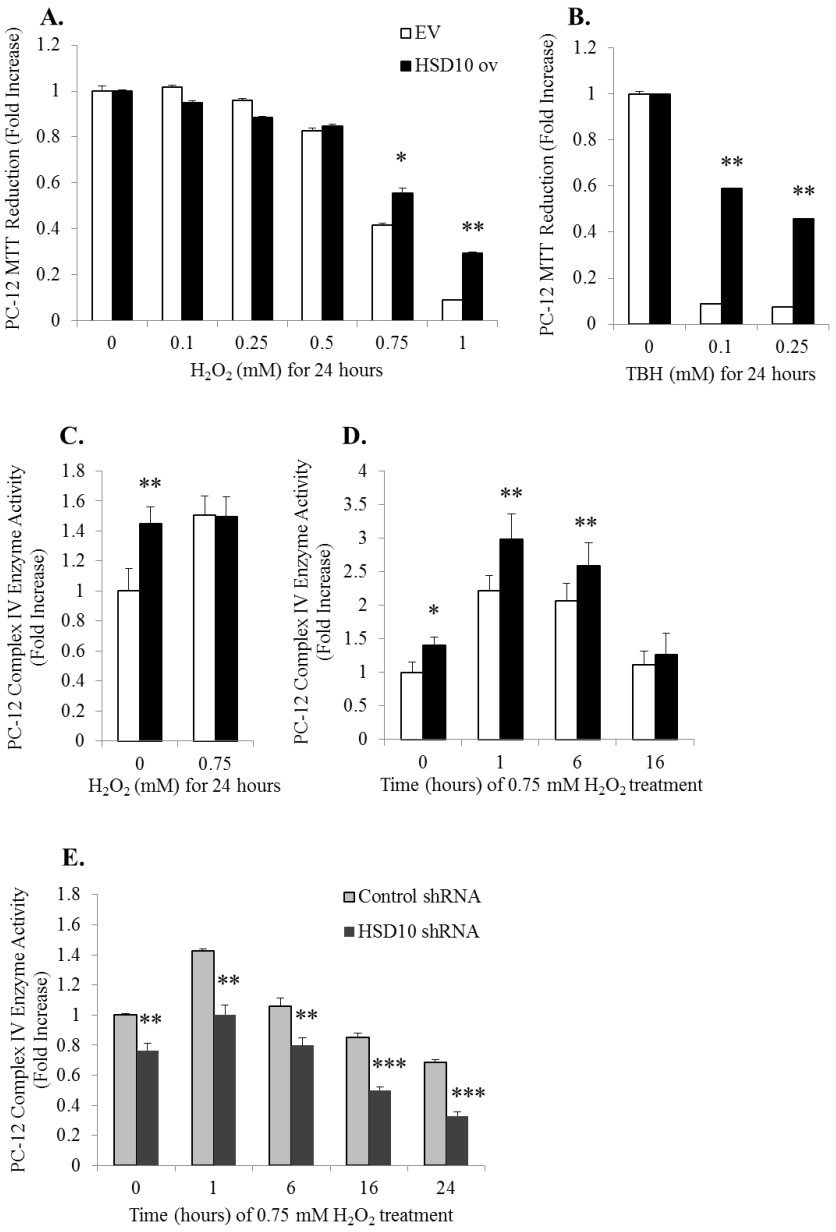

Figure 1-10: Effect of HSD10-modification on PC-12 cellular resistance to oxidative stress. **A-B.** Densitometry of MTT reduction in PC-12 transfected EV and HSD10 ov cells treated with **A)** 0, 0.1, 0.25, 0.5, 0.75, and 1 mM H_2O_2 (n=3 for all groups), and **B)** 0, 0.1, and 0.25 mM TBH for 24 hours (n=3 for all groups), displayed as fold increase relative to EV and HSD10 ov at the 0 mM time point. **C-D.** ETC complex IV enzyme activity was assessed in EV and HSD10 ov cells treated with 0.75 mM H_2O_2 for **C)** 24 hours (n=3), and **D)** 0, 1, 6, and 16 hours (n=6 for all time points), displayed as fold increase relative to EV at the 0 mM time point. **E.** ETC complex IV enzyme activity was assessed in control shRNA and HSD10 shRNA cells treated with 0.75 mM H_2O_2 for 0, 1, 6, 16, and 24 hours (n=4 for all time points), displayed as fold increase relative to control shRNA at the 0 mM time point. Data presented as mean ± SE. *P<0.05, **P<0.01, ***P<0.001 versus control groups. Adapted from Carlson, E.A. et al. (2015) *BMC Cancer* (152).

To provide further evidence for this concept, TUNEL staining was performed in the PC-12 HSD10 modified cell lines after treatment with 0 mM or 0.75 mM H_2O_2 for 24 hours (**Fig. 1-11 A** and **C**). As expected, both EV and HSD10 ov cells treated with H_2O_2 exhibited higher percentages of cells undergoing apoptosis (**Fig. 1-11 B, *p-values**), compared with the untreated matched control groups. However, the HSD10 ov treatment group had significantly less TUNEL staining compared to the EV treatment group (**Fig. 1-11 B, #p-value**), indicating that cells overexpressing HSD10 are more protected from stress-induced apoptosis induction.

Similarly, control shRNA and HSD10 shRNA cells treated with H_2O_2 displayed greater TUNEL staining (**Fig. 1-11 D, *p-values**), compared to the untreated matched control groups. Interestingly, untreated HSD10 shRNA cells showed higher percentages of cells undergoing apoptosis in comparison with untreated control shRNA cells (**Fig. 1-11 D, &p-values**). This implies that knockdown of HSD10 renders cells more vulnerable to apoptosis, even under normal conditions. Furthermore, the HSD10 shRNA treatment group had significantly more TUNEL staining compared to the control shRNA treatment group (**Fig. 1-11 D, ^p-values**), which suggests that cells lacking HSD10 are more susceptible to stress-induced apoptosis induction.

The data presented here support the concept that HSD10 overexpression increases pheochromocytoma cell resistance to cell death induced by oxidative stress, and that HSD10 knockdown renders the cells more susceptible to apoptosis induction. Together, this suggests that HSD10 may play a role in other cancer cell resistance.

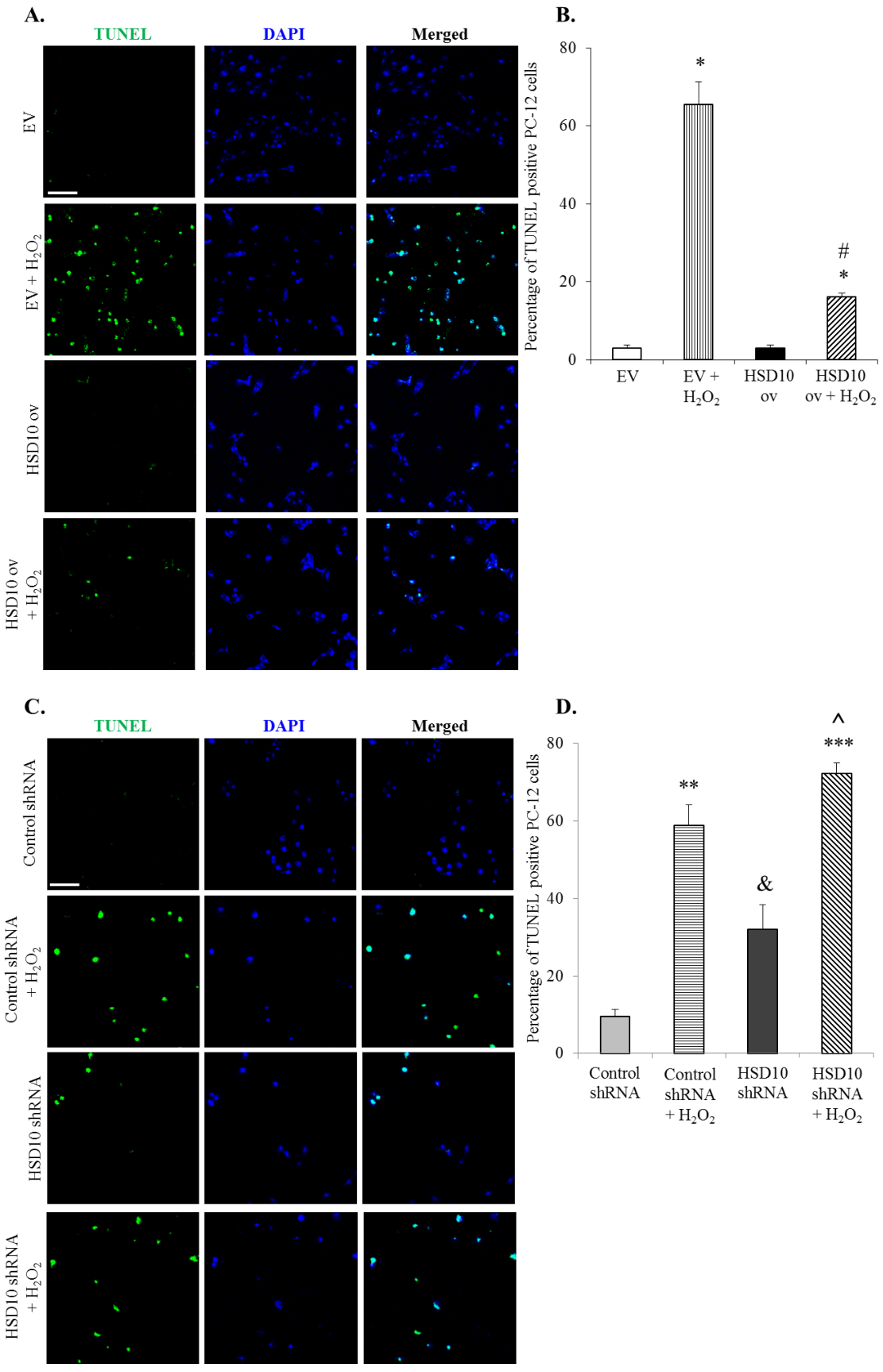
A.
TUNEL
DAPI
Merged
EV
EV + H2O2
HSD10 ov
HSD10 ov + H2O2
B.
Percentage of TUNEL positive PC-12 cells
80
60
40
20
0
*
#
*
EV
EV + H2O2
HSD10 ov
HSD10 ov + H2O2
C.
TUNEL
DAPI
Merged
Control shRNA
Control shRNA + H2O2
HSD10 shRNA
HSD10 shRNA + H2O2
D.
Percentage of TUNEL positive PC-12 cells
80
60
40
20
0
**
&
^
***
Control shRNA
Control shRNA + H2O2
HSD10 shRNA
HSD10 shRNA + H2O2

Figure 1-11: Assessment oxidative stress-induced cell death in PC-12 HSD10-transfected cells. A. Confocal microscopy demonstrating TUNEL staining of cells undergoing apoptosis (green), nuclear staining with DAPI (blue), and these two antigens co-localized (merged) in PC-12 transfected EV and HSD10 ov cells (**A**), control shRNA and HSD10 shRNA cells (**C**) treated with 0 mM and 0.75 mM H_2O_2 for 24 hours. Scale bar in **A** and **C**: 30 μm. **B.** Quantification of EV and HSD10 ov cell TUNEL staining (depicted in **A**) displayed as the percentage of TUNEL positive cells (n=4). **D.** Quantification of control shRNA and HSD10 shRNA cell TUNEL staining (depicted in **C**) displayed as the percentage of TUNEL positive cells (n=10). Data presented as mean ± SE. *P<0.01 versus EV and HSD10 ov non-treatment groups; **P<0.001 versus control shRNA non-treatment group; ***P<0.0001 versus HSD10 shRNA non-treatment group; #P<0.01 versus EV treatment group; &P<0.01 versus control shRNA non-treatment group; ^P<0.05 versus control shRNA treatment group. Adapted from Carlson, E.A. et al. (2015) *BMC Cancer* (152).

1.7. Interaction between HSD10 and CypD in Altered Pheochromocytoma Cells

Next, the mechanism behind the ability of HSD10 to regulate cancer cell growth and cell death resistance associated with mitochondrial function was examined. As the hypothesis of this dissertation is that HSD10 aids in cancer cell resistance by preventing MPTP-induced cell death via enhanced binding to CypD, the relationship between HSD10 and CypD was studied in the PC-12 overexpression cell lines.

Immunoblot analysis revealed that despite the large increase in HSD10 protein (**Fig. 1-12 A**), CypD protein expression remained similar between HSD10 ov cells and EV cells (**Fig. 1-12 B**); this is consistent with other studies of CypD in cancer (83). Interestingly, the decrease in HSD10 protein in HSD10 shRNA cells (**Fig. 1-12 C**) was paired with a reduction in CypD protein expression compared with control shRNA cells (**Fig. 1-12 D**), although CypD protein was still more prevalent than HSD10 protein in the HSD10 shRNA cells. This data indicates that while CypD expression remains level during HSD10 overexpression, it is negatively impacted by HSD10 reduction. This suggests that, due to the reductions in both HSD10 and CypD, cancer cells become more susceptible to cell death induction.

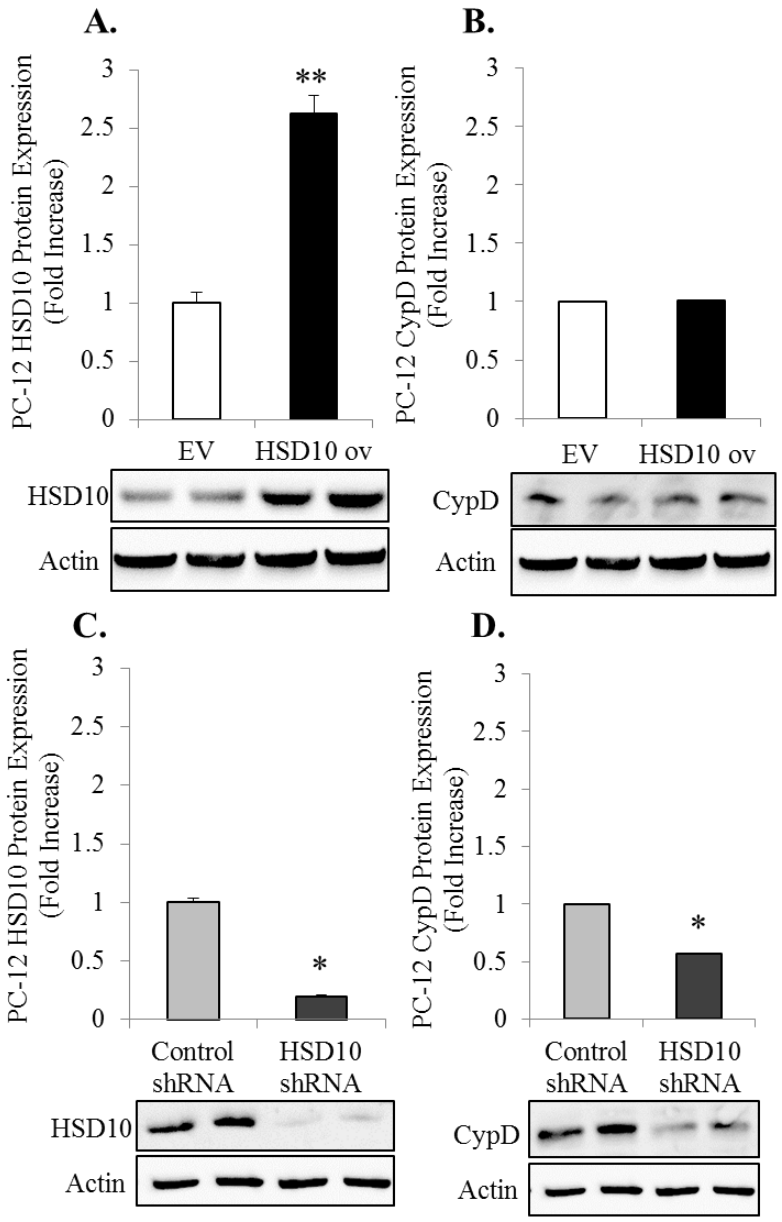

Figure 1-12: HSD10 and CypD abundance in PC-12 HSD10-transfected cells. PC-12 transfected cells were harvested for detection of protein expression using rabbit anti-HSD10 antibody (1:3000) and mouse anti-CypD antibody (1:8000) via immunoblotting. Actin (mouse anti-Actin antibody, 1:8000) was used as the loading control, and HSD10 and CypD expression were normalized to actin. **A-B.** EV and HSD10 ov whole cell lysates were analyzed for HSD10 (**A**) and CypD (**B**) protein expression (n=4). **C-D.** Control shRNA and HSD10 shRNA whole cell lysates were analyzed for HSD10 (**C**) and CypD (**D**) protein expression (n=4). Results are displayed as fold increase relative to EV for HSD10 ov, and control shRNA for HSD10 shRNA. Data presented as mean ± SE. *P<0.05, **P<0.01 versus EV and control shRNA groups. Adapted from Carlson, E.A. et al. (2015) *BMC Cancer* (152).

Furthermore, the co-localization of HSD10 and CypD within mitochondria was confirmed via co-immunofluorescence in the PC-12 overexpression cell lines (**Fig. 1-13 A**). The expression pattern of CypD did not change between EV and HSD10 ov cells (**Fig. 1-13 E**), which coincides with the CypD protein expression data shown in **Figure 1-12 B**. As expected, HSD10 levels were increased in HSD10 ov cells compared to EV cells (**Fig. 1-13 D**), consistent with the results in **Figures 1-1 A** and **1-2 B**.

Co-staining of HSD10 and CypD with the mitochondrial markers SODII and Hsp60, respectively, verified mitochondrial localization of the proteins (**Fig. 1-13 B-C**). Although CypD expression remained constant between EV and HSD10 ov cells, the increased expression of HSD10 in HSD10 ov cells appears to correspond with enhanced co-localization of HSD10 and CypD as shown in the merged images of **Figure 1-13 A**. This co-localization positions both proteins in close proximity, thus increasing the chance of binding capacity.

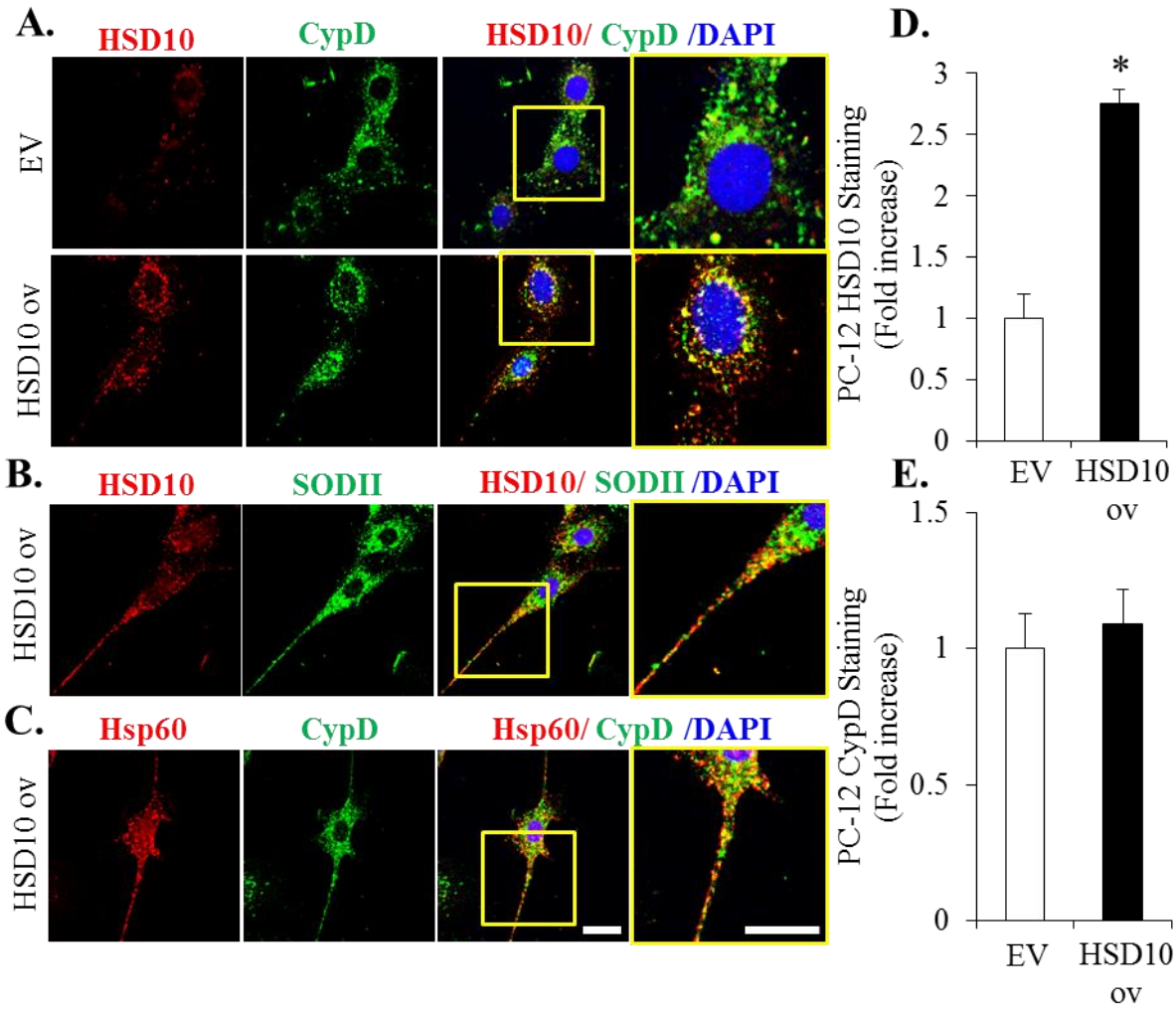

Figure 1-13: Localization of CypD in PC-12 HSD10-overexpression cells. PC-12 transfected cells were cultivated on chamber slides and proteins were detected using mouse anti-HSD10 (1:100) and rabbit anti-CypD (1:200), mouse anti-HSD10 (1:100) and rabbit anti-SODII (1:1000), or mouse anti-Hsp60 (1:1000) and rabbit anti-CypD (1:200). After incubation with anti-mouse Alexa Fluor 594 (1:2000) and anti-rabbit Alexa Fluor 488 (1:2000), cells were mounted in fluorescence mounting media. Confocal microscopy was used to visualize immuno-fluorescence staining of **A.** HSD10 alone (red), CypD alone (green), and these two antigens co-localized (yellow) with DAPI nuclear staining (blue) in EV and HSD10 ov PC-12 cells (scale bar: 20 μm). **B.** Immunofluorescence staining of HSD10 alone (red), mitochondrial marker SODII alone (green), and these two antigens co-localized (yellow) with DAPI (blue) in HSD10 ov PC-12 cells (scale bar: 20 μm). **C.** Immunofluorescence staining of CypD alone (green), mitochondrial marker Hsp60 alone (red), and these two antigens co-localized (yellow) with DAPI (blue) in HSD10 ov PC-12 cells (scale bar: 20 μm). **D-E.** Quantification of HSD10 and CypD fluorescence densities (depicted in **A**) displayed as fold increase relative to EV (n=4). Data presented as mean ± SE. *****P<0.01 versus control group. Adapted from Carlson, E.A. et al. (2015) *BMC Cancer* (152).

After confirming co-localization of the proteins, a Co-IP assay was performed to investigate HSD10-CypD interactions in the PC-12 overexpression cell lines. As shown in **Figure 1-14**, there was an enhanced interaction between HSD10 and CypD in HSD10 ov cells compared to EV cells, which was confirmed using both proteins as pull-down antibodies. This indicates that increased levels of HSD10 promote the formation of HSD10-CypD complexes.

Taken together, the results imply that an increased abundance of HSD10 in the vicinity of CypD leads to HSD10-CypD complex formation in PC-12 cells, conceivably preventing cell death induction. These findings further solidify the concept that HSD10 is important in promoting cancer growth and maintenance.

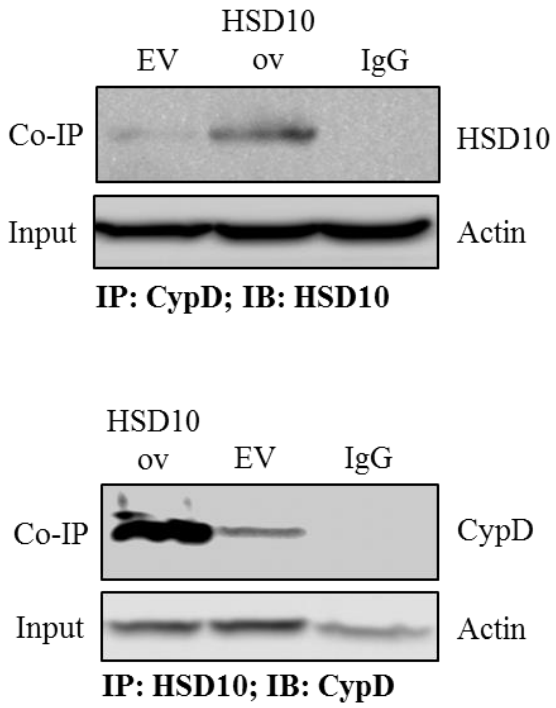

Figure 1-14: Enhanced interaction between HSD10 and CypD in PC-12 HSD10-overexpression cells. EV and HSD10 ov whole cell lysates were subjected to Co-IP with pull-down antibodies (3 µl rabbit anti-HSD10, 2 µl mouse anti-CypD, 3 µl rabbit IgG or 3 µl mouse serum). Immunoblotting was used to reveal the immunoprecipitated proteins with mouse anti-CypD (1:8000), rabbit anti-HSD10 (1:3000), and mouse anti-Actin (1:8000) as the loading control for the input. Adapted from Carlson, E.A. et al. (2015) *BMC Cancer* (152).

1.8. Impact of CypD-knockdown on Altered Pheochromocytoma Cells

After observing co-localization and enhanced binding between HSD10 and CypD in the PC-12 overexpression cells, the possible link was further studied via transient transfection with a siRNA oligonucleotide (**Table 7**) to knockdown CypD in the PC-12 HSD10 ov cells.

Immunoblot analysis showed a 45% reduction in CypD protein expression in the HSD10 ov-CypD siRNA cells compared to the HSD10 ov-control siRNA cells (**Fig. 1-15 A**). Also, the HSD10 ov-CypD siRNA cells exhibited a decrease in HSD10 protein (**Fig. 1-15 B**). This data, taken together with **Figure 1-12 C** and **D**, shows that upon HSD10-knockdown, CypD protein is reduced and that after CypD-knockdown, HSD10 protein is decreased. This provides further evidence that HSD10 and CypD are connected in cancer cells.

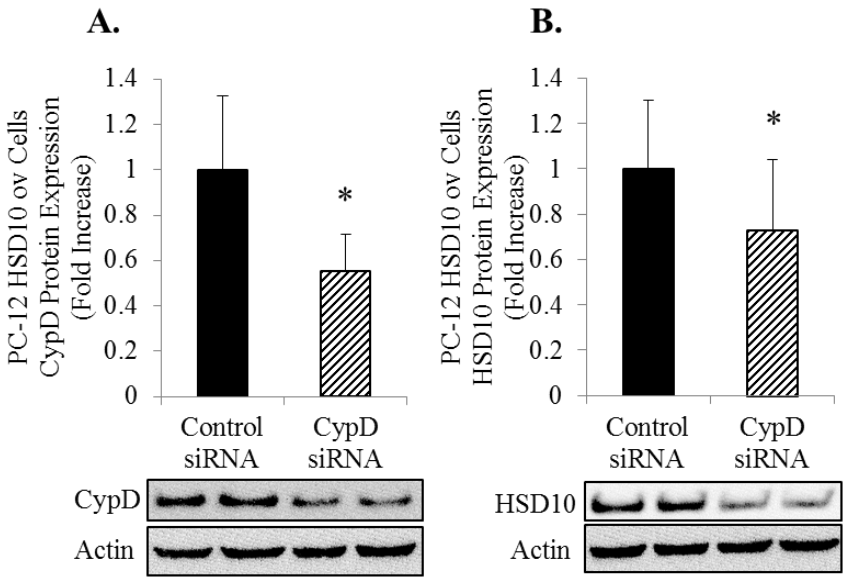

Figure 1-15: CypD-knockdown in PC-12 HSD10 ov cells. After transient transfection, PC-12 HSD10 ov cells were harvested for detection of protein expression using mouse anti-CypD antibody (1:6000) and rabbit anti-HSD10 antibody (1:2000) via immunoblotting. Actin (mouse anti-Actin antibody, 1:8000) was used as the loading control, and CypD and HSD10 expression were normalized to actin. **A-B.** Whole cell lysates were analyzed for CypD (**A**) and HSD10 (**B**) protein expression (n=4). Results are displayed as fold increase relative to control siRNA. Data presented as mean ± SE. *P<0.05 versus control siRNA group.

The effect of CypD knockdown on PC-12 HSD10 ov cell growth was examined using *in vitro* cell culture. Following transient transfection with CypD siRNA (**Table 7**), PC-12 HSD10 ov cells were plated in dishes at a constant density and grown over the course of seven days, with a dish counted each day. As demonstrated in **Figure 1-16**, both transfected cell groups grew at a similar rate during the first three days. By the fourth day, the CypD siRNA group had slightly fewer total cells compared to the control siRNA group.

The remainder of the days exhibited a trend toward reduced growth rate in the CypD siRNA cells in comparison to the control siRNA cells (**Fig. 1-16**). However, this decrease did not reach statistical significance, likely due to the extreme proliferative capabilities of the PC-12 HSD10 ov cells promoted by HSD10 itself. Thus, it would be beneficial to investigate the effect of CypD knockdown in PC-12 EV cells. Nevertheless, the trend toward decreased cell growth rate in the CypD siRNA cells suggests that HSD10 and CypD are associated in cancer.

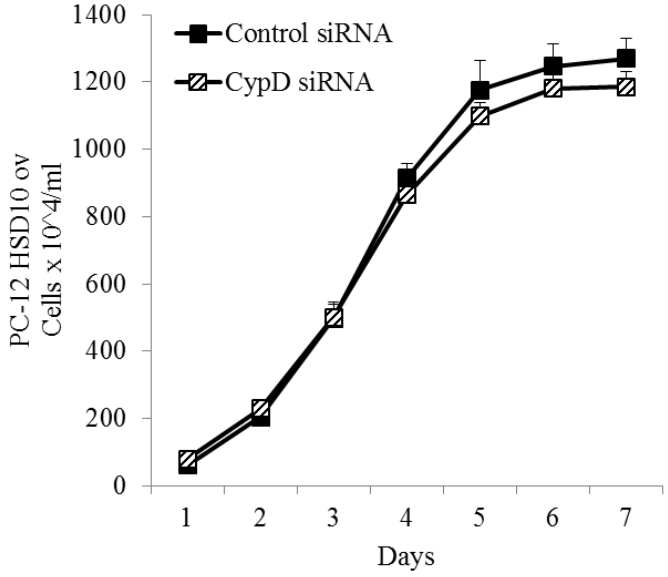

Figure 1-16: Effect of CypD-knockdown on *in vitro* PC-12 HSD10 ov cell growth. PC-12 HSD10 ov cells were plated at a constant density and transiently transfected using siRNA. Next, cells were counted over 7 days to determine cell growth rate. Growth curve of control siRNA (black ■) and CypD siRNA (black striped ■) cells displayed as cells x 10^4 per ml (n=4). Data presented as mean ± SE.

Next, the enzyme activity of ETC complex IV was tested to investigate whether CypD knockdown impacts mitochondrial respiration in PC-12 HSD10 ov cells. Complex IV enzyme activity was unchanged between the control siRNA and CypD siRNA groups (**Fig. 1-17 A**), suggesting that knockdown of CypD does not influence ETC functionality in the highly productive PC-12 HSD10 ov cells.

To confirm that CypD knockdown does not change the ETC system in PC-12 HSD10 ov cells, ATP content was assessed. In addition to the complex IV data, the level of ATP was unaltered in CypD siRNA cells compared to control siRNA cells (**Fig. 1-17 B**).

Together, the data implies that CypD knockdown does not affect PC-12 HSD10 ov cell respiration. This is not overly surprising, as CypD mainly functions as cell death inducer and may not be involved in energy metabolism. Thus, loss of CypD would not directly impact mitochondrial bioenergetics, especially in cells with an overabundance of HSD10, an enzyme which can influence many mitochondrial processes including metabolism.

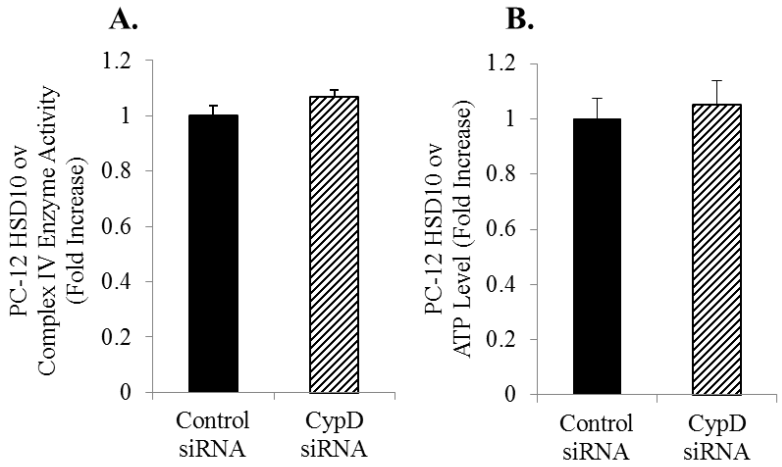

Figure 1-17: Consequence of CypD-knockdown on ETC complex IV enzyme activity and ATP level in PC-12 HSD10 ov cells. Following transient transfection, PC-12 HSD10 ov cells were harvested and tested for ETC complex IV enzyme activity (**A**) and cellular ATP content (**B**). Results are displayed as fold increase relative to control siRNA (n=4 for each assay). Data presented as mean ± SE.

As CypD is mainly involved in cell death induction, TUNEL staining was performed in the siRNA-transfected PC-12 HSD10 ov cells after treatment with 0 mM or 0.75 mM H_2O_2 for 24 hours (**Fig. 1-18 A**). As anticipated, both control siRNA and CypD siRNA cells treated with H_2O_2 displayed higher percentages of cells undergoing apoptosis (**Fig. 1-18 B, *p-values**), compared to the untreated matched control groups. A small trend toward greater cell death induction was observed in the CypD siRNA untreated group in comparison with the control siRNA group, although there was no statistical significance, providing a possible explanation for the small trend of decreased growth rate observed in the CypD siRNA group. Intriguingly, the CypD siRNA treatment group had significantly more TUNEL staining compared to the control siRNA treatment group (**Fig. 1-18 B, #p-value**), demonstrating that PC-12 HSD10 ov cells with less CypD are more susceptible to stress-induced apoptosis induction.

CypD has been observed to be overexpressed in many cancers (83), which often provides cancer cells protection against cell death due to its peptidyl prolyl isomerization activity (160). Similar to the data presented in **Figure 1-18**, Machida and associates previously showed that CypD-deficiency sensitized rat glioma cells to apoptosis (59). This implies that reducing the high amounts of endogenous CypD in certain cancer cells leads to induction of cell death.

Additionally, it is thought that interactions between CypD and specific mitochondrial proteins may be responsible for the anti-apoptotic phenomenon seen in cancers overexpressing CypD. For instance, binding of CypD to Bcl-2 (58) or HK-II (59) has been observed to suppress apoptotic cell death in cancer cells. Thus, **Figure 1-18** provides further support of this concept and identifies HSD10 as another binding partner for the anti-apoptotic effect of CypD in cancer.

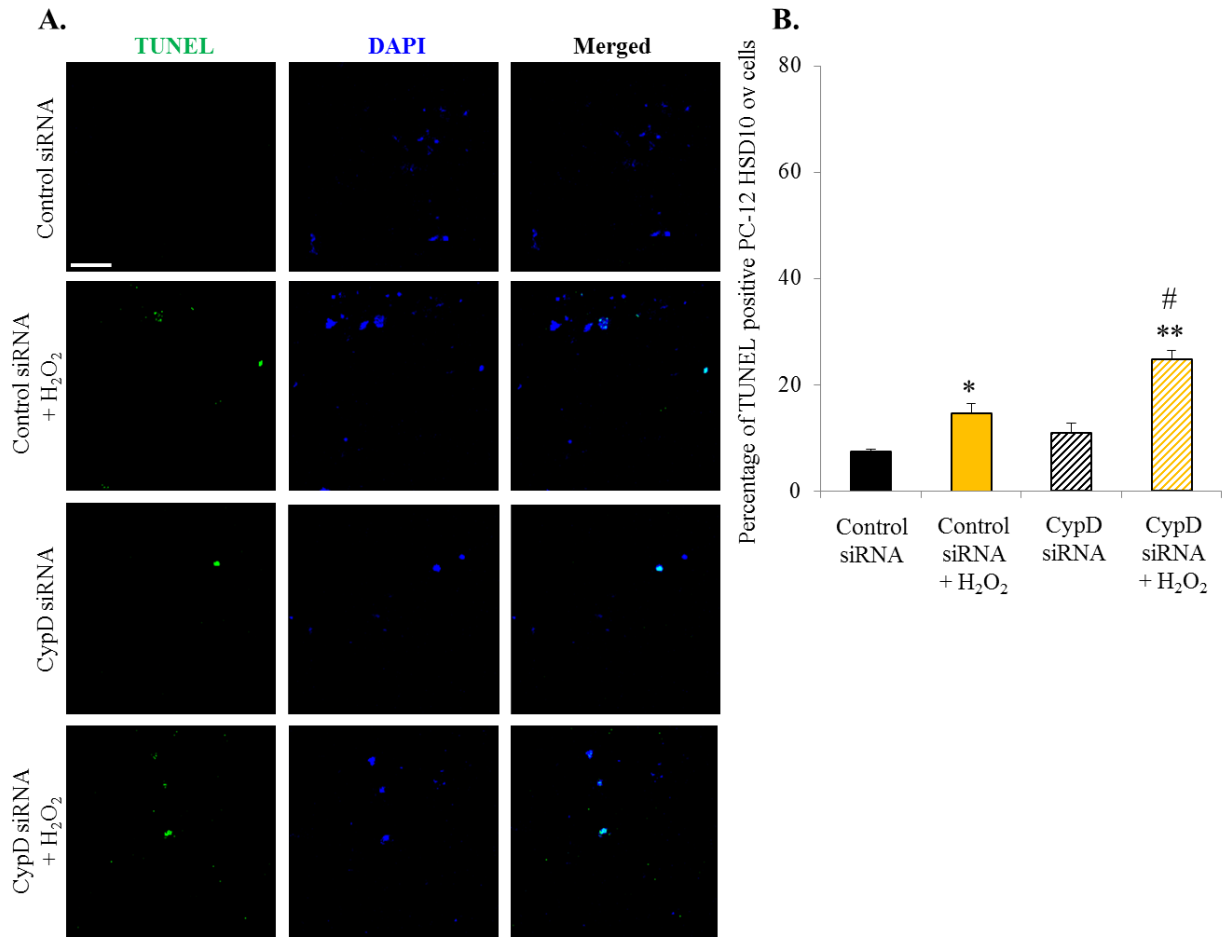

Figure 1-18: Effect of CypD-knockdown on oxidative stress-induced cell death in PC-12 HSD10 ov cells. After transient transfection, cell death induction was assessed in PC-12 HSD10 ov cells. **A.** Confocal microscopy demonstrating TUNEL staining of cells undergoing apoptosis (green), nuclear staining with DAPI (blue), and these two antigens co-localized (merged) in control siRNA and CypD siRNA cells treated with 0 mM and 0.75 mM H_2O_2 for 24 hours. Scale bar in **A**: 30 µm. **B.** Quantification of control siRNA and CypD siRNA cell TUNEL staining (depicted in **A**) displayed as the percentage of TUNEL positive cells (n=10). Data presented as mean ± SE. *P<0.01, **P<0.001 versus control siRNA and CypD siRNA non-treatment groups; #P<0.01 versus control siRNA treatment group.

1.9. Interim Conclusion

Chapter 1 examined the effect of HSD10 modification in rat pheochromocytoma cells to assess the importance of HSD10 in cancer (**Fig. 1-19**). Overexpression of HSD10 in PC-12 cells was associated with increased energy production, enhanced cell growth rate, and protection against stress-induced cell death induction. This was likely due to the enhanced complex formations between HSD10 and CypD.

Knockdown of HSD10 in PC-12 cells correlated with reduced energy production, decreased cell growth rate, and diminished resistance against stress-induced cell death, possibly caused by the lost interaction of HSD10 with CypD. Furthermore, knockdown of CypD in PC-12 HSD10 ov cells was accompanied by increased susceptibility of cells to stress-induced cell death induction; however, no changes were observed in energy production.

Taken altogether, these results suggest that HSD10 plays an important role in cancer cell growth and energy metabolism. Moreover, the data indicates that HSD10 and CypD together are involved in cancer cell resistance to cell death. Additional studies are needed to further examine the role of the interaction of HSD10 with CypD in relation to cancer cell death.

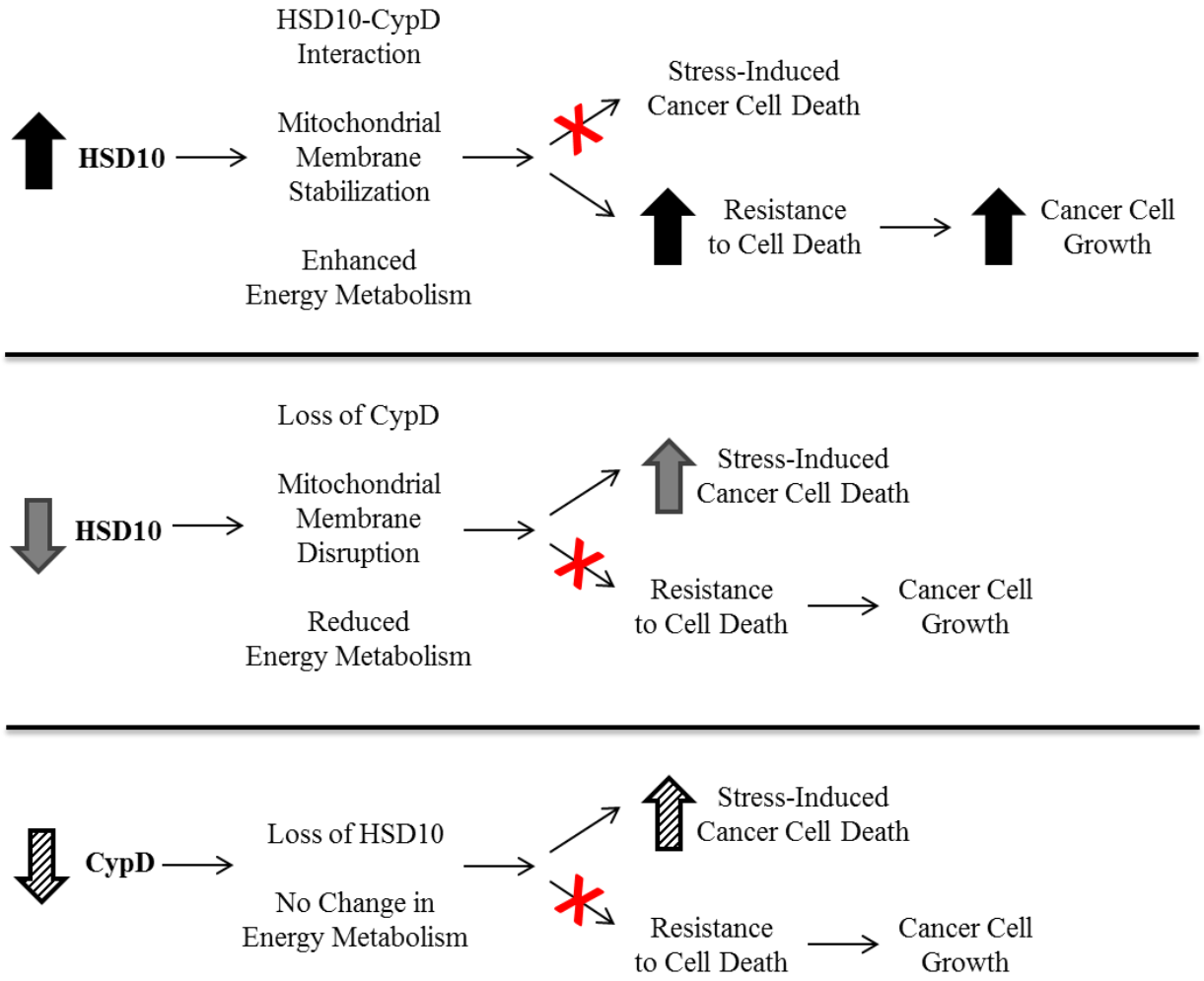

Figure 1-19: Chapter 1 summary of the effect of HSD10 on PC-12 cancer cell progression. Black arrows: increased HSD10 in PC-12 cells correlates with increased HSD10-CypD complex formation, enhanced mitochondrial membrane stabilization, and heightened energy production; this leads to cancer cell survival through enhanced cellular resistance to cell death, resulting in increased cancer cell growth. Gray arrows: decreased HSD10 in PC-12 cells is associated with mitochondrial membrane disruption, reduced energy production, and decreased CypD protein; this results in reduced cancer cell survival due to stress-induced cell death. Black-striped arrows: decreased CypD in PC-12 HSD10 ov cells is accompanied by reduced HSD10 protein, but no change in energy production; this sensitizes cancer cells to stress-induced cell death.

RESULTS

Chapter 2: Influence of HSD10 on Altered Breast Cancer Cells

Although early detection and improved treatments have increased patient survival rates (161), breast cancer remains the second leading cause of cancer-related deaths among women (162). This is largely due to rapid replication of tumor cells and enhanced resistance to available breast cancer therapies. After initially determining that HSD10 may promote tumor growth in pheochromocytoma cells, the role of HSD10 in cancer was further investigated in relation to human breast cancer. Using similar techniques from **Chapter 1**, breast cancer cell growth rate was observed in wild type cells to determine growth patterns and correlations in regard to HSD10 endogenous expression.

The MCF7, MCF10A, MDA-MB-231, and T47D breast cancer cell lines were used for the HSD10 transfection studies detailed in **Section 2.3.** and onward in this chapter. As in **Chapter 1**, breast cancer cell growth rate was observed in HSD10-transfected cell lines to determine if HSD10 influences breast tumor cell proliferation in cell culture. Once it was observed that HSD10 alteration correlates with differing growth patterns in breast cancer cells, mitochondrial processes were examined to explore the impact of HSD10 on intracellular function. The goal of this chapter was to establish working models of human breast cancer cell lines with altered HSD10.

2.1. HSD10 Content in Wild-Type Breast Cancer Cell Lines

To investigate the role of HSD10 in breast cancer cells, the relative amount of HSD10 was measured in a panel of wild-type human breast cancer cell lines (**Fig. 2-1**). Upon comparison of the relative expression levels of HSD10 total RNA in the panel of human breast cancer cell lines, the MCF10A, MCF7, and MDA-MB-231 cell lines were chosen for HSD10 overexpression as they all exhibited low to median levels of HSD10 (**Fig. 2-1, Lane 2 green bar, Lane 4 red bar, and Lane 9 purple bar**). Additionally, MCF10A cells are described as non-tumorigenic breast cells compared to other breast cancer cell lines; thus these cells were used to investigate whether HSD10 is a tumor-initiating factor. Furthermore, T47D cells were selected for HSD10 knockdown since this line had considerably high levels of HSD10 relative to the other cell lines (**Fig. 2-1, Lane 17 blue bar**).

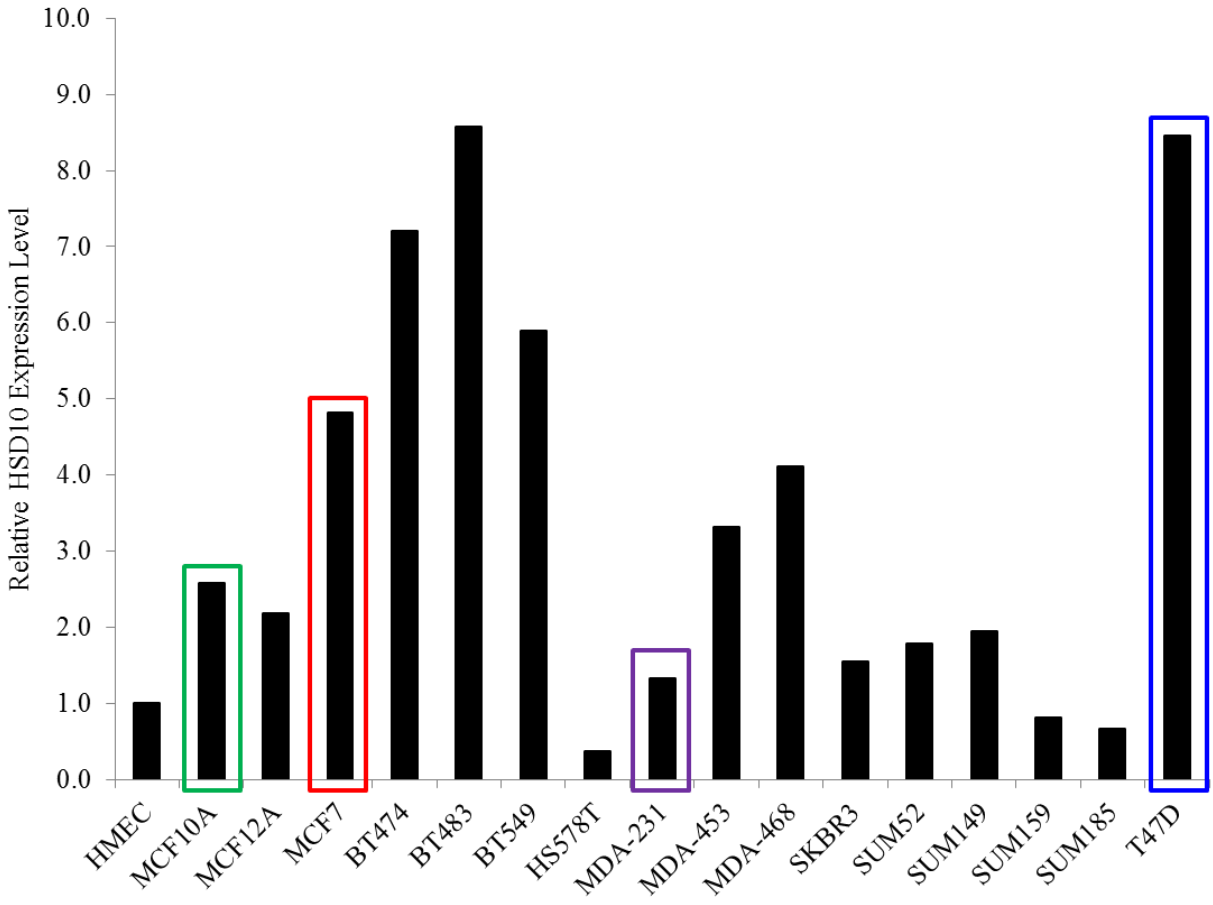

Figure 2-1: Abundance of HSD10 in a panel of breast cancer cell lines. Total RNA isolated from multiple human breast cancer cell lines was transcribed into cDNA and subjected to qRT-PCR with primers for human HSD10. qRT-PCR was normalized against GAPDH and relative HSD10 expression levels were calculated using a standard curve. Lanes: 1) HMEC, 2) MCF10A, 3) MCF12A, 4) MCF7, 5) BT474, 6) BT483, 7) BT549, 8) HS578T, 9) MDA-MB-231, 10) MDA-MB-453, 11) MDA-MB-468, 12) SKBR3, 13) SUM52, 14) SUM149, 15) SUM159, 16) SUM185, 17) T47D.

These four human breast cancer cell lines were used for further studies, in addition to rat pheochromocytoma cells (**Table 10**). Immunoblot analysis of the selected cell lines further demonstrated HSD10 protein expression patterns, which were similar to that of the total RNA content depicted in the breast cancer panel for T47D, MCF7, MCF10A, and MDA-MB-231 cells (**Fig. 2-2 A**). CypD protein levels correlated with the expression pattern of HSD10 for the four breast cancer cell lines (**Fig. 2-2 B**).

Before altering HSD10 content in the chosen breast cancer cell lines for the studies detailed in later in this chapter, these wild-type cells were evaluated for natural cell growth rate.

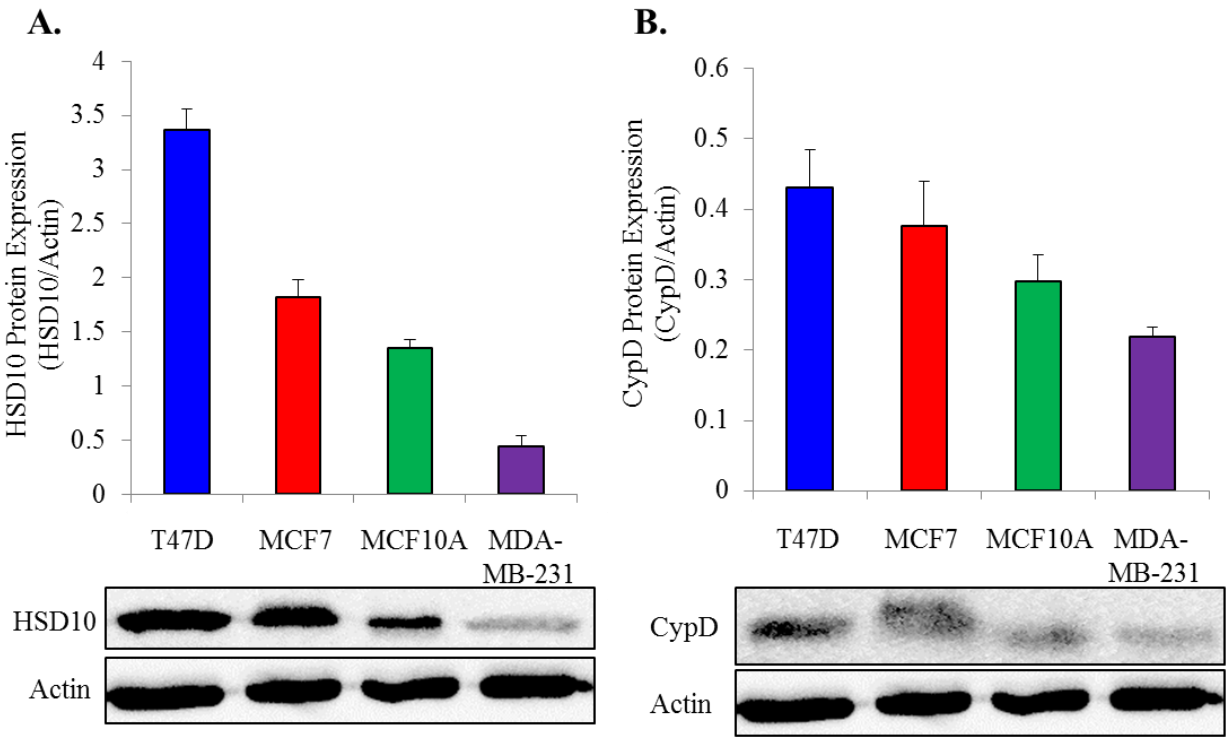

Figure 2-2: HSD10 and CypD protein expression pattern in four breast cancer cell lines. Wild-type T47D, MCF7, MCF10A, and MDA-MB-231 breast cancer cells were harvested for detection of protein expression using rabbit anti-HSD10 antibody (1:1000) and mouse anti-CypD antibody (1:8000) via immunoblotting. Actin (mouse anti-Actin antibody, 1:4000) was used as the loading control with HSD10 and CypD expression both normalized to actin. **A.** Whole cell lysates were analyzed for HSD10 protein expression (n=3 for all groups). **B.** Whole cell lysates were analyzed for CypD protein expression (n=3 for all groups). Data presented as mean ± SE.

2.2. In Vitro *Wild-Type Breast Cancer Cell Growth Curve Analysis*

In order to determine baseline cell growth and observe natural cell behavior for the four breast cancer cell lines, cell growth curves over ten days were performed using wild-type T47D, MCF7, MCF10A, and MDA-MB-231 cells. As depicted in **Figure 2-3**, MCF10A cells initially grew at a faster rate compared to T47D and MCF7 cells. Interestingly, MCF10A cells grow in a monolayer formation; once the dish is covered, the growth of new cells appeared to decline and the current cells sickened and died (**Fig. 2-3, green line**, MCF10A downward curve trend from days 7-10). This growth pattern is consistent with the specific cell type: MCF10A is a non-tumorigenic breast cell line in which the cells form a monolayer and do not form large masses when growth space is limited.

Clumping of cells into large masses is indicative of a tumorigenic cell line, which was exhibited by both T47D and MCF7 cells. These two cell types grew very slowly in clumped groups in the initial days of the growth curve (**Fig. 2-3**, days 1-3). By the fourth day, cell growth had increased and remained fairly constant throughout the rest of the experiment. In the end, the T47D cell line attained the highest number of cells out of the four cell lines (**Fig. 2-3, blue line**, day 10), and the MCF7 cells reached a little over half of the total T47D cell number (**Fig. 2-3, red line**, day 10). Both of these cell lines continued to grow in large clumps across the surface of the dish and did not form a monolayer, indicative of a carcinoma cell line.

The metastatic MDA-MB-231 cell line grew at a rate similar to the T47D and MCF7 cells (**Fig. 2-3, purple line**, days 1-6). Intriguingly, the cells formed a monolayer first and then began clumping as space became limited. Over days seven through ten, the MDA-MB-231 cell number declined, likely due to a lack of growth space following cell clumping.

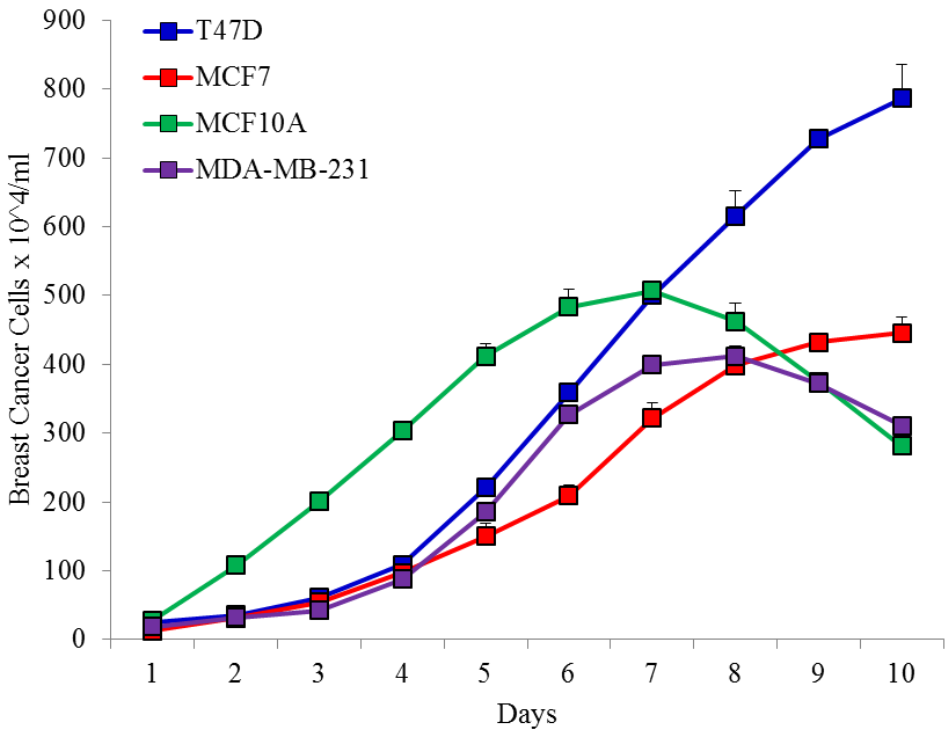

Figure 2-3: Natural cell growth pattern in four breast cancer cell lines. T47D, MCF7, MCF10A, and MDA-MB-231 cells were plated at a constant density and counted over the course of 10 days for determination of wild-type cell growth rate. MCF10A (green ■) cells initially grew at a faster rate compared to the other cell lines, but climaxed around day 7. The T47D (blue ■) and MCF7 (red ■) cell lines grew at a constant rate, although MCF7 cells grew more slowly in comparison to T47D cells. MDA-MB-231 (purple ■) cells grew at a rate similar to the T47D and MCF7 cells, but peaked around day 8. Data presented as mean ± SE.

2.3. Generation of HSD10-transfected Breast Cancer Cell Lines

Succeeding lentiviral transfection, MCF7, MDA-MB-231, and MCF10A cells expressing either an empty CSCW vector or an HSD10 overexpression CSCW vector (**Table 9**) were subjected to immunoblotting for analysis of protein content. HSD10 protein expression was increased by approximately 2-fold in MCF10A HSD10 ov cells (**Fig. 2-4 A**), MDA-MB-231 HSD10 ov cells (**Fig. 2-4 C**), and MCF7 HSD10 ov cells (**Fig. 2-4 D**) in comparison with the respective controls.

Additionally, HSD10 knockdown was performed in T47D cells via lentiviral transfection using a shRNA oligonucleotide (**Table 7**). Immunoblot analysis determined that HSD10 protein expression was significantly reduced by 70% in T47D HSD10 shRNA-transfected cells in comparison with T47D control shRNA-transfected cells (**Fig. 2-4 B**). These experiments verify that HSD10 overexpression in MCF7, MDA-MB-231, and MCF10A cells and HSD10 knockdown in T47D cells was successful.

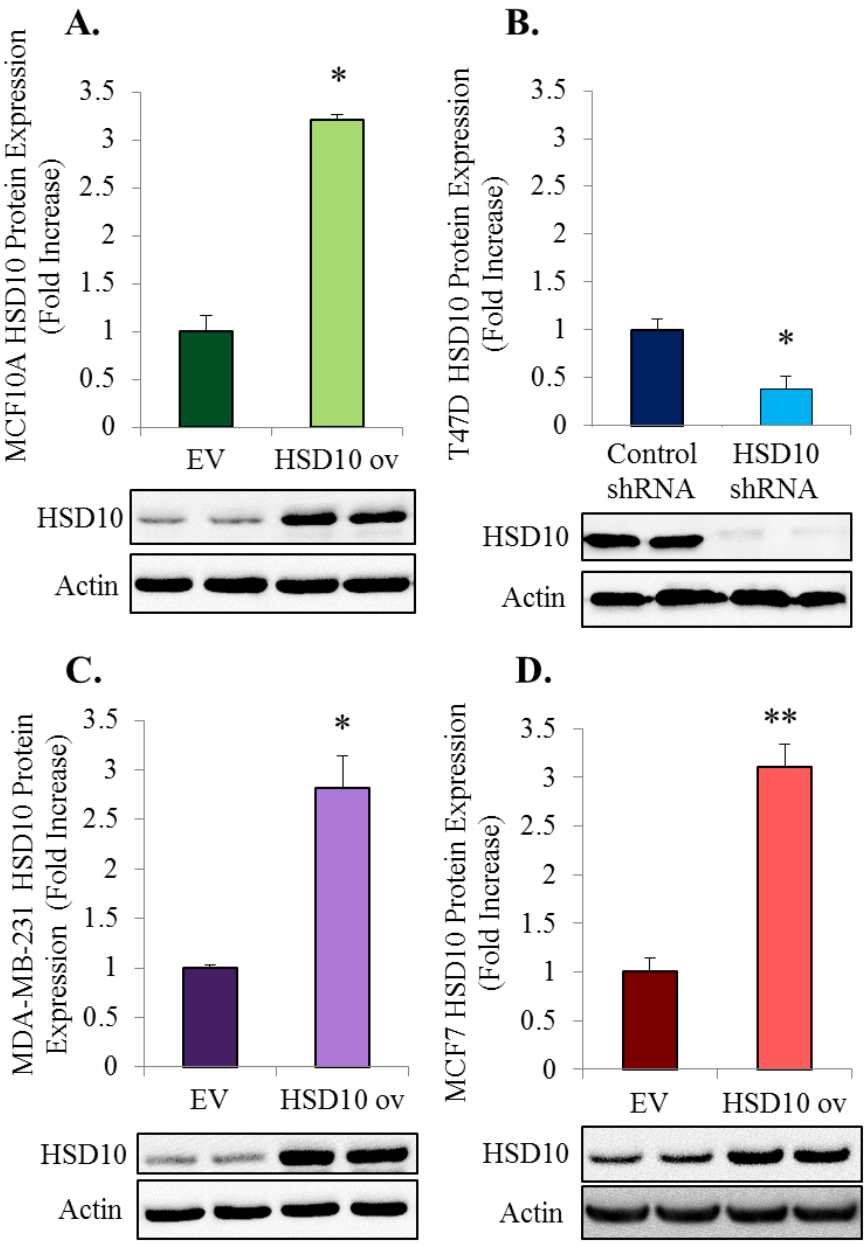

Figure 2-4: Generation of HSD10-transfected breast cancer cells. MCF10A, T47D, MDA-MB-231, and MCF7 transfected cells were harvested for detection of protein expression using rabbit anti-HSD10 antibody (1:3000) via immunoblotting. Actin (mouse anti-Actin antibody, 1:8000) was used as the loading control and HSD10 expression was normalized to actin. **A.** MCF10A EV and HSD10 ov whole cell lysates were analyzed for HSD10 protein expression and displayed as fold increase relative to MCF10A EV (n=3). **B.** T47D Control shRNA and HSD10 shRNA whole cell lysates were analyzed for HSD10 protein expression and displayed as fold increase relative to T47D control shRNA (n=3). **C.** MDA-MB-231 EV and HSD10 ov whole cell lysates were analyzed for HSD10 protein expression and displayed as fold increase relative to MDA-MB-231 EV (n=4). **D.** MCF7 EV and HSD10 ov whole cell lysates were analyzed for HSD10 protein expression and displayed as fold increase relative to MCF7 EV (n=4). Data presented as mean ± SE. *P<0.05, **P<0.01 versus control group.

2.4. Localization of HSD10 in HSD10-transfected Breast Cancer Cells

Furthermore, to ensure that the effects observed in HSD10-transfected breast cancer cells were not due to impaired localization of excess HSD10, immunofluorescence staining of all modified breast cancer cell lines was used to show the localization of HSD10 to mitochondria.

Similar to the previous observations in the PC-12 cells (**Chapter 1**), the fluorescence intensity of HSD10 was significantly increased in MCF10A HSD10 ov cells in comparison with MCF10A EV cells (**Fig. 2-5 A-B**). Additionally, the merged picture of **Figure 2-5 A** demonstrates increased localization of HSD10 to mitochondria in the MCF10A HSD10 ov cells. Similar HSD10 staining intensity and mitochondria localization was observed in the MDA-MB-231 HSD10 ov cells (**Fig. 2-5 E-F**) and MCF7 HSD10 ov cells (**Fig. 2-5 G-H**), compared with the respective EV control cells. Furthermore, the intensity of HSD10 staining was decreased in T47D HSD10 shRNA cells compared to T47D control shRNA cells (**Fig. 2-5 C-D**), confirming the success of HSD10 knockdown.

As in the PC-12 cells (**Chapter 1**), upregulation of HSD10 does not appear to affect the mitochondrial localization of the enzyme. Also, downregulation of HSD10 does not seem to hinder mitochondrial targeting. The diminished co-staining of HSD10 with Mito Tracker Red is anticipated to be the result of the large decrease in HSD10.

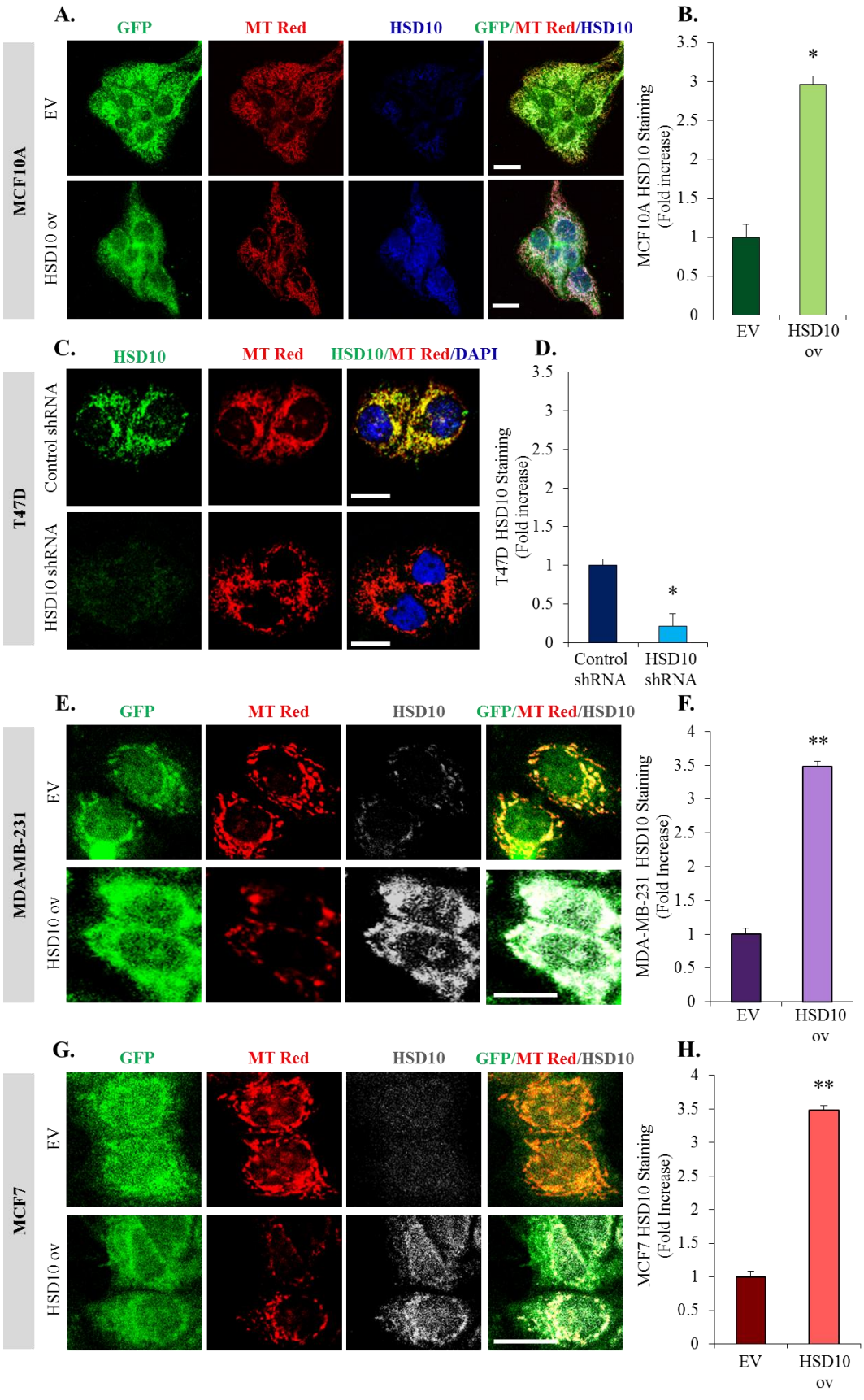
A.
GFP
MT Red
HSD10
GFP/MT Red/HSD10
MCF10A
EV
HSD10 ov
B.
MCF10A HSD10 Staining (Fold increase)
EV
HSD10 ov
C.
HSD10
MT Red
HSD10/MT Red/DAPI
T47D
Control shRNA
HSD10 shRNA
D.
T47D HSD10 Staining (Fold increase)
Control shRNA
HSD10 shRNA
E.
GFP
MT Red
HSD10
GFP/MT Red/HSD10
MDA-MB-231
EV
HSD10 ov
F.
MDA-MB-231 HSD10 Staining (Fold Increase)
EV
HSD10 ov
G.
GFP
MT Red
HSD10
GFP/MT Red/HSD10
MCF7
EV
HSD10 ov
H.
MCF7 HSD10 Staining (Fold Increase)
EV
HSD10 ov

Figure 2-5: Localization of HSD10 in HSD10-transfected breast cancer cells. MCF10A, T47D, MDA-MB-231, and MCF7 transfected cells were cultivated on chamber slides and proteins were detected using mouse anti-HSD10 antibody (1:300) and Mito Tracker Red (1:500). After incubation with anti-mouse Alexa Fluor 488 (1:500), cells were mounted in fluorescence mounting media. Confocal microscopy was used to visualize immunofluorescence staining of **A.** GFP alone (green), Mito Tracker Red alone (red), HSD10 alone (blue), and these three antigens co-localized (white) in EV and HSD10 ov MCF10A cells (scale bar: 20 μm). **B.** Quantification of HSD10 immunofluorescence staining (depicted in **A**) displayed as fold increase relative to MCF10A EV (n=6). **C.** Immunofluorescence staining of HSD10 alone (green), Mito Tracker Red alone (red), and merged with blue DAPI nuclear staining (yellow) in control shRNA and HSD10 shRNA T47D cells (scale bar: 20 μm). **D.** Quantification of HSD10 immunofluorescence staining (depicted in **C**) displayed as fold increase relative to T47D control shRNA (n=6). **E.** GFP alone (green), Mito Tracker Red alone (red), HSD10 alone (gray), and these three antigens co-localized (white) in EV and HSD10 ov MDA-MB-231 cells (scale bar: 20 μm). **F.** Quantification of HSD10 immunofluorescence staining (depicted in **E**) displayed as fold increase relative to MDA-MB-231 EV (n=10). **G.** GFP alone (green), Mito Tracker Red alone (red), HSD10 alone (gray), and these three antigens co-localized (white) in EV and HSD10 ov MCF7 cells (scale bar: 20 μm). **H.** Quantification of HSD10 immunofluorescence staining (depicted in **G**) displayed as fold increase relative to MCF7 EV (n=10). Data presented as mean ± SE. *P<0.01, *P<0.001 verses control group.

2.5. In Vitro *HSD10-transfected Breast Cancer Cell Growth Curve Analysis*

The consequence of HSD10 alteration on breast cancer cell growth was studied using *in vitro* cell culture growth curves. MCF10A HSD10-overexpression, T47D HSD10-knockdown, MDA-MB-231 HSD10-overexpression, and MCF7 HSD10-overexpression cell lines were plated at a constant density in 100-mm dishes and grown over the course of nine to ten days, with a dish counted every day. Interestingly, MCF10A HSD10 ov cells grew at approximately the same rate as MCF10A EV cells over nine days until the dishes were fully confluent (**Fig. 2-6 A**).

This data suggests that HSD10 may not be a tumor-initiating factor, since overexpression did not affect growth rate in the non-tumorigenic MCF10A cells. Instead, it is highly probably that HSD10 is a tumor-promoting factor in previously-induced cancer cells, based on much of the evidence in this dissertation. Due to the growth curve results in **Fig. 2-6 A** and the theory that HSD10 is not a tumor-initiator, the MCF10A cell line was viewed as a poor candidate for the creation of an HSD10-overexpression stably transfected cell model.

Knockdown of HSD10 in T47D cells led to a considerable decrease in growth rate compared with control shRNA T47D cells (**Fig. 2-6 B**). This result matched the PC-12 HSD10-knockdown growth curve depicted in **Chapter 1**. As T47D cells are true cancer cells, this result implies that HSD10 may promote cancerous cell growth in cell culture, while having little to no effect in non-cancerous breast cells. Considering the growth curve results, the T47D cell line was subjected to further testing for corroboration that it would be a successful HSD10-knockdown stably transfected cell model.

Overexpression of HSD10 in MDA-MB-231 cells did not result in any change in cell growth rate (**Fig. 2-6 C**), despite the fact that it is a metastatic cancer cell line. It is possible that this observation is due in part to the lack of endocrine receptors in the MDA-MB-231 cell line

(163). As HSD10 plays a role in steroidogenesis, and many HSD17B family members have been implicated in hormone-related cancers, it is plausible that ER-negative breast cancers are not influenced by HSD10. Further study is needed to investigate this possibility.

Last, HSD10 overexpression in MCF7 cells did not elicit any statistically significant changes in cell growth rate. There was a slight increase in MCF7 HSD10 ov cell growth from days seven to nine (**Fig. 2-6 D**), compared to MCF7 EV cells. This may be explained by the ability of HSD10 to limit stress-induced cell death. Once the dishes were confluent on the sixth day, the MCF7 EV cells may have been unable to compete for space and thus underwent apoptosis. In contrast, it is possible that the MCF7 HSD10 ov cells were able to continue growing and remained protected from cell death induction due to the high amounts of HSD10.

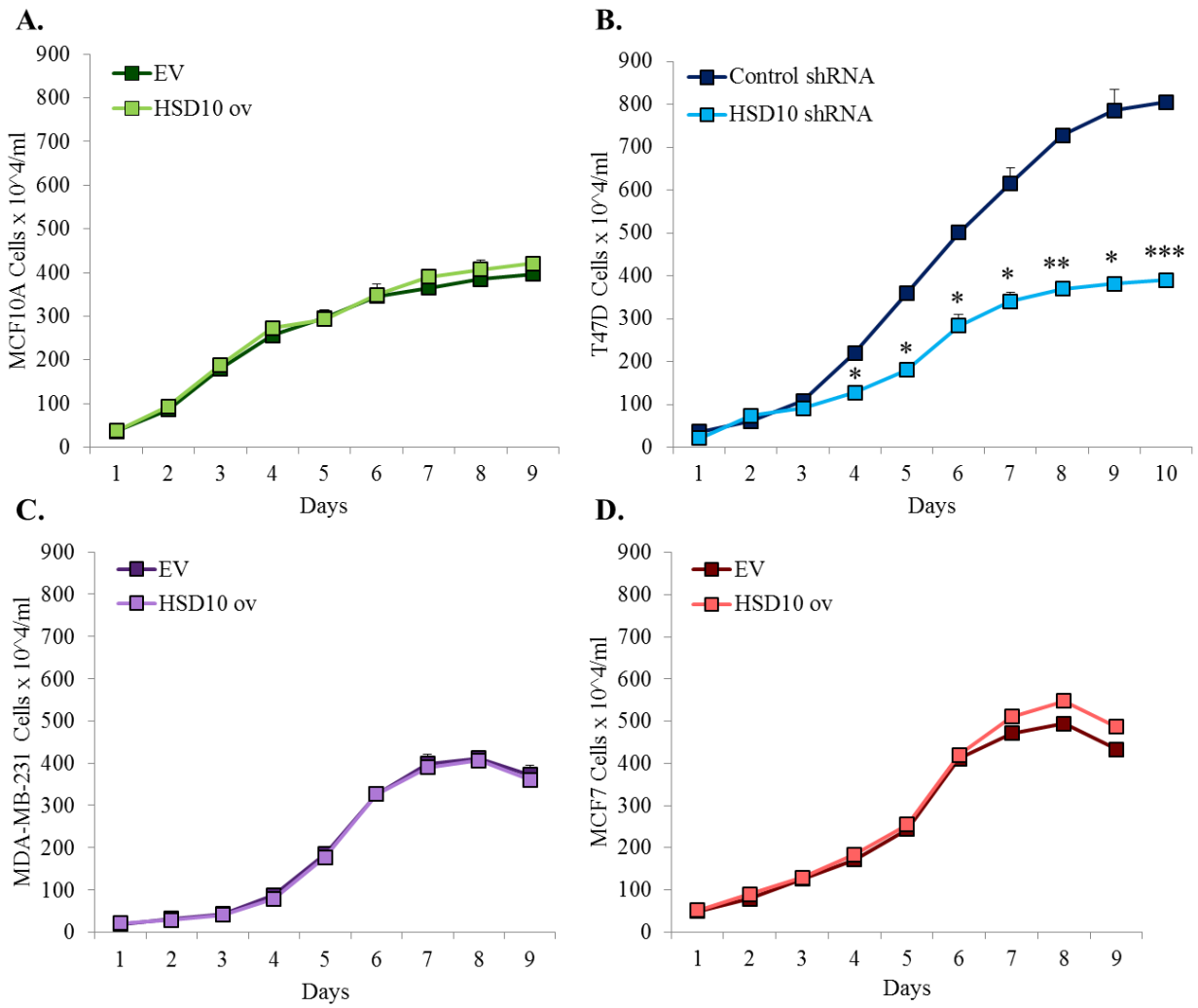

Figure 2-6: Effect of HSD10-modification on *in vitro* breast cancer cell growth. MCF10A, T47D, MDA-MB-231, and MCF7 transfected cells plated at a constant density were grown and counted over the course of 9-10 days to determine cell growth rate. **A.** Growth curve of MCF10A EV (dark green ■) and MCF10A HSD10 ov (light green ■) cells displayed as cells x 10^4 per ml (n=4). **B.** Growth curve of T47D control shRNA (dark blue ■) and T47D HSD10 shRNA (light blue ■) cells depicted as cells x 10^4 per ml (n=4). **C.** Growth curve of MDA-MB-231 EV (dark purple ■) and MDA-MB-231 HSD10 ov (light purple ■) cells displayed as cells x 10^4 per ml (n=4). **D.** Growth curve of MCF7 EV (dark red ■) and MCF7 HSD10 ov (light red ■) cells displayed as cells x 10^4 per ml (n=4). Data presented as mean ± SE. *****P<0.01, ******P<0.001, *******P<0.0001 versus control shRNA group.

2.6. Effect on Altered Breast Cancer Mitochondrial Function

As mitochondrial functions were altered upon HSD10-transfection in the PC-12 cells (**Chapter 1**), the effect of HSD10 on mitochondrial function was also studied in the modified breast cancer cells. ETC complex I, II, III, and IV enzyme activities were tested to examine the effect of HSD10 alteration on mitochondrial respiration.

Interestingly, complex I enzyme activity for the T47D-transfected cells remained unchanged between the two groups (**Fig. 2-7 A**), while complexes II and III had a slight trend toward decreased activity in HSD10 shRNA cells in comparison with control shRNA cells (**Fig. 2-7 B-C**), although not statistically significant. Complex IV enzyme activity was greatly diminished in the HSD10 shRNA group compared to the control shRNA group (**Fig. 2-7 D**).

The differences observed in the T47D-transfected cells as compared to the PC-12-tranfected cells used previously may be explained by focusing on the natural levels of HSD10 in the wild-type cells. Since wild-type T47D cells express very high levels of endogenous HSD10, perhaps these cells are able to compensate for HSD10 knockdown to a greater degree than wild-type PC-12 cells which express mid-range levels of HSD10.

Regardless of the disparities, the statistically significant reduction in complex IV enzyme activity and trends toward reduced complex II and III enzyme activity in the T47D HSD10 shRNA cells parallels the decreased ETC complex enzyme activities in the PC-12 HSD10 shRNA cells. Together, this data demonstrates that the phenotype resulting from HSD10 knockdown is largely preserved across two cancer cell lines.

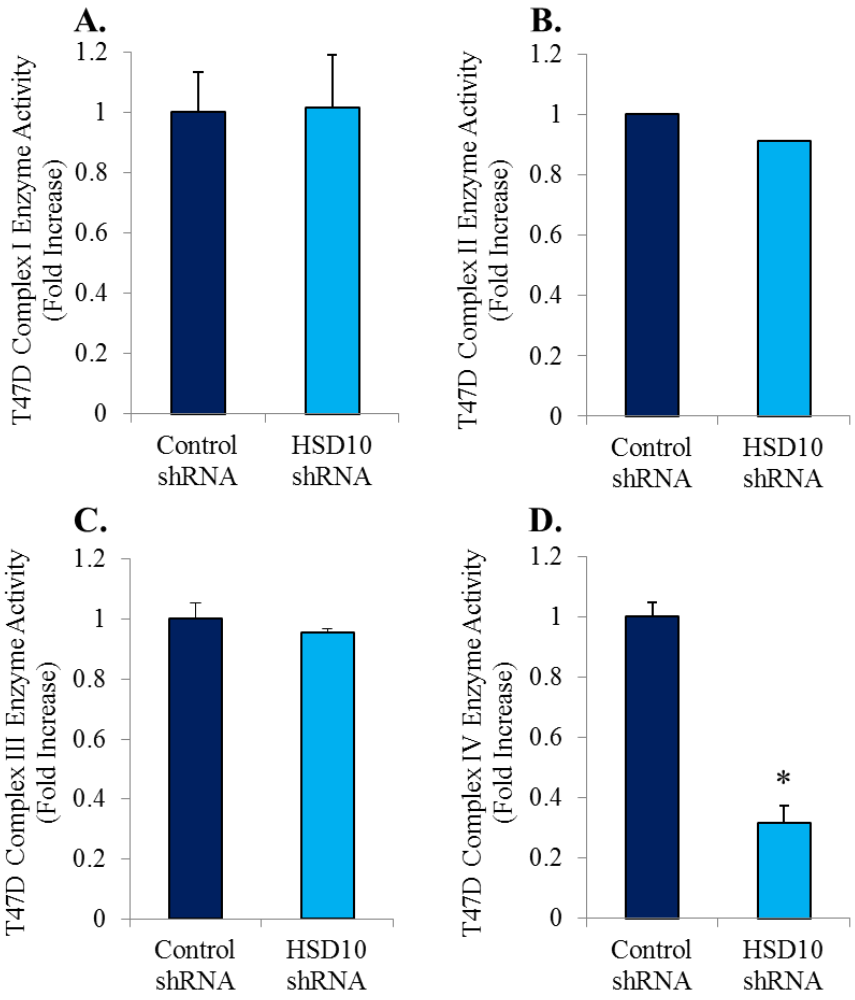

Figure 2-7: Examination of ETC enzyme activities in HSD10-transfected breast cancer cells. T47D transfected cells were harvested and tested for ETC complex I (**A**), II (**B**), III (**C**), and IV (**D**) enzyme activities. Results are displayed as fold increase relative to control shRNA (n=5 for each assay). Data presented as mean ± SE. *P<0.001 versus control group.

Lastly, since complex IV enzyme activity was reduced in T47D HSD10 shRNA cells, ATP production was assessed to determine the effect of this change. Similar to the PC-12 HSD10 shRNA cells in **Chapter 1**, the level of ATP was significantly reduced in T47D HSD10 shRNA cells compared to T47D control shRNA cells (**Fig. 2-8**). This provides further evidence that HSD10 alteration is important across two cancer cell lines.

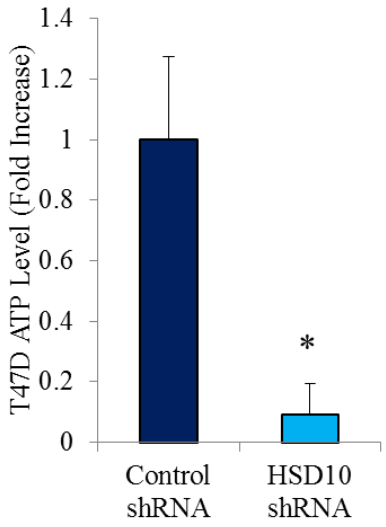

Figure 2-8: Assessment of ATP production in HSD10-transfected breast cancer cells. T47D transfected cells were harvested for determination of cellular ATP content. Densitometry of results displayed as fold increase relative to control shRNA (n=4). Data presented as mean ± SE. *****P<0.01 versus control group.

2.7. Interim Conclusion

Chapter 2 investigated the effect of HSD10 alteration in a different type of human cancer to confirm or disprove the importance of HSD10 across cancers. Since overexpression of HSD10 did not induce MCF10A cancer development, it is probable that HSD10 is a tumor-promoting factor (**Fig. 2-9**). Therefore, it is likely that HSD10 alteration is more problematic in cancerous cells, as compared to non-tumorigenic cells.

Additionally, knockdown of HSD10 in T47D cells displayed a similar phenotype to the PC-12 HSD10-knockdown cells. This shows that the resultant phenomenon following HSD10 alteration is conserved across two known cancer cell lines, providing further evidence that HSD10 has an integral role in cancer growth. Further studies are necessary to examine whether the HSD10-mediated phenotype is observed in other cancer types, and to determine which cancers are most affected.

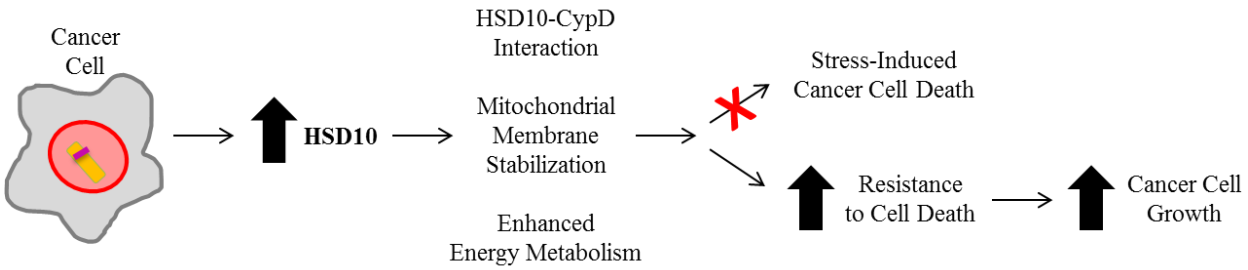

Figure 2-9: Chapter 2 summary of the effect of HSD10 on cancer cell progression. In cancer cells, increased HSD10 levels correlate with increased HSD10-CypD complex formation, enhanced mitochondrial membrane stabilization, and heightened energy production. This leads to cancer cell survival through enhanced cellular resistance to cell death, resulting in increased cancer cell growth.

RESULTS

Chapter 3: The Future Outlook for HSD10 in Cancer

Upon determination of the significant role HSD10 plays in PC-12 cancer progression in **Chapter 1** and testing four human breast cancer cell lines with HSD10 alteration in **Chapter 2**, several future directions for this project will be outlined in the following chapter.

To begin, it is highly recommended that stably-transfected cell lines with HSD10 overexpression and HSD10 knockdown be created prior to performing any experiments. Essentially, stable expression of HSD10 will yield more accurate results over a longer period of time, as compared to transient or lentiviral transfection.

3.1. Stable Expression of HSD10 in Breast Cancer Cell Lines

The goal of Chapter 2 was to establish working models of human breast cancer cell lines with differential expression of HSD10. Out of the four studied cell lines, it was anticipated that two would be chosen for creation of stable cell lines.

Lentiviral transfection significantly increased HSD10 protein content in the MCF10A and MDA-MB-231 cell lines (**Fig. 2-4 A** and **C**). However, this was not accompanied by changes in cell growth rate (**Fig. 2-6 A** and **C**). Thus, it was determined that the MCF10A and MDA-MB-231 cell lines were unsuitable candidates for stable transfection.

On the contrary, lentiviral transfection significantly decreased HSD10 protein expression in the T47D cell line (**Fig. 2-4 B**), which correlated with a marked reduction in cell growth rate (**Fig. 2-6 B**). Following the successful change in T47D cell growth after HSD10 knockdown, ETC complex enzyme activities and ATP content were examined. Reductions in complex IV enzyme activity and ATP levels were detected, demonstrating that the HSD10 knockdown cell phenotype was consistent to the observations in PC-12 cells (**Chapter 1**). Therefore, the T47D breast cancer cell line is considered an appropriate candidate for stable knockdown of HSD10.

Interestingly, lentiviral transfection significantly increased HSD10 protein content in the MCF7 cell line (**Fig. 2-4 D**), which was accompanied by a trend toward enhanced cell growth rate (**Fig. 2-6 D**), although there was no statistical significance. Due to time constraints, ETC complex enzyme activity and ATP levels were not tested. However, despite the limited change in cell growth, it is recommended to use the MCF7 breast cancer cell line for preliminary studies of stable overexpression of HSD10. It is possible that stable transfection will provide more accurate evidence as to whether or not HSD10 overexpression affects MCF7 cell growth rate.

3.2. In Vitro *and* In Vivo *Analysis of Stably-transfected HSD10 Breast Cancer Cell Lines*

Upon the creation of stable breast cancer cell lines, immunoblotting and immunofluorescence staining should be done to verify the degree of successful overexpression or knockdown of HSD10 in the cell lines.

Next, *in vitro* cell growth rate curves must be performed to examine whether the stable, artificial overexpression or knockdown of endogenous HSD10 influences breast cancer cell growth rate. Due to the success of lentiviral HSD10 knockdown correlating with diminished T47D cell growth rate (**Fig. 2-6 B**), it is expected that the stable reduction of HSD10 in the same cell line will yield comparable results. In regards to the MCF7 cell line, which showed a trend toward increased cell growth following lentiviral HSD10 overexpression (**Fig. 2-6 D**), it is possible that the stable overexpression of HSD10 in MCF7 cells will reveal that cell growth rate is affected by HSD10 alteration in the cells. If this observation is made, then the MCF7 cell line is an appropriate model to study the effect of stable HSD10 overexpression in breast cancer. If no changes in the MCF7 cells are observed, then other breast cancer cell lines will need to be assessed to achieve a suitable cell line for stable overexpression of HSD10. The panel of breast cancer cell lines depicted in **Figure 2-1** should be utilized to choose cell lines with low to median levels of endogenous HSD10, which will simplify experiments for artificial overexpression of HSD10. Additionally, since wild-type MCF7 cells exhibit median levels of endogenous HSD10, this cell line may also be used as an alternative HSD10 knockdown model in addition to the T47D cell line.

Once two stably-transfected breast cancer cell lines, which yield significant effects on cell growth, have been generated, the subsequent step is to analyze the phenotype of the stable cell lines in animals. As cancer cells often behave differently in cell culture dishes as compared

to a living organism, it is necessary to investigate whether the stably-modified breast cancer cell lines will exhibit similar growth patterns under more natural parameters, such as the tumor-microenvironment and nutrient-rich conditions. Based on **Figure 1-4**, female SCID mice provide a suitable model for observing tumor formation *in vivo*. Thus, it is recommended that mammary fat-pad injections of the stably-transfected cell lines be performed in mice. Tumors should be monitored and measured several times per week, for at least three months, or until humane endpoints are reached. The length of time necessary for tumor nodules to form will vary depending on the cell line and inoculation volume; however, T47D and MCF7 cells typically need at least three months to form (164, 165). If HSD10 levels affect *in vivo* tumor growth using the stably-modified breast cancer cells, similar to the observations in the stably-transfected PC-12 *in vivo* tumor study (**Fig. 1-4**), it provides more convincing, clinically significant evidence that HSD10 plays a key role in breast cancer progression.

After it is confirmed that stable overexpression and knockdown of HSD10 influence breast cancer *in vitro* cell growth and *in vivo* tumor formation, the effects of HSD10-modification on cellular function must be analyzed. Although the experiments detailed in **Chapter 1** provide an in-depth assessment and convincing data for the impact of HSD10-alteration on cancer cell function, this work was all performed in a rat adrenal gland tumor cell line. While the rat is a well-established animal model for investigating human disease states, rat cells alone will not provide adequate information for translation into human disease for clinical study. Therefore, it is highly advised to examine cellular function in the stably-transfected human breast cancer cell lines utilizing the same techniques performed in the PC-12 cells.

Since HSD10 is a mitochondrial enzyme, mitochondrial function must be examined by assessing ETC complex I, II, III, and IV enzyme activities, as well as ATP content in the

HSD10-modified breast cancer cells. Additionally, testing mitochondrial membrane permeability in the stably-transfected breast cancer cells will provide information regarding the health of the mitochondria. This will lead to the investigation of cellular resistance to oxidative stress conditions using functional assays such as complex enzyme activity. If HSD10-alteration confers the breast cancer cells resistance capabilities, cell death assays such as TUNEL staining must be used for clarification. As similar results for complex IV enzyme activity and cellular ATP content were obtained in the lentiviral HSD10 knockdown T47D cells (**Fig. 2-7 D** and **Fig. 2-8**) compared to the PC-12 HSD10 knockdown cells (**Fig. 1-5 D** and **Fig. 1-7**), it is anticipated that the growth and cellular function-related phenotypes associated with HSD10 reduction will remain accurate for the stable HSD10 knockdown T47D cell line.

Once the phenotypes previously observed for HSD10 overexpression and knockdown are further solidified with evidence in the stable breast cancer cell lines, the mechanism of action for HSD10 in cancer progression needs to be thoroughly investigated. **Chapter 1** began to examine the physical interaction of HSD10 with CypD in the PC-12 cells. The studies need to be performed in the stably-transfected human breast cancer cell lines, including immunoblotting and co-immunofluorescence staining to assess the impact of HSD10 overexpression or reduction on CypD protein levels, as well as Co-IPs under baseline and oxidative stress conditions to examine whether HSD10 and CypD interact in the modified breast cancer cells. If the phenotype data of HSD10-modification is sustained in PC-12 cells, it is likely that the interaction between HSD10 and CypD will occur in different cell lines as well. Furthermore, CypD translocation studies using mitochondrial matrix and IM fractions need to be performed to examine the impact of HSD10 on CypD function. According to our overall hypothesis, overexpression of HSD10 in cancer cells limits the ability of CypD to translocate to the IM under stress conditions, thereby

preventing cell death induction; this results in the enhanced cell growth rate in the HSD10 overexpression cells. Thus, these studies would determine if the interaction of HSD10 with CypD is preventing the translocation of CypD to the IM in the stable HSD10 overexpression breast cancer cells. Likewise, CypD translocation should be examined in the stable HSD10 knockdown breast cancer cells to assess whether reduction in HSD10 disrupts its interaction with CypD, thus permitting CypD to translocate to the IM and induce cell death.

In addition to examining the physical interaction between HSD10 and CypD, knockdown and overexpression studies targeting CypD can be performed to investigate the interface between the two proteins. **Chapter 1** also began to study the role of HSD10 with CypD by using siRNA to reduce CypD protein in the PC-12 HSD10 ov cells. As siRNA transfection efficacy and duration is often transitory (166), it is advised to use a CypD-specific shRNA oligonucleotide (167) for transfection in the breast cancer cells. Wild-type T47D cells are an appropriate choice for CypD knockdown, as the cells express high levels of endogenous HSD10 and CypD. Following CypD knockdown, immunoblotting and immunofluorescence must be done to confirm the degree of CypD protein reduction in the human breast cancer cells. Next, studies should be completed to assess whether the phenotype of CypD-modification matches the phenotype observed for HSD10-alteration. An *in vitro* cell growth curve should be performed to examine how knockdown of CypD affects breast cancer cell growth rate; if there is difference in cell growth, an *in vivo* study would provide further evidence as to whether CypD knockdown has any impact on tumor formation in animals. Furthermore, Co-IPs, CypD translocation, and cell death assays would determine whether reduction of CypD effects the HSD10-CypD interaction and cell death induction to a similar degree as HSD10 knockdown. If the phenotypes of CypD knockdown and HSD10 reduction are equivalent in the same cell line, such as the T47D breast

cancer cells, the evidence will successfully demonstrate that HSD10 mediates breast cancer cell growth rate and resistance to cell death induction via interaction with CypD.

Finally, whole transcriptome RNA sequencing may be used to analyze the changing cellular transcriptome, post-transcriptional modifications, and gene function and expression in the HSD10-modified cancer cell lines. Such experiments would facilitate the identification of potential signal transduction pathways and genetic factors involved in HSD10-CypD-mediated tumor growth.

3.3. Effect of HSD10 Inhibition on Cancer Cell Growth

After observing the protective role of HSD10 overexpression in PC-12 cancer cells and the destructive consequences of HSD10 knockdown in **Chapter 1**, the final step of the project will be to examine the effect of synthesized small molecule HSD10 inhibitors (generated by the Yan lab (168)) on cancer cell growth.

The synthesized A1 and A5 HSD10 inhibitor compounds (169) are structurally very similar, differing only by the addition of an ester group to A1 (**Fig. E-A** and **E-B**). The compounds exhibit comparable capacities to bind HSD10 (**Fig. E-C** and **E-D**), with A5 displaying a slightly higher binding affinity for HSD10. Additionally, the A1 and A5 inhibitors disrupt HSD10 enzymatic activity to an equivalent degree (**Fig. E-E** and **E-F**), although compound A5 exhibits the most potent inhibitory effect.

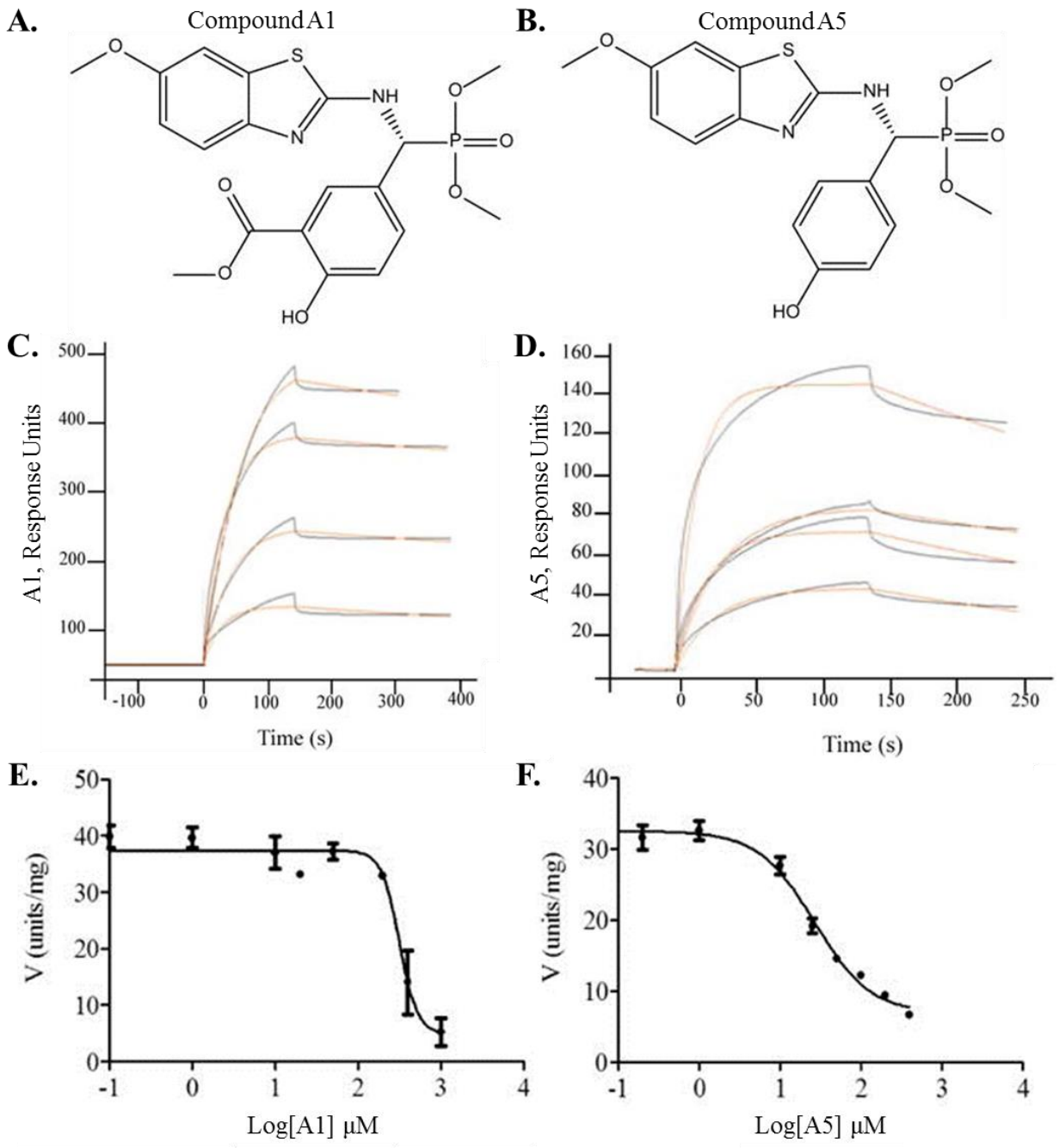

Figure E: Characterization of small molecule HSD10 inhibitors. Structures of the synthesized small molecule HSD10 inhibitors A1 (**A**) and A5 (**B**). HSD10 inhibitors A1 (**C**) and A5 (**D**) bound to immobilized human recombinant HSD10 protein in a dose-dependent manner as depicted by Surface Plasmon Resonance (SPR); globally fit data (black lines) were overlaid with experimental data (red lines). SPR results of the compound binding affinities for HSD10 revealed K_d values of 496 nM for A1 and 291 nM for A5. Inhibition of HSD10 enzymatic activity in the presence of the synthesized A1 (**E**) and A5 (**F**) inhibitors corresponded with K_i values of 96.6±19.4 µM and 14.9±1.4 µM, respectively. Adapted from Valasani, K.R. et al. (2014) *Curr Alzheimer Res* (169).

As shown in **Figure 3-1**, the HSD10 enzymatic A5 inhibitor does not disrupt HSD10 protein expression in either PC-12 EV or HSD10 ov cells.

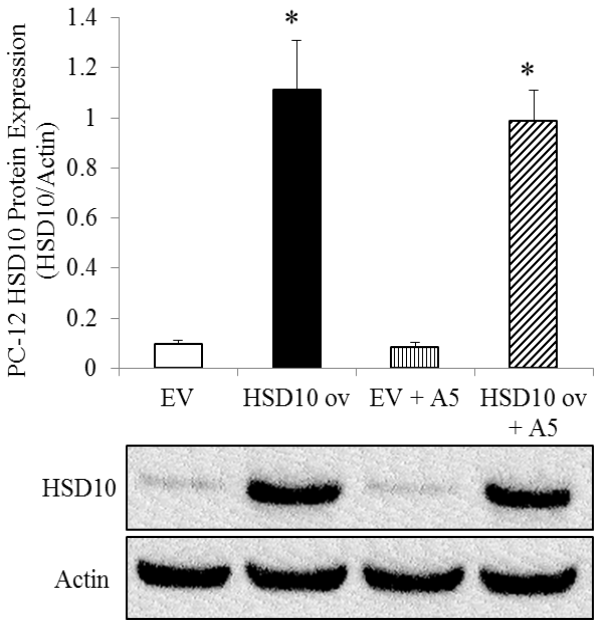

Figure 3-1: HSD10 enzyme inhibition does not affect HSD10 protein expression in PC-12 HSD10-transfected cells. PC-12 EV and HSD10 ov cells were treated with 0 μM or 150 μM A5 inhibitor for 24 hours and then harvested for detection of HSD10 protein expression using rabbit anti-HSD10 antibody (1:3000). Actin (mouse anti-Actin antibody, 1:8000) was used as the loading control and HSD10 protein expression was normalized to actin (n=4 for each group). Data presented as mean ± SE. *P<0.01 versus control groups.

Following treatment of PC-12 cells with the two HSD10 inhibitors, growth rate analysis was used to determine which HSD10 inhibitor was more effective in several of the cancer cell lines used in this dissertation. Additionally, the effect of HSD10 inhibition on tumor growth was assessed using the PC-12 HSD10 ov *in vivo* tumor mouse model.

3.3.1. In Vitro *and* In Vivo *HSD10-transfected Pheochromocytoma Cell Growth Analysis with HSD10 Inhibitors*

The effect of HSD10 inhibition on PC-12 cell growth was examined using *in vitro* cell growth rate experiments. PC-12 EV and HSD10 ov cells were plated in dishes at a constant density, treated with 0, 50, 100, 150, 200, 250, or 300 μM A1 (**Fig. 3-2**) or A5 inhibitor (**Fig. 3-3**), and then grown over the course of seven days. Each day, the number of cells was counted in one dish. Both of the HSD10 inhibitors reduced EV cell growth rate in a dose-dependent manner (**Fig. 3-2 A** and **Fig. 3-3 A**), with the A5 inhibitor having a more significant effect.

There was little to no affect for either inhibitor on HSD10 ov cell growth rate (**Fig. 3-2 B** and **Fig. 3-3 B**). This is possibly due to the differing amounts of HSD10 between the two PC-12 cell lines. As the HSD10 ov cells have a significantly higher abundance of artificial HSD10 and grow extremely fast, the same dosage of small molecule HSD10 inhibitor has a larger quantity of HSD10 to bind and inhibit, thus diminishing the efficacy of the compounds. Undeniably, the *in vivo* data shown in **Figure 3-4** further confirms the theory that the PC-12 HSD10 ov cells are unaffected by the HSD10 inhibitors. The animal study revealed that there was no statistical difference between the untreated HSD10 ov tumors and the HSD10 ov tumors treated with the stronger HSD10 inhibitor A5 over one month.

Due to these results, it is advised to study HSD10 inhibition in unmodified cancer cell lines with varying endogenous HSD10 levels. Additionally, cancer cells that form tumors slowly over the course of several months in animals would provide a better model for cancer research, as many cancers are considered chronic diseases that can last months or years. Ideally, slower growing tumors would allow more time for the HSD10 inhibitors to work toward slowing and/or halting the tumor growth rate.

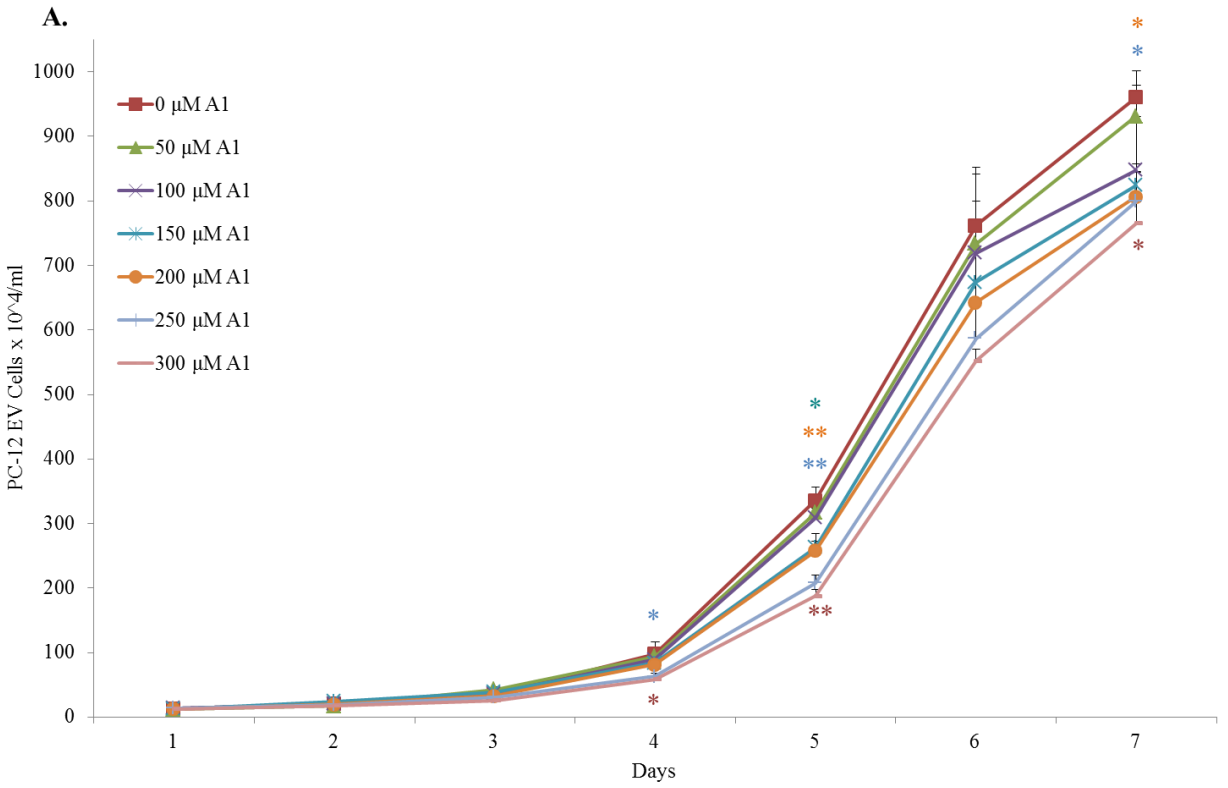
A.
PC-12 EV Cells x 10^4/ml
Days
0 µM A1
50 µM A1
100 µM A1
150 µM A1
200 µM A1
250 µM A1
300 µM A1

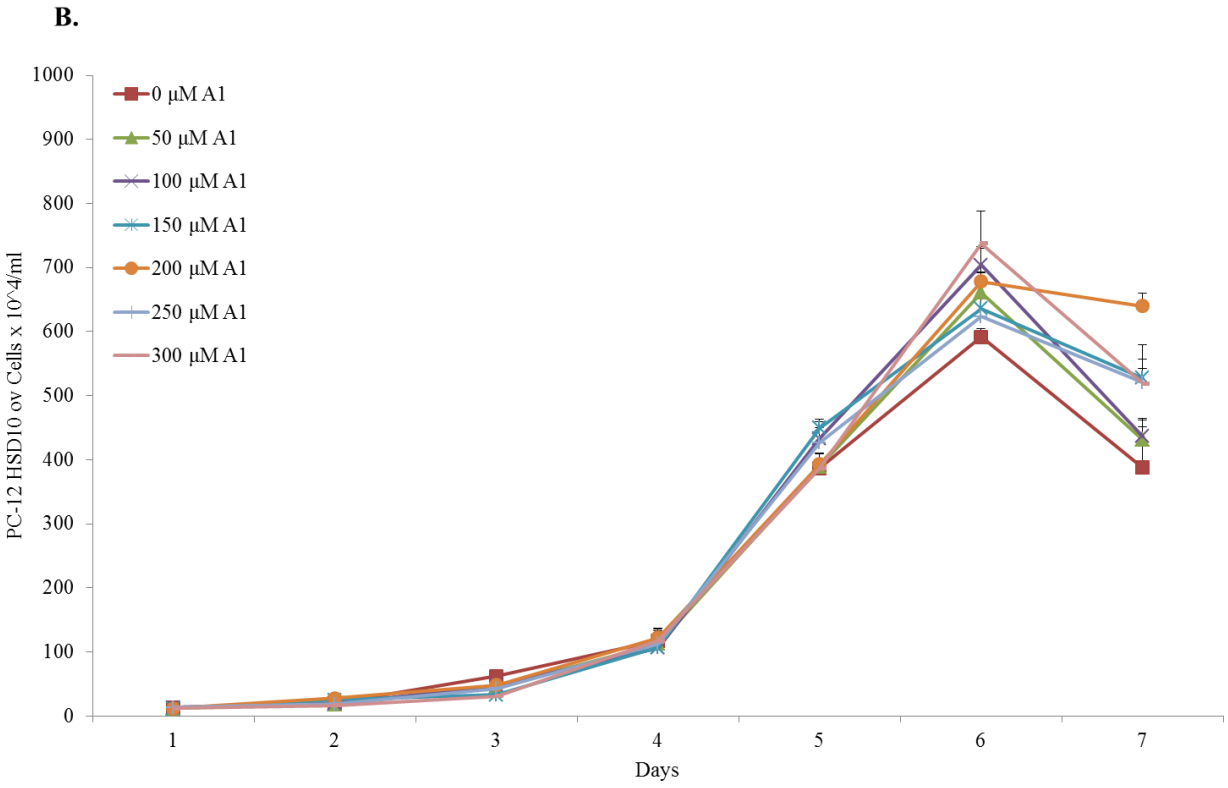
B.
PC-12 HSD10 ov Cells x 10^4/ml
Days
0 µM A1
50 µM A1
100 µM A1
150 µM A1
200 µM A1
250 µM A1
300 µM A1

Figure 3-2: HSD10 A1 inhibitor reduces *in vitro* growth rate in PC-12 EV cells. PC-12 transfected cells were plated at a constant density in low glucose DMEM media and treated with 0, 50, 100, 150, 200, 250, or 300 μM A1 HSD10 inhibitor. The cells were then grown and counted over the course of 7 days to determine cell growth rate. **A.** Growth curve of EV 0 μM A1 (red ■), EV 50 μM A1 (green ▲), EV 100 μM A1 (purple ×), EV 150 μM A1 (teal ♦), EV 200 μM A1 (orange ●), EV 250 μM A1 (blue ▏), and EV 300 μM A1 (pink ▬) depicted as cells x 10^4 per ml (n=4). **B.** Growth curve of HSD10 ov 0 μM A1 (red ■), HSD10 ov 50 μM A1 (green ▲), HSD10 ov 100 μM A1 (purple ×), HSD10 ov 150 μM A1 (teal ♦), HSD10 ov 200 μM A1 (orange ●), HSD10 ov 250 μM A1 (blue ▏), and HSD10 ov 300 μM A1 (pink ▬) depicted as cells x 10^4 per ml (n=4). Data presented as mean ± SE. Pink *P<0.05, **P<0.001 for 300 μM against 0 μM; Blue *P<0.05, **P<0.001 for 250 μM against 0 μM; Orange *P<0.05, **P<0.01 for 200 μM against 0 μM; Teal *P<0.01 for 150 μM against 0 μM.

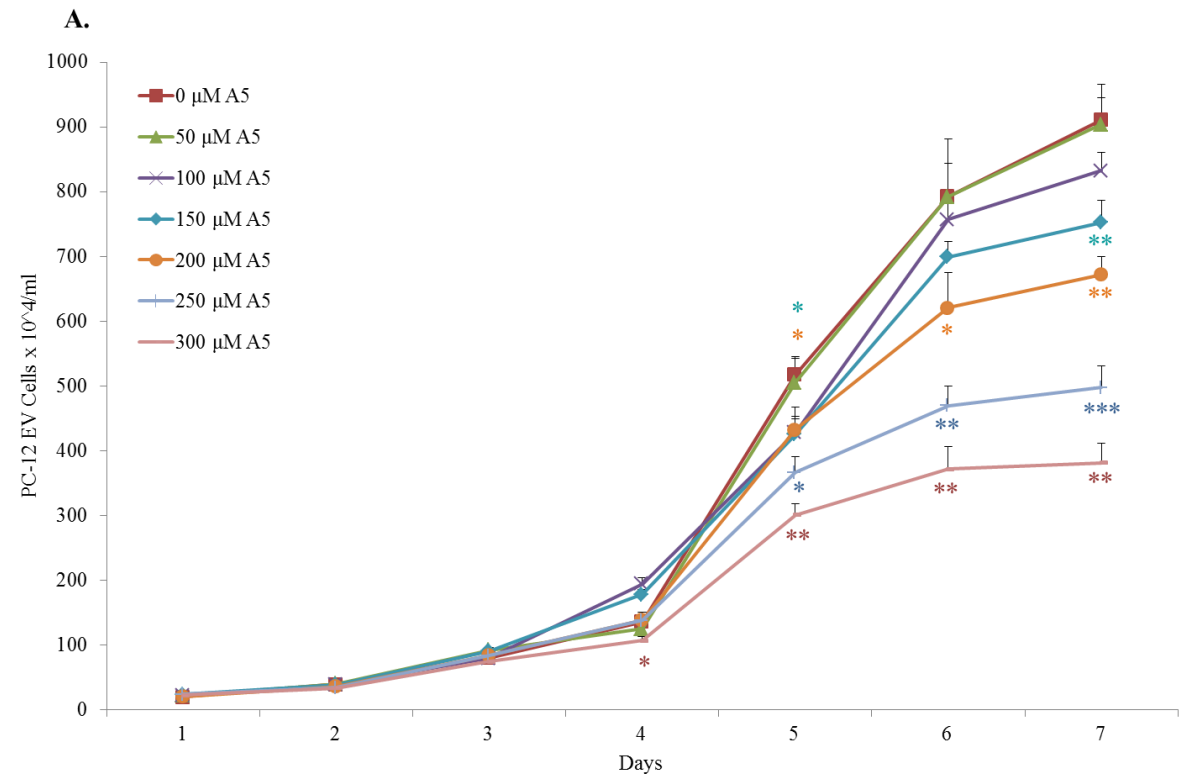
A.
PC-12 EV Cells x 10^4/ml
Days
0 µM A5
50 µM A5
100 µM A5
150 µM A5
200 µM A5
250 µM A5
300 µM A5

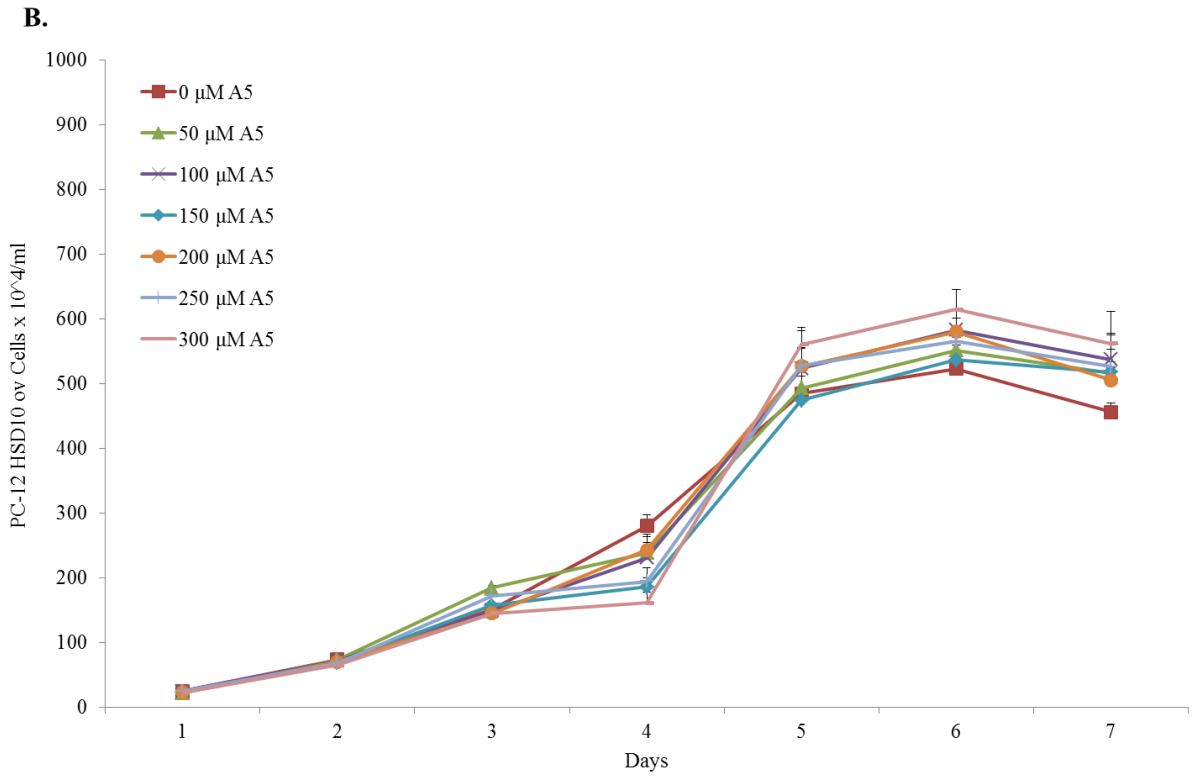
B.
PC-12 HSD10 ov Cells x 10^4/ml
Days
0 µM A5
50 µM A5
100 µM A5
150 µM A5
200 µM A5
250 µM A5
300 µM A5

Figure 3-3: HSD10 A5 inhibitor reduces *in vitro* growth rate in PC-12 EV cells. PC-12 transfected cells were plated at a constant density in low glucose DMEM media and treated with 0, 50, 100, 150, 200, 250, or 300 μM A5 HSD10 inhibitor. The cells were then grown and counted over the course of 7 days to determine cell growth rate. **A.** Growth curve of EV 0 μM A5 (red ■), EV 50 μM A5 (green ▲), EV 100 μM A5 (purple ×), EV 150 μM A5 (teal ♦), EV 200 μM A5 (orange ●), EV 250 μM A5 (blue ▏), and EV 300 μM A5 (pink ▬) depicted as cells x 10^4 per ml (n=4). **B.** Growth curve of HSD10 ov 0 μM A5 (red ■), HSD10 ov 50 μM A5 (green ▲), HSD10 ov 100 μM A5 (purple ×), HSD10 ov 150 μM A5 (teal ♦), HSD10 ov 200 μM A5 (orange ●), HSD10 ov 250 μM A5 (blue ▏), and HSD10 ov 300 μM A5 (pink ▬) depicted as cells x 10^4 per ml (n=4). Data presented as mean ± SE. Pink *P<0.05, **P<0.0001 for 300 μM against 0 μM; Blue *P<0.01, **P<0.001, ***P<0.0001 for 250 μM against 0 μM; Orange *P<0.05, **P<0.001 for 200 μM against 0 μM; Teal *P<0.05, **P<0.01 for 150 μM against 0 μM.

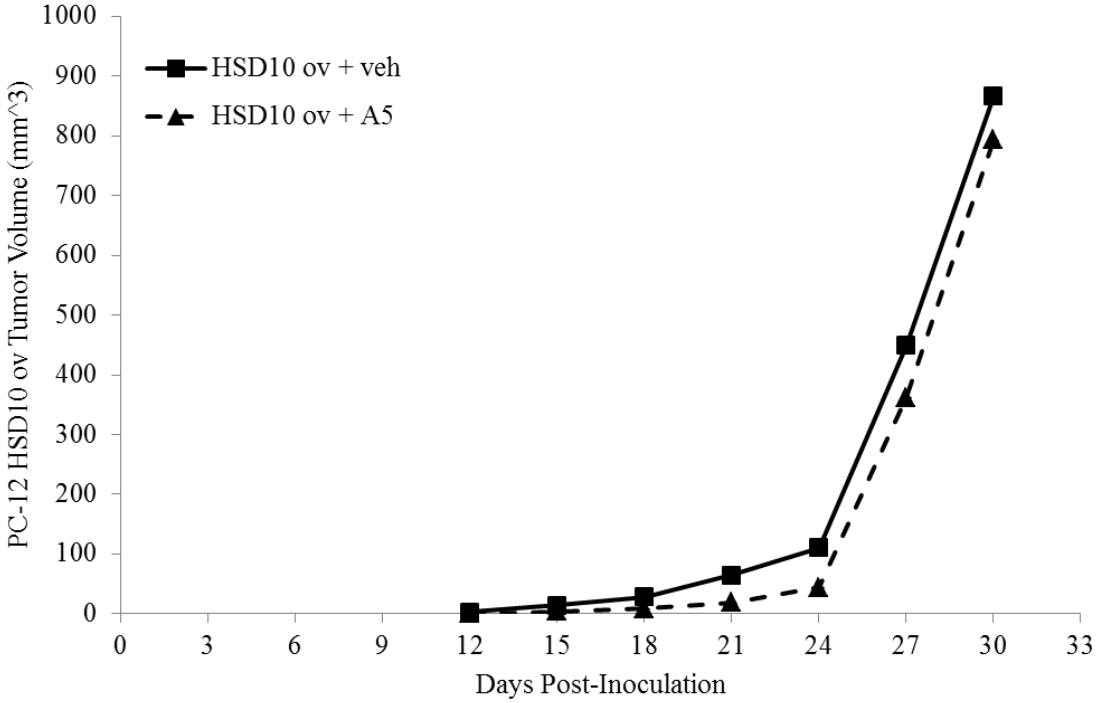

Figure 3-4: HSD10 A5 inhibitor has minimal effect on *in vivo* PC-12 HSD10 ov tumor growth. PC-12 transfected HSD10 ov cells were pretreated with either nothing or 150 μM A5 HSD10 inhibitor 24 hours prior to injection into the mammary fat pad tissue of 8 two-month old female SCID mice. On Day 15, mice received either vehicle (sterilized saline) or 10 mg/kg A5 HSD10 inhibitor via intraperitoneal injection; this was repeated every three days until the experiment end. Quantification of tumor growth in all SCID mice treated with vehicle (n=8; ■, solid line) or A5 HSD10 inhibitor (n=8; ▲, dashed line) grown over a total of 30 days, depicted in tumor volume (mm^3). Data presented as mean.

3.3.2. **In Vitro *and* In Vivo *Breast Cancer Cell Growth Analysis with HSD10 Inhibitors***

After completing the pilot studies for the two HSD10 inhibitors in the PC-12 cells, the next step was to examine the effect of the compounds on wild-type cancer cell lines with endogenous HSD10. Due to time-constraints, 0 μM and 150 μM doses were used to test the efficacy of the HSD10 inhibitors in the T47D and MCF7 human breast cancer cell lines. Cells were plated in dishes at a constant density, treated with either 0 μM, 150 μM A1, or 150 μM A5, and then grown and counted over ten days.

From the second day of the experiment, both of the HSD10 inhibitors decreased T47D cell growth rate (**Fig. 3-5**), with the A5 inhibitor having a more significant effect (**Fig. 3-5**, ▲ dotted line). Due to this promising preliminary data, it is anticipated that a T47D *in vivo* tumor model would provide an advantageous foundation for future HSD10 inhibitor studies. Furthermore, many studies have shown that T47D tumors often grow in animals gradually over three months up to one year (164). As it is theorized in **Section 3.3.1** that slow growing tumors will allocate more time for the HSD10 inhibitors to effect tumor growth rate, the T47D cell line is a suitable candidate for *in vivo* experiments utilizing the HSD10 compounds.

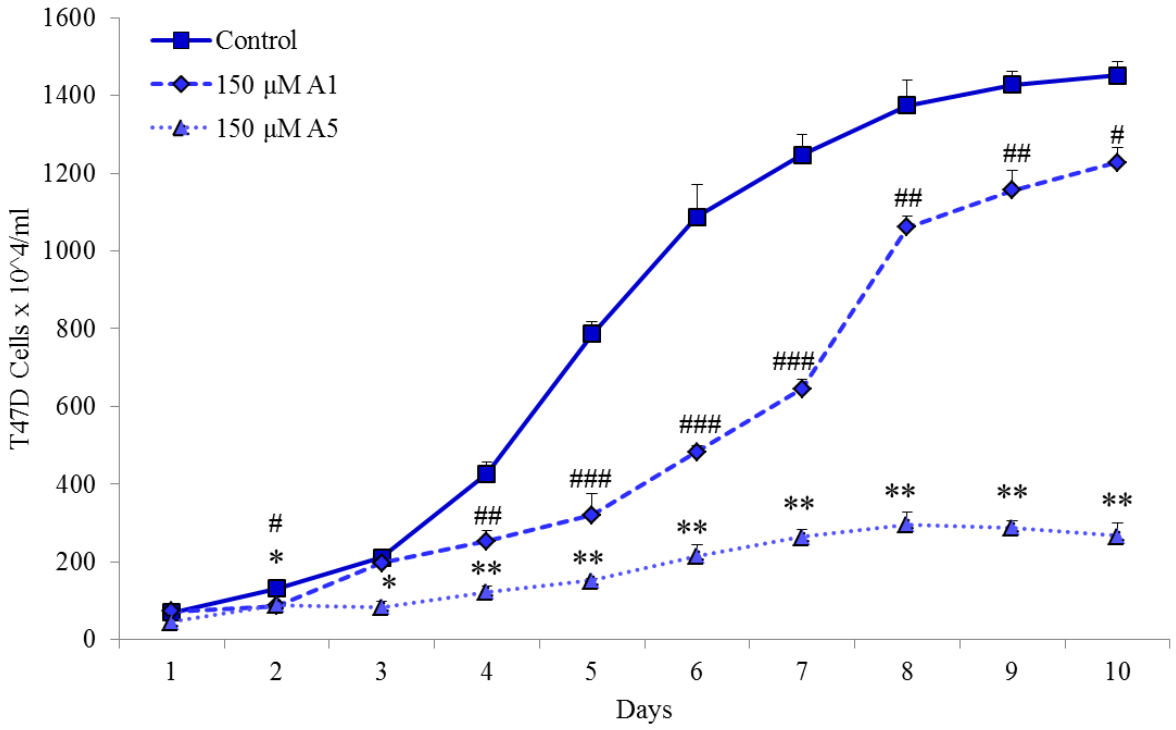

Figure 3-5: Effect of HSD10 inhibition on *in vitro* T47D cell growth. T47D wild-type cells were plated at a constant density and treated with either 150 µM A1 or 150 µM A5 HSD10 inhibitors. The cells were then grown and counted over the course of 10 days to determine cell growth rate. Growth curve of untreated control (■, solid line) versus either A1-treated (♦, dashed line) or A5-treated (▲, dotted line) depicted as cells x 10^4 per ml (n=4). Data presented as mean ± SE. #P<0.01, ##P<0.001, ###P<0.0001 versus control group for A1 inhibitor; *P<0.01, **P<0.0001 versus control group for A5 inhibitor.

The A5 inhibitor also reduced MCF7 cell growth rate (**Fig. 3-6**, ▲ dotted line). However, the A1 inhibitor was ineffective in the MCF7 cells. Since the A5 inhibitor was successful in decreasing the cell growth rate of PC-12 EV, T47D, and MCF7 cells, it is recommended for use in all future studies involving HSD10 inhibition.

Additionally, it is suggested that the MCF7 breast cancer cell line be retained as an alternative to the T47D breast cancer cell line for future *in vivo* HSD10 inhibitor studies, as MCF7 cells behave similarly to T47D cells (165).

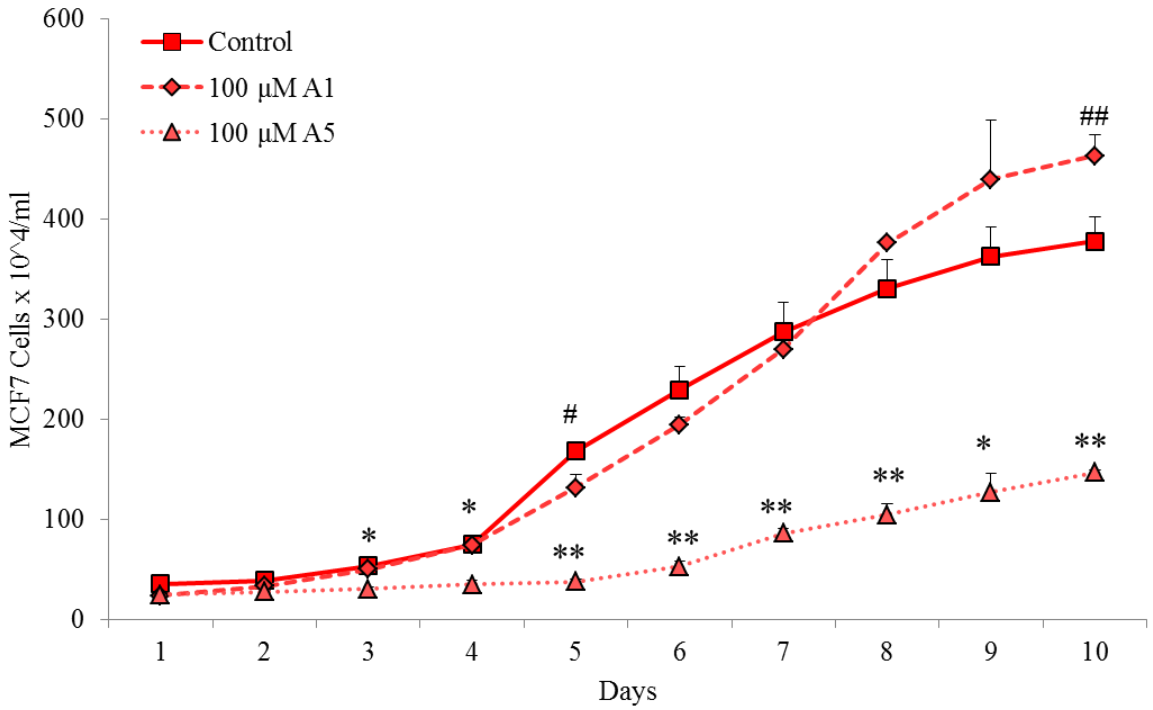

Figure 3-6: Effect of HSD10 inhibition on *in vitro* MCF7 cell growth. MCF7 wild-type cells were plated at a constant density and treated with either 100 µM A1 or 100 µM A5 HSD10 inhibitors. The cells were then grown and counted over the course of 10 days to determine cell growth rate. Growth curve of untreated control (■, solid line) versus either A1-treated (♦, dashed line) or A5-treated (▲, dotted line) displayed as cells x 10^4 per ml (n=4). Data presented as mean ± SE. #P<0.05, ##P<0.01 versus control group for A1 inhibitor; *P<0.001, **P<0.0001 versus control group for A5 inhibitor.

Studies with HSD10 inhibitors must be performed *in vivo* to assess the efficacy of HSD10 inhibition on reducing tumor formation and growth rate in animals. These experiments would provide clinically relevant data regarding the pharmacological capabilities of HSD10 inhibitors in cancer treatment.

Additionally, since blocking enzymes can yield different consequences as opposed to reducing protein, cell culture studies need to be completed to investigate the mechanism of action for the HSD10 inhibitors. TUNEL staining utilizing wild-type breast cancer cells, such as T47D, and the compounds will assess whether inhibition of HSD10 promotes cancer cell death.

This would suggest that the HSD10 inhibitors slow cancer cell growth rate and tumor formation by inducing cell death. If no significant changes are observed, cell-cycle analysis using flow cytometry should be used to determine if inhibition of HSD10 affects cell proliferation. This would indicate that the HSD10 inhibitors hinder cancer cell growth and tumor progression via slowing and/or blocking cell replication.

3.4. Interim Conclusion

Chapter 3 discussed future directions for the project investigating HSD10 in cancer progression. Using stably-transfected cells lines with HSD10 overexpression or HSD10 knockdown, it was recommended that all assays and experiments detailed in **Chapters 1** and **2** be performed in the human breast cancer cell lines. This will provide the necessary human-specific data for confirmation of the role of HSD10 in breast cancer.

Moreover, several mechanistic studies involving the interaction between HSD10 and CypD were outlined, including Co-IP, CypD translocation, and cell death assays utilizing HSD10-modified as well as CypD-modified human breast cancer cell lines. Further investigation into the relationship between HSD10 and CypD will elucidate the mechanism underlying the growth rate and cellular functional phenotypes initially observed in the PC-12 cells.

Finally, experiments with the HSD10 compounds were suggested, as they may produce clinically relevant data regarding the potential use of HSD10 inhibitors as anti-cancer therapeutics (**Fig. 3-7**). These studies would provide an important foundation for targeting HSD10 as a novel cancer treatment.

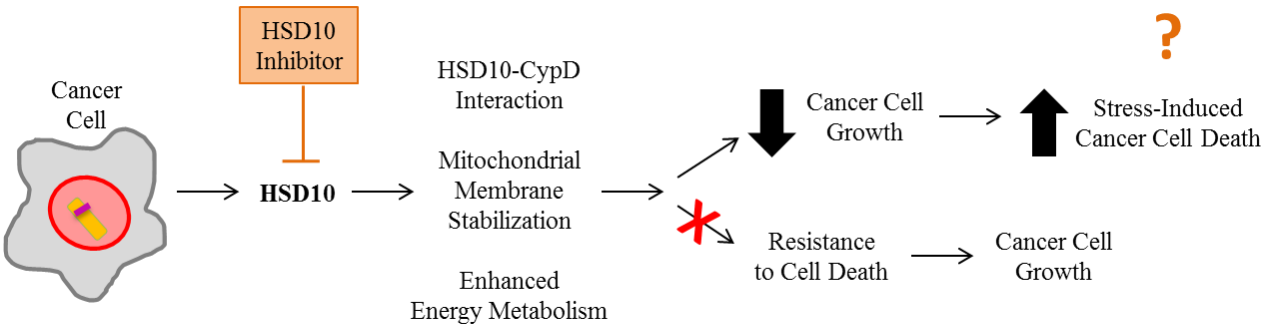

Figure 3-7: Chapter 3 summary of the future outlook for HSD10 inhibition in cancer. In cancer cells, HSD10 levels correlate with HSD10-CypD complex formation, mitochondrial membrane stabilization, and heightened energy production, which leads to cancer cell survival through enhanced cellular resistance to cell death. Upon HSD10 inhibition, cancer cell growth rate is reduced, possibly by increased cell death induction or reduced cell replication.

DISCUSSION

This study demonstrated for the first time that PC-12 pheochromocytoma cells overexpressing HSD10 grow significantly faster in cell culture and form larger tumors at a faster rate in SCID mice. It was theorized that HSD10 promotes enhanced cell growth through altered mitochondrial function, as enhanced complex IV enzyme activity and ATP production in PC-12 cells overexpressing HSD10 was observed. Knockdown of HSD10 negatively impacted PC-12 cell growth and mitochondrial function; all ETC complex activities were considerably reduced, as well as ATP generation. This diminished energy production is likely responsible for the reduced growth rate observed in cell culture. The possibility that HSD10 may confer protection in cancer cells was also evaluated. Upregulation of HSD10 permitted PC-12 cells to maintain a higher functional capacity with reduced cell death induction under chemical-induced oxidative stress. Knockdown of HSD10 reversed PC-12 cellular resistance capabilities, which led to heightened cell death induction under baseline and oxidative stress conditions.

Additionally, the mechanism of action underlying the phenotype observed following HSD10 modification was investigated by assessing the interaction of HSD10 with CypD. In HSD10-overexpressing PC-12 cells, enhanced complex formation was observed between HSD10 and CypD using co-IP, which possibly explains the lower cell death induction rate in cells with a surplus of HSD10. Knockdown of CypD in PC-12 cells overexpressing HSD10 resulted in a trend toward lower cell growth rate, but no changes in energy metabolism, suggesting that the slight decrease in proliferation is due to cell death. As expected, knockdown of CypD in PC-12 cells overexpressing HSD10 revealed an increase in cell death induction under oxidative stress conditions compared to matched control cells.

Next, this phenomenon was investigated in four human breast cancer cell lines in order to broaden the scope of cancers that are potentially influenced by HSD10. MCF10A breast cells, as well as MCF7 and MDA-MB-231 breast cancer cells were modified to overexpress HSD10, while T47D breast cancer cells were altered to lower HSD10 levels. Overexpression of HSD10 did not alter the growth rate of either the MCF10A or MDA-MB-231 cells. In MCF7 cells, HSD10 overexpression resulted in a slight trend toward increased cell growth rate, although not in a statistically significant way. Nevertheless, HSD10 knockdown significantly reduced T47D cell growth rate. Similar to the PC-12 cells, lowering of HSD10 levels in the T47D cells reduced complex IV enzyme activity and ATP production, indicating that the phenotype of HSD10 knockdown is sustained across two different cancers.

Taken together, these findings provide evidence that HSD10 mediates cancer cell growth and resistance to death-inducing environments via interaction with CypD. This section will provide a detailed discussion of the results in context with the current literature.

In Vivo Mouse Model

The use of an *in vivo* xenograft mouse model demonstrated that PC-12 HSD10-overexpressing cells grew faster and formed larger tumors over 32 days, as opposed to vector control tumors (**Fig. 1-4**). While there are limited *in vivo* xenograft studies involving PC-12 cells, Freed et al. revealed that following implantation of PC-12 cells into the striatum of Sprague-Dawley rats, the number of cells remained unchanged over 20 weeks without continued tumor growth (158). This is consistent with the minimal growth observed in PC-12 EV tumors and provides further support for the tumor-promoting capability of HSD10.

Due to the inability of PC-12 EV cells to form measureable tumors *in vivo*, it was unrealistic to establish a xenograft mouse model using PC-12 cells to assess the effect of HSD10 knockdown on tumor growth. While animal data is lacking for the effect of HSD10 knockdown on PC-12 tumor formation, the cell culture evidence strongly shows that reduction of HSD10 is accompanied by deficits in energy metabolism, cell growth, and resistance to cell death in PC-12 and T47D cells. Hence, it is predicted that HSD10 knockdown will limit tumor growth *in vivo*.

As outlined in **Chapter 3**, stable HSD10 knockdown in T47D cells would provide a suitable foundation for analysis of tumor growth *in vivo*, as this cell line forms consistent, slow-growing tumors within three to six months (164). The use of T47D cells is also highly recommended for *in vivo* studies assessing the efficacy of HSD10 inhibitors, as HSD10-overexpressing PC-12 cells showed little to no change in tumor growth between vehicle-treated and HSD10 inhibitor-treated animals (**Fig. 3-4**). As the PC-12 HSD10 overexpression cells demonstrate exceptionally high metabolic and replication rates, it is anticipated that the tumors will be largely unresponsive to HSD10 inhibition *in vivo*. Thus, this cell line is not a good choice for the additional *in vivo* studies pertaining to this project.

Effect of HSD10-Alteration on Cancer Cell Function

Cell Proliferation and Energy Metabolism

Typically, tumors exhibit increased cell proliferation compared to noncancerous tissues. Similarly, HSD10-overexpressing PC-12 cells demonstrated an enhanced cell growth rate in cell culture (**Fig. 1-3 A**). This phenomenon is likely due to altered processes within mitochondria, as large amounts of HSD10 localized with mitochondria in HSD10-overexpressing cells. Although the Warburg effect of elevated glycolytic ATP production in cancer cells is widely recognized (7), many groups have revealed that mitochondria in tumor cells are able to operate both respiratory pathways (34). As elevated ATP production was observed in HSD10-overexpressing cells (**Fig. 1-7**), it is possible that HSD10 provides additional energy metabolites for the cells.

Among its many functions, HSD10 is involved in the breakdown of fatty acids and branched chain amino acids, primarily isoleucine. In the isoleucine metabolism pathway, HSD10 catalyzes the NADH-dependent oxidation of 2-methyl-3-hydroxybutyryl-CoA to 2-methyl-acetoacetyl-CoA (115, **Schematic 8**). The end products, acetyl-CoA and propionyl-CoA, are then used in the TCA cycle to generate ATP.

β-oxidation is also a source of ketone bodies that can provide energy for the liver (170), heart (171), brain (172), and other organs when glucose levels are low. When glycolysis is inhibited, two acetyl-CoA molecules condense to form acetoacetyl-CoA, which then forms into the ketone bodies, acetoacetate and BHB (173). These substrates can then be taken up by mitochondria where they are reconverted to acetyl-CoA and used to fuel the TCA cycle (174). Although HSD10 does not play an essential role in ketone metabolism under physiological conditions, Yan et al. suggests that it may assist the mitochondrial enzyme normally responsible for BHB oxidation, β-hydroxybutyrat-dehydrogenase, under cellular stress situations (127).

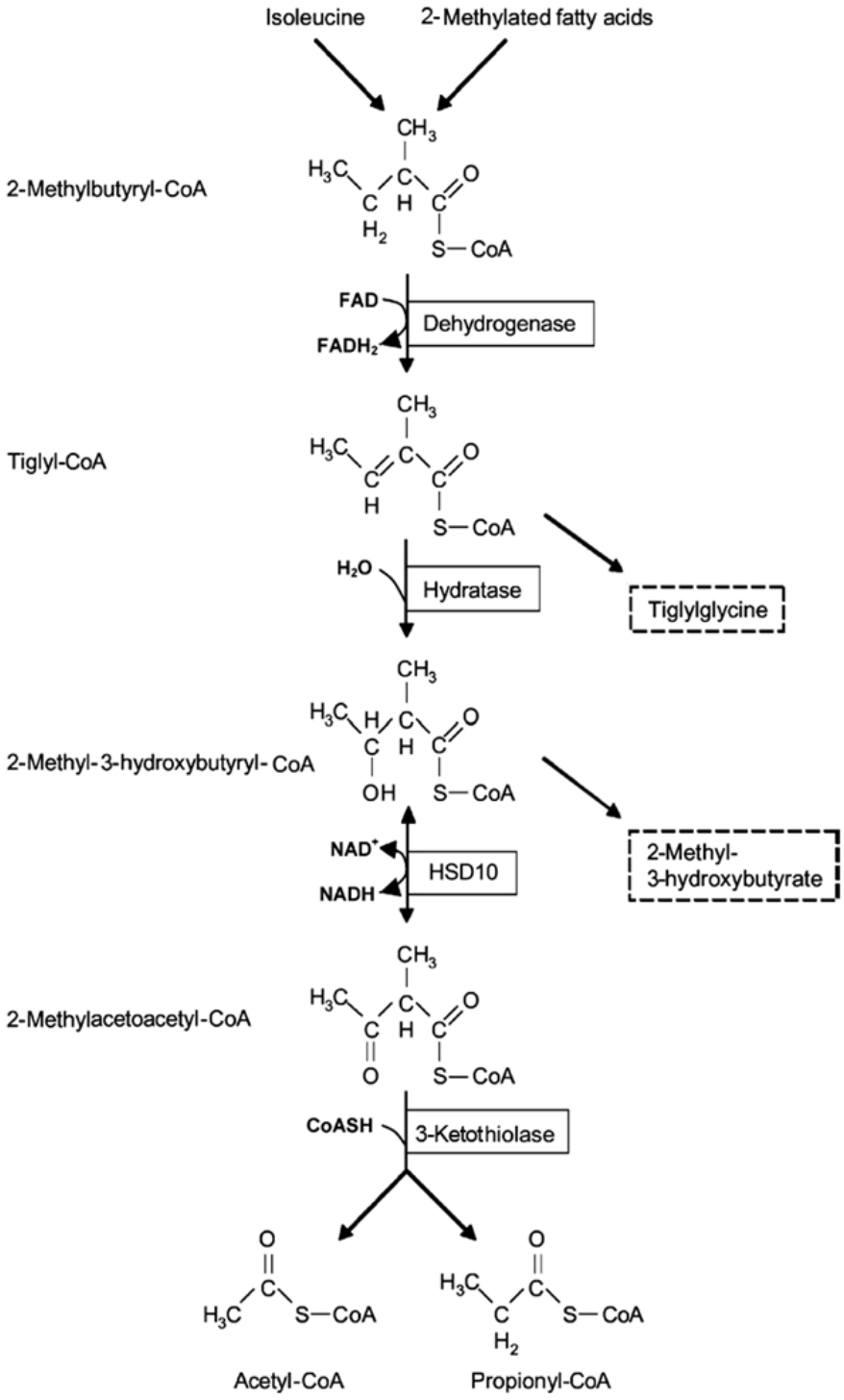

Schematic 8: Role of HSD10 in the isoleucine metabolism pathway. Isoleucine is metabolized in several steps via different enzymes. HSD10 catalyzes the NADH-dependent oxidation of 2-methyl-3-hydroxybutyryl-CoA to 2-methyl-acetoacetyl-CoA. End products are acetyl-CoA and propionyl-CoA which are vital substrates for other metabolic pathways involved in the production of ATP. Adapted from Zschocke, J. et al. (2000) *Pediatr Res* (113).

Studies have shown that tumor animal models utilize BHB as an energy source. For instance, Kallinowski et al. observed that BHB concentrations increased in the tumors of nude rats as tumor blood flow decreased (175). Additionally, Pavlides et al. recently discovered that BHB is upregulated in caveolin-1 null mice and proposed that epithelial cancer cells directly take in stromal-derived BHB to drive tumor progression and eventual metastasis (176). With cancer cells already displaying heightened ATP generation, the addition of another source of energy via the enzymatic capability of HSD10 would enhance energy production even further. This could lead not only to alterations in mitochondrial bioenergetics, but also to changes in mitochondrial signal transduction pathways, including resistance to cell death.

ETC complex IV enzyme activity was also increased in the PC-12 HSD10-overexpressing cells (**Fig. 1-5 D**), likely contributing to the ability of ATP synthase to generate additional ATP. The increase seen in complex IV, but not observed in complex I-III, could be attributed to the rate-limiting capability of complex IV (177). The enhanced energy production implies that mitochondrial processes are highly functional in the PC-12 cells with HSD10 overexpression. This was further verified by the consistent enzymatic activity of citrate synthase (**Fig. 1-8**) and enhanced mitochondrial membrane potential (**Fig. 1-9 B-C**). Hyperpolarization of the mitochondrial membrane in HSD10-overexpressing PC-12 cells would aid in the protection against membrane depolarization and cell death induction, thereby permitting mitochondria to continue generating energy to fuel cell growth.

Conversely, HSD10-underexpressing PC-12 and T47D cells both exhibited decreased cell growth rate in cell culture (**Fig. 1-3 B** and **Fig. 2-6 B**, respectively). This phenotype is likely due to the deficits observed in several mitochondrial processes. All ETC complex enzyme activities were significantly diminished following HSD10 knockdown in the PC-12 cells (**Fig. 1-5**), as

well as complex IV enzyme activity in the T47D HSD10-underexpressing cells (**Fig. 2-7 D**). Additionally, cellular ATP levels were reduced in the PC-12 HSD10 knockdown cells (**Fig. 1-7**) and T47D HSD10 knockdown cells (**Fig. 2-8**). Taken together, these findings indicate that reduction of HSD10 disrupts cancer cell mitochondrial function and structure.

Furthermore, loss of endogenous HSD10 could be considered a stressor in cancer cells, as it was accompanied by decreased citrate synthase enzyme activity in the PC-12 HSD10-underexpressing cells (**Fig. 1-8**). As citrate synthase is a pacemaker enzyme in the TCA cycle, it is commonly used as a quantitative marker enzyme to assess the content of intact mitochondria (178, 179). Therefore, the reduction in citrate synthase enzyme activity indicates that the PC-12 HSD10 knockdown cellular mitochondria are dysfunctional under baseline conditions. This was further confirmed after examination of the mitochondrial membrane potential using TMRM dye, which revealed that fewer PC-12 HSD10 knockdown mitochondria had intact membranes (**Fig. 1-9 D-E**). In accordance with other studies, TMRM provided accurate results under the non-quench mode used in the experiment (180-182). Thus, HSD10 reduction correlated with diminished energy production, which was likely caused by mitochondrial energy metabolism disruption and membrane potential loss.

Also, cell viability was examined using the MTT reduction assay, which utilizes the reduction of MTT by NADH in the cytoplasm to measure metabolic activity (183). It is presently understood that the amount of MTT formazan product is proportional to the number of living cells (184). No significant changes were observed between all PC-12 cell groups at baseline, although there was a slight trend toward decreased MTT reduction in HSD10 knockdown cells (**Fig. 1-9 A**). This result suggests that the changes seen in the ETC complexes and ATP production are due to differences in PC-12 cell growth rate, and not cell death induction.

However, the significance of the MTT reduction assay has been seriously questioned recently (185), as there is a high rate of variability, including undetected toxicity or false proliferation results (186). Such inconsistences are likely caused by variable assay conditions which can alter metabolic activity, and consequently the MTT dye reduction without affecting cell viability (187). Furthermore, changes in baseline and stress-induced cell death were observed in the PC-12 HSD10-transfected cells, calling into question the PC-12 MTT assay findings. Duplication of the experiment may provide insight into the MTT assay data, or it may yield inconstant results. Alternative cell viability assays that would likely provide more reliable results include the protease viability marker assay (188) and the ATP assay (189), which was utilized in this thesis.

Cellular Resistance to Stress Stimuli and Cell Death

In addition to heightened cell proliferation, tumors often display enhanced resistance to cell death when compared to noncancerous tissues. Correspondingly, HSD10-overexpressing PC-12 cells demonstrated increased resistance to oxidative stress-induced cell death (**Fig. 1-11 A-B**) compared to matched control cells. This phenotype is likely caused by the hyperpolarized mitochondrial membrane, which grants HSD10-overexpressing PC-12 mitochondria the ability to maintain higher functioning processes, such as energy metabolism (**Fig. 1-10 C-D**), during death-inducing situations compared to matched controls.

The MTT reduction assay was also used to assess cell viability under oxidative stress conditions, namely H_2O_2 and TBH (**Fig. 1-10 A** and **B**, respectively). The results were similar to the ETC complex IV enzyme activity data (**Fig. 1-10 C-D**), indicating that overexpression of HSD10 confers PC-12 cells protection against stress-induced cellular dysfunction. However, as

mentioned previously, the MTT assay as a viability assay is under debate (185, 186). Thus, it must be stated that the MTT results alone would be considered debatable. Nevertheless, the additional experiment examining complex IV enzyme activity under stress conditions provides further support for the resistance phenotype of the PC-12 HSD10 overexpression cells.

While the TUNEL assay is a well-accepted histological method for cytotoxicity via detection of apoptotic cells (190), it has various limitations. For instance, cells undergoing active gene transcription can yield false-positive TUNEL results (191). Also, several studies have shown that TUNEL cannot always distinguish between cells undergoing apoptosis and necrosis (192, 193). Hence, other cytotoxicity assays, such as caspase-3 activity (194) or Annexin V (195), should be used in combination with TUNEL to validate apoptotic cell death. Additionally, it would be beneficial to evaluate whether HSD10 overexpression impacts necrotic cell death, thus determining the favored cell death pathway involved. The measurement of LDH release is a useful approach for the detection of necrosis, and would provide the necessary evidence pertaining to which cell death pathway is involved in the HSD10-modificed cells (196). Likewise, autophagy should be examined in relation to HSD10-modification, as many cancer cells exhibit defective autophagy which can promote tumor growth despite cellular stress (197). Immunoblotting and immunofluorescence can be employed to detect the endogenous levels of autophagy-related proteins, including LC3-I, LC3-II, and Beclin-1. Inhibitors, such as Bafilomycin A1, which block the degradation of autolysosome content, should also be used to assess autophagic flux (198).

On the contrary, HSD10-underexpressing PC-12 cells exhibited decreased resistance to oxidative stress-induced cell death (**Fig. 1-11 C-D**), conceivably due to deficits in the mitochondrial membrane potential and energy metabolism. Indeed, PC-12 cells with HSD10

knockdown displayed reduced complex IV enzyme activity under both baseline and oxidative stress conditions (**Fig. 1-10 E**), providing additional evidence that reduction of HSD10 disrupts cancer cell mitochondrial function and cell death resistance capabilities.

Similar to the PC-12 HSD10 overexpression data, additional cytotoxicity experiments are necessary to confirm the increased stress-induced apoptotic induction shown by TUNEL staining in the PC-12 HSD10 knockdown cells. Also, an LDH release assay would provide evidence as to whether the necrotic cell death pathway is implicated following HSD10 knockdown. Furthermore, the endogenous levels of autophagy-related proteins should be examined via immunoblotting and immunofluorescence to investigate if autophagy is impacted by HSD10 knockdown. Moreover, an MTT assay was not performed to assess cell viability in the PC-12 HSD10-underexpressing cells treated with H_2O_2. While the MTT assay alone may have limitations, it would further solidify the complex IV enzyme activity findings. Other cell viability assays, such as the protease viability marker assay previously mentioned, would also provide added support.

Overall, the PC-12 cellular data indicate that HSD10 is an important component underlying cancer cell resistance to cell death. Upon the introduction of a death-inducing stimulus, cancer cells with an abundance of HSD10 remain highly functional (**Schematic 9.1**) and less susceptible to cell death (**Schematic 9.2**). In contrast, cancer cells with low levels of HSD10 are more prone to mitochondrial dysfunction (**Schematic 9.3**) and less resistant to cell death induced by stress (**Schematic 9.4**).

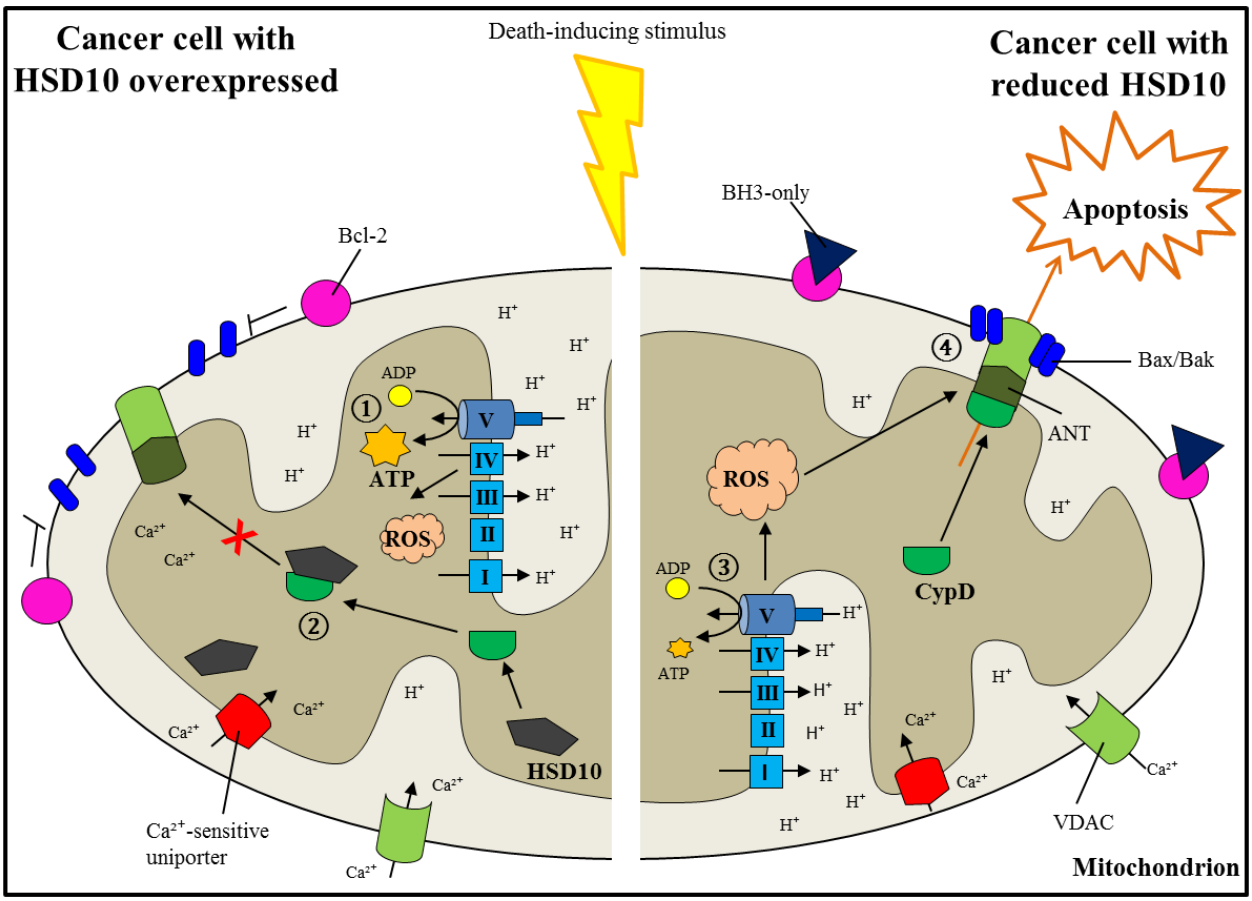

Schematic 9: Consequence of HSD10 expression in cancer cells under death-inducing conditions. Cancer cells overexpressing HSD10 are **1)** able to maintain a high state of energy metabolism and **2)** prevent MPTP-mediated apoptosis via interaction with CypD under oxidative stress situations. Conversely, cancer cells with reduced levels of HSD10 are **3)** unable to produce sufficient energy and **4)** succumb to cell death induced by CypD translocation in an oxidative stress environment.

Role of HSD10-CypD Interaction in Cancer

In **Chapter 1**, it was proposed that the phenotype observed in the PC-12 HSD10 overexpression cells was caused by increased binding with CypD. In the PC-12 cells, CypD protein levels remained constant despite overexpression of HSD10 (**Fig. 1-12 A-B**). This result was rather unexpected as CypD is often overexpressed in certain cancers (83, 160). Theoretically, overexpression of HSD10 would have a limited effect on CypD expression, as CypD protein is already abundant in cancer cells. Furthermore, Co-IP revealed an enhanced interaction between HSD10 and CypD in PC-12 HSD10-overexpressing cells compared to match control cells under baseline conditions (**Fig. 1-14**). Due to the evidence demonstrating that the PC-12 HSD10-overexpressing cells were more resilient against stress-induced cell death, assessing the effect of oxidative stress on the HSD10-CypD interaction would strengthen the role of HSD10 and CypD in cancer progression and aggressiveness.

Co-IP is a commonly used method for examining protein-protein interactions (199, 200); however, it has a few limitations that must be addressed. For instance, the use of complex mixtures, instead of purified proteins, can make it difficult to determine that the two proteins-of-interest bind to one another directly (201). Moreover, Co-IP cannot yield quantitative data pertaining to the affinity of interactions (202). Also, Co-IP data has been mainly used for detection of interactions between pairs of proteins, not co-complex relationships. Geva et al. recently devised a novel way for analyzing whole protein complex detection from Co-IP results by detecting sets of prey that co-associate with the same set of baits (203). As both HSD10 and CypD have been shown to bind other factors, this method would provide important information regarding a possible complex formation involving HSD10, CypD, and other factors, such as Bcl-2 (58), HK-II (59), or ER (150).

In contrast to the unchanged expression in the PC-12 HSD10-overexpressing cells, knockdown of HSD10 correlated with reduced CypD protein expression (**Fig. 1-12 C-D**), which indicates that CypD levels are negatively affected by HSD10 reduction in cancer cells. Since the TUNEL assay demonstrated that the PC-12 HSD10 knockdown cells were more vulnerable to both baseline and stress-induced cell death, Co-IPs would be essential for evaluation of the effect of HSD10 knockdown at baseline and under oxidative stress conditions on the HSD10-CypD interaction. Performing Co-IPs in the PC-12 cells with HSD10 reduction would provide necessary data to further elucidate the role of HSD10 and CypD in cancer.

Next, the effect of CypD knockdown in the PC-12 HSD10-overexpressing cells was investigated. Reduction of CypD was accompanied by a decrease in HSD10 protein content in the PC-12 HSD10 overexpression cells (**Fig. 1-15 A-B**), matching the previously mentioned results showing that HSD10 reduction correlates with reduced CypD expression in wild-type PC-12 cells. This data strengthens the hypothesis that HSD10 and CypD are connected in cancer. However, knockdown of CypD did not significantly alter PC-12 HSD10-overexpressing cell growth (**Fig. 1-16**), although a small trend toward decreased growth rate was observed. This data suggests that HSD10 could be a potential upstream modulator controlling CypD-induced mitochondrial perturbation.

Several explanations are possible for this result. First, it is likely that the PC-12 HSD10-overexpression cells are a poor model for assessing the role of factors other than HSD10. The extreme proliferative capabilities observed in this particular cell line are undoubtedly promoted by the artificial overexpression of HSD10 itself. Wild-type PC-12 cells would provide a favorable alternative for the evaluation of CypD knockdown, as HSD10 levels would be natural. Second, it is possible that the use of siRNA to knockdown CypD was ineffective for the duration

of the cell growth curve experiment (166). While the small difference in growth rate between the control and CypD knockdown cells is observed, it does not shift further apart, suggesting that the siRNA-mediated gene silencing may not be effective. For a short-term experiment, lentiviral transfection using shRNA to knockdown CypD could be employed to determine the effect on cell growth rate (167). Third, it is feasible that CypD knockdown does not affect cell growth rate due to intracellular changes. Mitochondrial bioenergetics and/or signal transduction pathways, such as apoptosis, may be altered upon CypD knockdown as a compensatory mechanism to maintain mitochondrial function and protect the affected cancer cells.

As there was a trend, but no significant difference, toward decreased cell growth rate following CypD knockdown in the PC-12 HSD10-overexpressing cells, it was not surprising that cellular energy metabolism processes were unaffected (**Fig. 1-17 A-B**). Since CypD is involved in cell death induction, it is possible that loss of CypD does not directly impact the mitochondrial energy production processes. Recently, several groups have discovered that CypD deficiency prevents diet-induced obesity by increasing glucose metabolism and ATP production in mice (204, 205). Additionally, Shulga et al. demonstrated that inactivation of CypD promotes the detachment of HKII from the MPTP, leading to the stimulation of mitochondrial bioenergetics in cancer cells (206). This evidence suggests that knockdown of CypD promotes mitochondrial bioenergetics, thereby providing an additional explanation for the consistently high, unaltered energy metabolic results. Furthermore, the HSD10 overexpression phenotype of the PC-12 cell line aids in the maintenance of high functioning mitochondrial bioenergetics, in addition to the consequence of CypD knockdown. As these mitochondria are already functioning at a higher capacity than wild-type PC-12 cells, it is logical that knockdown of CypD would not provide a synergistic affect.

The energy metabolism results indicate that despite the reduction of CypD, the PC-12 HSD10-overexpressing cells still exhibit similar functional rates, which correlate with similar cell growth rates. However, since a small trend toward decreased cell growth rate was observed in the CypD knockdown cells, a TUNEL assay was performed to examine cell death induction. The control PC-12 HSD10-overexpressing cells and CypD knockdown PC-12 HSD10-overexpressing cells both showed low percentages of apoptotic cells at baseline (**Fig. 1-18 B**). The CypD knockdown group exhibited a slight trend toward increased cell death induction versus the control group, although this trend was not statistically significant. However, despite the lack of statistical significance, the trend of slightly increased cell death under baseline conditions matches the trend of marginally lowered cell growth rate at baseline for the CypD knockdown PC-12 HSD10-overexpressing cells. Thus, it is logical that the slightly reduced cell growth rate is due to a minor elevation in cell death induction, at baseline conditions.

Under an oxidative stress situation, reduction of CypD rendered the PC-12 HSD10-overexpressing cells more vulnerable to cell death induction in comparison to the control PC-12 HSD10-overexpressing cells (**Fig. 1-18 B**). This indicates that regardless of the presence of HSD10, the PC-12 cells with less CypD were more susceptible to stress-induced apoptosis. However, this phenomenon is a bit incongruous with the overall hypothesis of this thesis. If CypD levels are reduced, theoretically, HSD10 levels are reduced to a similar degree, as demonstrated via immunoblotting (**Fig. 1-15 B**). Logically, the remaining CypD may still be bound to HSD10, thereby preventing CypD from inducing MPTP-mediated cell death. However, increased cell death is observed under stress conditions following CypD and HSD10 lowering. One possibility is that small amounts of unbound CypD are able to translocate to the IM and

induce cell death (**Schematic 10.2**). This is logical, as HSD10 is able to bind to many different substrates, thereby providing CypD with a limited opportunity to function independently.

Alternatively, the results advocate a different mechanism of action that involves a super-complex of proteins. As CypD interactions with other proteins, such as Bcl-2 (58) and HK-II (59), have been observed to prevent apoptosis in cancer cells, it is possible that a super-complex exists between HSD10, CypD, Bcl-2, HK-II, and potentially other mitochondrial proteins (**Schematic 10.1**). For example, if the expression of HK-II is unchanged when HSD10 and CypD levels are reduced, it is hypothetical that unbound HK-II molecules are able to induce pro-apoptotic Bax/Bak-mediated cell death under stress situations (**Schematic 10.3**). Co-IPs would be necessary to investigate the possibility of a super-complex between these proteins, prior to additional exploration of its role in cancer progression and cell death induction.

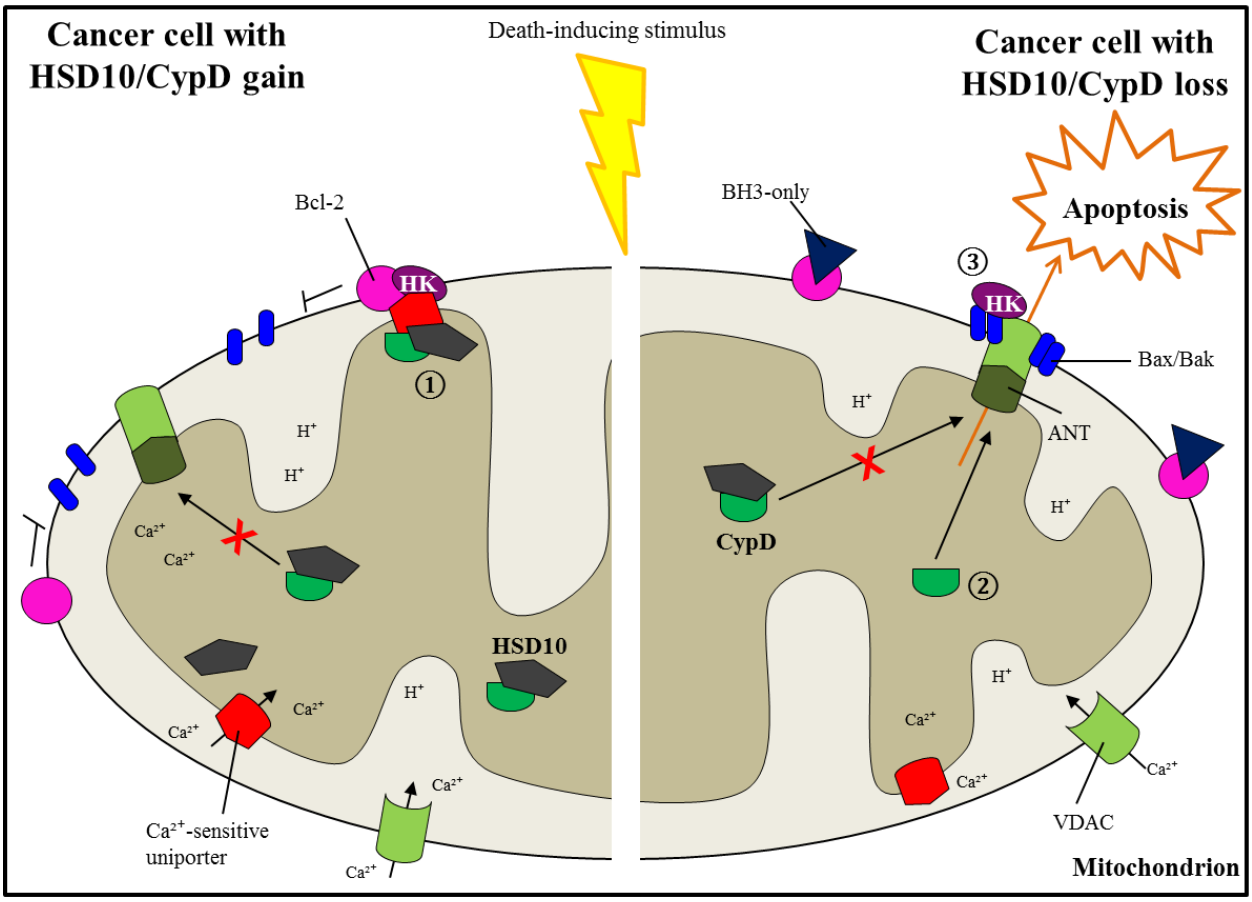

Schematic 10: Hypothetical super-complex of HSD10, CypD, Bcl-2, HK-II, and/or other proteins. Cancer cells overexpressing HSD10 and CypD are **1)** able to form a super-complex with Bcl-2, HK-II, and possibly other proteins to prevent apoptosis under death-inducing conditions. In the event of HSD10 and CypD protein loss in cancer cells, **2)** other components of the super-complex are released, such as HK-II, which can mediate cell death induction in response to a death-inducing stimulus.

Potential Role of HSD10-ER Interaction in Breast Cancer

It was postulated in **Chapter 2** that the unchanged phenotype of the MDA-MB-231 breast cancer cells after lentiviral HSD10 overexpression (**Fig. 2-6 C**) was due to the triple negative status of the cell line. MDA-MB-231 cells do not express ERs, progesterone receptors, or human epidermal growth factor receptor 2 (207). As HSD10 belongs to the HSD17B family which catalyzes the interconversion of dehydroepiandrosterone (DHEA) to androstanediol (adiol), androstenedione to testosterone, and estrone to E2, respectively (208, **Schematic 10**), it is possible that the role of HSD10 in cancer progression is specific to hormone-related tumors.

Currently, four publications have examined HSD10 in cancer. He et al. demonstrated that certain malignant prostate cells with increased HSD10 expression are able to generate higher amounts of dihydrotestosterone (DHT) from adiol, compared to control cells (118). Since DHT is the most potent androgen, HSD10 overexpression may promote prostate cancer growth via the favored conversion of adiol to DHT. Additionally, Salas et al. found that HSD10 gene expression was up-regulated in osteosarcoma patients categorized as poor responders to chemotherapy (148). Androgens and estrogens have been linked with bone tumor incidence (209-211), indicating a role for HSD10 with steroids in a variety of cancer types. Connecting these findings, Jernberg et al. showed that prostate-to-bone metastases expressed higher levels of HSD10 compared to non-malignant prostate and primary prostate tumor tissue (149), which may provide cells with the capacity to convert larger quantities of androgens into more potent androgens, thus promoting cancer growth and aggressiveness.

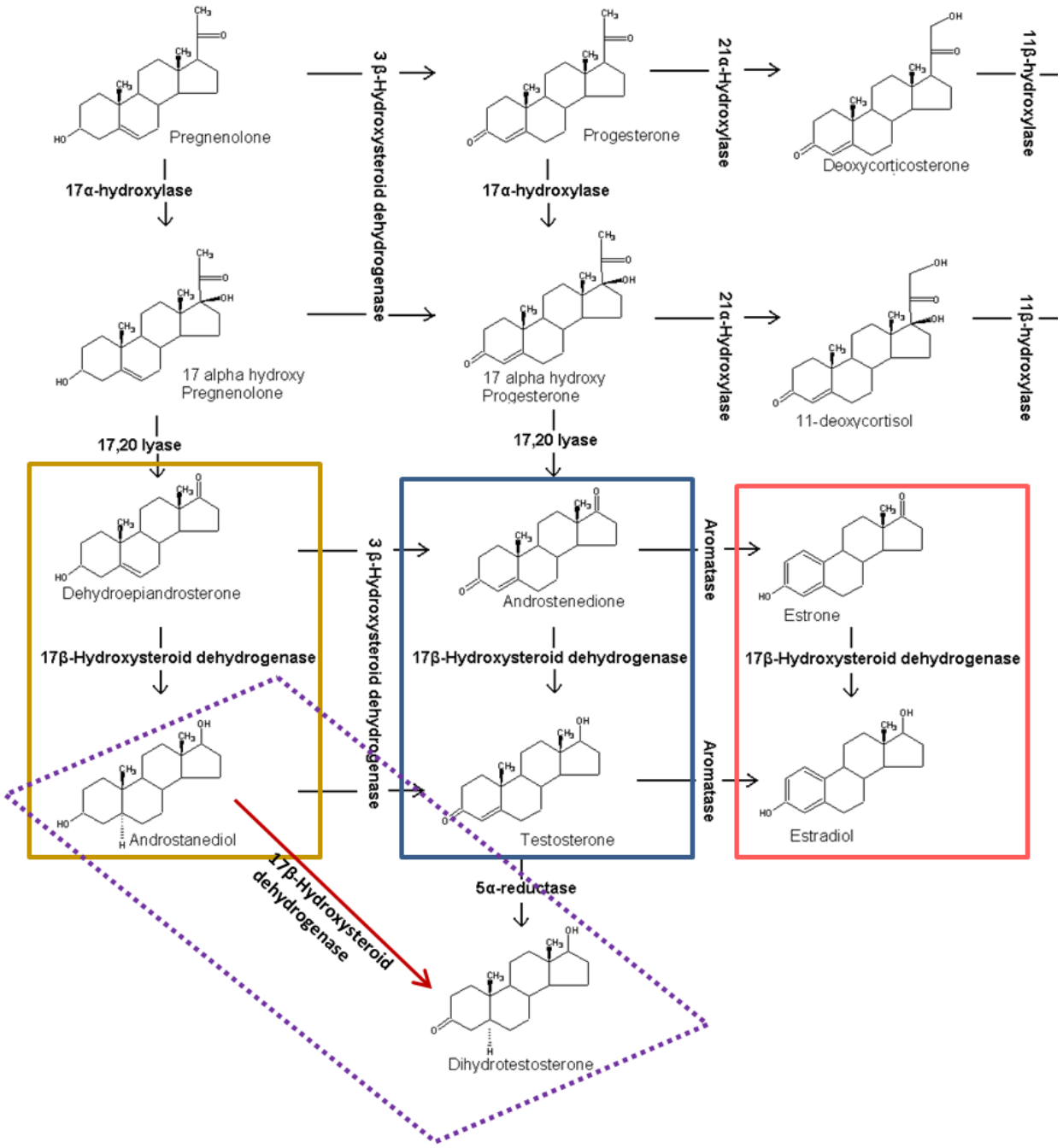

Schematic 11: Role of HSD10 in the steroidogenesis pathway. During steroidogenesis, members of the HSD17B family catalyze the interconversion of dehydroepiandrosterone (DHEA) to androstanediol (adiol; gold bar), androstenedione to testosterone (blue bar), and estrone to estradiol (E2; pink bar). The HSD17B family can also catalyze the oxidation of adiol to dihydrotestosterone (DHT; purple dotted bar). Adapted from Häggström, M. (2014) *Wiki J Med* (212).

Lastly, Carlson et al. demonstrated that PC-12 cells overexpressing HSD10 exhibit increased cell growth rate and resistance to stress-induced cell death (152). PC-12 cells do not express ERα (213); nevertheless, ERβ protein has been detected in the cells, albeit minimal expression (214). Interestingly, it was previously discovered by Nilsen et al. that PC-12 cells express both ERα and ERβ upon nerve growth factor treatment (215), suggesting that cell stimulation could induce ER expression. Moreover, Charalampopoulos et al. showed that androgen receptors specific for DHEA are present on the membrane surface of PC-12 cells (216), providing further evidence for an involvement of HSD10 with steroids in cancer.

Since the future goal of the project is to examine HSD10 in breast cancer, the remainder of this section will predominantly focus on the potential role of estrogen with HSD10. While both ER subtypes are expressed in the cardiovascular system, immune system, nervous system, and reproductive system of humans, ERα is predominantly expressed in the reproductive system (217) whereas ERβ is largely expressed in the nervous system (218). Of the four breast cancer cell lines used in this dissertation, T47D and MCF7 cells are ER-positive (219), while MCF10A and MDA-MB-231 cells are ER-negative (220).

It is widely recognized that estrogens play a major role in promoting breast epithelial cell proliferation (221, 222). Accordingly, the role of estrogen as a breast carcinogen is under active investigation. It has been postulated that estrogens induce tumorigenic effects through binding to ERα (223). Acting through ERα would allow estrogens to exert a potent stimulus on breast cell growth via actions on the enhanced production of growth factors (224). However, as reported in a recent study, ERα knockout mice expressing the Wnt-1 oncogene still developed mammary tumors, indicating that estrogens may cause breast cancer through a non-ERα-mediated mechanism, such as genotoxicity (225, 226).

As specified, HSD17B catalyzes the interconversion of estrone and E2 (208). A highly potent estrogen, the carcinogenicity of E2 has been successfully demonstrated by the transformation of human breast epithelial cells (227, 228). This supports the concept that E2 can act as a carcinogenic agent without the presence of ERα. Nevertheless, it is possible that ERβ or other mechanisms could play a role in the transformation of human breast epithelial cells.

HSD10 was observed to bind to ERα in rat cardiomyocyte mitochondria (150), which inhibited the conversion of E2 to estrone. It is possible that in breast cancer cells, as well as other hormone-dependent cancers, HSD10 forms a complex with ERα, thereby disrupting the conversion of highly toxic E2 to less potent estone. Without free HSD10 to catalyze the reaction, E2 accumulates in the breast cancer cells and stimulates uncontrolled cell proliferation. This event may underlie hormone-dependent cancer cell growth, which may provide a novel avenue for hormone therapy involving HSD10. Further research is necessary to specify which ERs HSD10 is able to interact with in cancer cells to investigate this theory.

Concluding Remarks

The results presented in this thesis provide a promising platform for further research to elucidate the mechanism underlying HSD10-mediated cancer cell growth and cell death resistance. As HSD10 overexpression granted pheochromocytoma cells enhanced cellular proliferative and cell death resistant capabilities, targeted inhibition of HSD10 in cancer cells may provide a novel treatment method. Furthermore, since lowering of HSD10 in pheochromocytoma cells was accompanied by increased vulnerability to stress-induced apoptosis, simultaneous application of a HSD10-specific inhibitor with current anti-cancer therapies that induce cell death may afford an effective combinatorial treatment. Classic options of cytotoxic agents include cisplatin (229), etoposide (230), paclitaxel (231), or doxorubicin (232). Also, CypD knockdown in pheochromocytoma cells with overexpression of HSD10 rendered the cells more susceptible to stress-induced cell death; thus, manipulation of CypD may deliver an additional way of treating cancer patients.

Furthermore, after verifying that HSD10 is important in rat adrenal gland tumor cell growth, the subsequent step was to investigate its role in human cancers. HSD10 knockdown reduced T47D breast cancer cell growth rate and was accompanied by decreased energy production, providing a compelling start toward examining HSD10 in human breast cancer. The effect of HSD10 in breast cancer development will be especially compelling as HSD10 is able to regulate estrogen steroidogenesis (125). Furthermore, fellow HSD10 family member HSD17B type 1 was discovered as a novel target for endocrine therapy in certain breast cancer patients (233-235). Thus, evaluating the effect of HSD10 on human cancers would then provide vital information as to its translational implications as a biomarker and/or treatment target.

REFERENCES

1. Stewart, B.W., and Wild, C.P. (2014) World Cancer Report 2014. *International Agency for Research on Cancer Nonserial Publication, World Health Organization Press*: 1-630.
2. Siegel, R., Naishadham, D., and Jemal, A. (2013) Cancer statistics, 2013. *CA: A Cancer Journal for Clinicians* **63**, 11-30.
3. Kim, J. J., and Tannock, I. F. (2005) Repopulation of cancer cells during therapy: an important cause of treatment failure. *Nature Reviews: Cancer* **5**, 516-525.
4. Land, H., Parada, L. F., and Weinberg, R. A. (1983) Tumorigenic conversion of primary embryo fibroblasts requires at least two cooperating oncogenes. *Nature* **304**, 596-602.
5. Herman, J. G., Latif, F., Weng, Y., Lerman, M. I., Zbar, B., Liu, S., Samid, D., Duan, D. S., Gnarra, J. R., Linehan, W. M., and et al. (1994) Silencing of the VHL tumor-suppressor gene by DNA methylation in renal carcinoma. *Proceedings of the National Academy of Sciences of the United States of America* **91**, 9700-9704.
6. Masutani, C., Kusumoto, R., Yamada, A., Yuasa, M., Araki, M., Nogimori, T., Yokoi, M., Eki, T., Iwai, S., and Hanaoka, F. (2000) Xeroderma pigmentosum variant: from a human genetic disorder to a novel DNA polymerase. *Cold Spring Harbor Symposia on Quantitative Biology* **65**, 71-80.
7. Warburg, O. (1956) On respiratory impairment in cancer cells. *Science* **124**, 269-270.
8. Tang, H. L., Yuen, K. L., Tang, H. M., and Fung, M. C. (2009) Reversibility of apoptosis in cancer cells. *British Journal of Cancer* **100**, 118-122.
9. Wallace, D. C. (2012) Mitochondria and cancer. *Nature Reviews: Cancer* **12**, 685-698.

10. Perkins, G., Renken, C., Martone, M. E., Young, S. J., Ellisman, M., and Frey, T. (1997) Electron tomography of neuronal mitochondria: three-dimensional structure and organization of cristae and membrane contacts. *Journal of Structural Biology* **119**, 260-272.

11. Imanishi, H., Hattori, K., Wada, R., Ishikawa, K., Fukuda, S., Takenaga, K., Nakada, K., and Hayashi, J. (2011) Mitochondrial DNA mutations regulate metastasis of human breast cancer cells. *PloS One* **6**, doi: 10.1371/journal.pone.0023401.

12. Shidara, Y., Yamagata, K., Kanamori, T., Nakano, K., Kwong, J. Q., Manfredi, G., Oda, H., and Ohta, S. (2005) Positive contribution of pathogenic mutations in the mitochondrial genome to the promotion of cancer by prevention from apoptosis. *Cancer Research* **65**, 1655-1663.

13. Ma, Y., Bai, R. K., Trieu, R., and Wong, L. J. (2010) Mitochondrial dysfunction in human breast cancer cells and their transmitochondrial cybrids. *Biochimica et Biophysica Acta* **1797**, 29-37.

14. Warburg, O. (1956) On the origin of cancer cells. *Science* **123**, 309-314.

15. Anderson, S., Bankier, A. T., Barrell, B. G., de Bruijn, M. H., Coulson, A. R., Drouin, J., Eperon, I. C., Nierlich, D. P., Roe, B. A., Sanger, F., Schreier, P. H., Smith, A. J., Staden, R., and Young, I. G. (1981) Sequence and organization of the human mitochondrial genome. *Nature* **290**, 457-465.

16. Chang, D. D., and Clayton, D. A. (1985) Priming of human mitochondrial DNA replication occurs at the light-strand promoter. *Proceedings of the National Academy of Sciences of the United States of America* **82**, 351-355.

17. Tseng, L. M., Yin, P. H., Chi, C. W., Hsu, C. Y., Wu, C. W., Lee, L. M., Wei, Y. H., and Lee, H. C. (2006) Mitochondrial DNA mutations and mitochondrial DNA depletion in breast cancer. *Genes, Chromosomes and Cancer* **45**, 629-638.

18. Mambo, E., Chatterjee, A., Xing, M., Tallini, G., Haugen, B. R., Yeung, S. C., Sukumar, S., and Sidransky, D. (2005) Tumor-specific changes in mtDNA content in human cancer. *International Journal of Cancer* **116**, 920-924.

19. Chihara, N., Amo, T., Tokunaga, A., Yuzuriha, R., Wolf, A. M., Asoh, S., Suzuki, H., Uchida, E., and Ohta, S. (2011) Mitochondrial DNA alterations in colorectal cancer cell lines. *Journal of Nippon Medical School = Nippon Ika Daigaku Zasshi* **78**, 13-21.

20. Yin, P. H., Wu, C. C., Lin, J. C., Chi, C. W., Wei, Y. H., and Lee, H. C. (2010) Somatic mutations of mitochondrial genome in hepatocellular carcinoma. *Mitochondrion* **10**, 174-182.

21. Sanchez-Cespedes, M., Parrella, P., Nomoto, S., Cohen, D., Xiao, Y., Esteller, M., Jeronimo, C., Jordan, R. C., Nicol, T., Koch, W. M., Schoenberg, M., Mazzarelli, P., Fazio, V. M., and Sidransky, D. (2001) Identification of a mononucleotide repeat as a major target for mitochondrial DNA alterations in human tumors. *Cancer Research* **61**, 7015-7019.

22. Nomoto, S., Yamashita, K., Koshikawa, K., Nakao, A., and Sidransky, D. (2002) Mitochondrial D-loop mutations as clonal markers in multicentric hepatocellular carcinoma and plasma. *Clinical Cancer Research: An Official Journal of the American Association for Cancer Research* **8**, 481-487.

23. Miyazono, F., Schneider, P. M., Metzger, R., Warnecke-Eberz, U., Baldus, S. E., Dienes, H. P., Aikou, T., and Hoelscher, A. H. (2002) Mutations in the mitochondrial DNA D-Loop region occur frequently in adenocarcinoma in Barrett's esophagus. *Oncogene* **21**, 3780-3783.

24. Bai, R. K., Chang, J., Yeh, K. T., Lou, M. A., Lu, J. F., Tan, D. J., Liu, H., and Wong, L. J. (2011) Mitochondrial DNA content varies with pathological characteristics of breast cancer. *Journal of Oncology* **2011**, doi: 10.1155/2011/496189.

25. Yu, M., Zhou, Y., Shi, Y., Ning, L., Yang, Y., Wei, X., Zhang, N., Hao, X., and Niu, R. (2007) Reduced mitochondrial DNA copy number is correlated with tumor progression and prognosis in Chinese breast cancer patients. *IUBMB Life* **59**, 450-457.

26. McCormack, J. G. (1985) Characterization of the effects of Ca2+ on the intramitochondrial Ca2+-sensitive enzymes from rat liver and within intact rat liver mitochondria. *Biochemical Journal* **231**, 581-595.

27. Yankovskaya, V., Horsefield, R., Tornroth, S., Luna-Chavez, C., Miyoshi, H., Leger, C., Byrne, B., Cecchini, G., and Iwata, S. (2003) Architecture of succinate dehydrogenase and reactive oxygen species generation. *Science* **299**, 700-704.

28. McCormack, J. G., Halestrap, A. P., and Denton, R. M. (1990) Role of calcium ions in regulation of mammalian intramitochondrial metabolism. *Physiological Reviews* **70,** 391-425.

29. Takehara, Y., Kanno, T., Yoshioka, T., Inoue, M., and Utsumi, K. (1995) Oxygen-dependent regulation of mitochondrial energy metabolism by nitric oxide. *Archives of Biochemistry and Biophysics* **323**, 27-32.

30. Nalin, C. M., and Cross, R. L. (1982) Adenine nucleotide binding sites on beef heart F1-ATPase. Specificity of cooperative interactions between catalytic sites. *Journal of Biological Chemistry* **257**, 8055-8060.

31. Carlson, E. A., Rao, V. K., and Yan, S. S. (2013) From a cell's viewpoint: targeting mitochondria in Alzheimer's disease. *Drug Discovery Today: Therapeutic Strategies* **10**, doi: 10.1016/j.ddstr.2014.04.002.

32. Domenis, R., Bisetto, E., Rossi, D., Comelli, M., and Mavelli, I. (2012) Glucose-modulated mitochondria adaptation in tumor cells: a focus on ATP synthase and inhibitor factor 1. *International Journal of Molecular Sciences* **13**, 1933-1950.

33. Isidoro, A., Martinez, M., Fernandez, P. L., Ortega, A. D., Santamaria, G., Chamorro, M., Reed, J. C., and Cuezva, J. M. (2004) Alteration of the bioenergetic phenotype of mitochondria is a hallmark of breast, gastric, lung and oesophageal cancer. *Biochemical Journal* **378**, 17-20.

34. Bellance, N., Benard, G., Furt, F., Begueret, H., Smolkova, K., Passerieux, E., Delage, J. P., Baste, J. M., Moreau, P., and Rossignol, R. (2009) Bioenergetics of lung tumors: alteration of mitochondrial biogenesis and respiratory capacity. *International Journal of Biochemistry and Cell Biology* **41**, 2566-2577.

35. Weber, K., Ridderskamp, D., Alfert, M., Hoyer, S., and Wiesner, R. J. (2002) Cultivation in glucose-deprived medium stimulates mitochondrial biogenesis and oxidative metabolism in HepG2 hepatoma cells. *Biological Chemistry* **383**, 283-290.

36. Smolkova, K., Bellance, N., Scandurra, F., Genot, E., Gnaiger, E., Plecita-Hlavata, L., Jezek, P., and Rossignol, R. (2010) Mitochondrial bioenergetic adaptations of breast cancer cells to aglycemia and hypoxia. *Journal of Bioenergetics and Biomembranes* **42**, 55-67.

37. Rodriguez-Enriquez, S., Carreno-Fuentes, L., Gallardo-Perez, J. C., Saavedra, E., Quezada, H., Vega, A., Marin-Hernandez, A., Olin-Sandoval, V., Torres-Marquez, M. E., and Moreno-Sanchez, R. (2010) Oxidative phosphorylation is impaired by prolonged hypoxia in breast and possibly in cervix carcinoma. *International Journal of Biochemistry and Cell Biology* **42**, 1744-1751.

38. Carlson, E. A., and Yan, S. S. (2014) Disrupting cancer cell function by targeting mitochondria. *Integrative Cancer Science and Therapeutics* **1**, doi: 10.15761/ ICST.1000105.

39. Turrens, J. F. (2003) Mitochondrial formation of reactive oxygen species. *Journal of Physiology* **552**, 335-344.

40. McCord, J. M., and Fridovich, I. (1969) Superoxide dismutase. An enzymic function for erythrocuprein (hemocuprein). *Journal of Biological Chemistry* **244**, 6049-6055.

41. Mutisya, E. M., Bowling, A. C., and Beal, M. F. (1994) Cortical cytochrome oxidase activity is reduced in Alzheimer's disease. *Journal of Neurochemistry* **63**, 2179-2184.

42. Young-Collier, K. J., McArdle, M., and Bennett, J. P. (2012) The dying of the light: mitochondrial failure in Alzheimer's disease. *Journal of Alzheimer's Disease: JAD* **28**, 771-781.

43. Sawyer, D. E., Roman, S. D., and Aitken, R. J. (2001) Relative susceptibilities of mitochondrial and nuclear DNA to damage induced by hydrogen peroxide in two mouse germ cell lines. *Redox Report: Communications in Free Radical Research* **6**, 182-184.

44. Ishikawa, K., Takenaga, K., Akimoto, M., Koshikawa, N., Yamaguchi, A., Imanishi, H., Nakada, K., Honma, Y., and Hayashi, J. (2008) ROS-generating mitochondrial DNA mutations can regulate tumor cell metastasis. *Science* **320**, 661-664.

45. Toyokuni, S., Okamoto, K., Yodoi, J., and Hiai, H. (1995) Persistent oxidative stress in cancer. *FEBS Letters* **358**, 1-3.

46. Kumar, B., Koul, S., Khandrika, L., Meacham, R. B., and Koul, H. K. (2008) Oxidative stress is inherent in prostate cancer cells and is required for aggressive phenotype. *Cancer Research* **68**, 1777-1785.

47. Mochizuki, T., Furuta, S., Mitsushita, J., Shang, W. H., Ito, M., Yokoo, Y., Yamaura, M., Ishizone, S., Nakayama, J., Konagai, A., Hirose, K., Kiyosawa, K., and Kamata, T. (2006) Inhibition of NADPH oxidase 4 activates apoptosis via the AKT/apoptosis signal-regulating kinase 1 pathway in pancreatic cancer PANC-1 cells. *Oncogene* **25**, 3699-3707.

48. Pelicano, H., Lu, W., Zhou, Y., Zhang, W., Chen, Z., Hu, Y., and Huang, P. (2009) Mitochondrial dysfunction and reactive oxygen species imbalance promote breast cancer cell motility through a CXCL14-mediated mechanism. *Cancer Research* **69**, 2375-2383.

49. Anastasiou, D., Poulogiannis, G., Asara, J. M., Boxer, M. B., Jiang, J. K., Shen, M., Bellinger, G., Sasaki, A. T., Locasale, J. W., Auld, D. S., Thomas, C. J., Vander Heiden, M. G., and Cantley, L. C. (2011) Inhibition of pyruvate kinase M2 by reactive oxygen species contributes to cellular antioxidant responses. *Science* **334**, 1278-1283.

50. Al-Nasser, I., and Crompton, M. (1986) The reversible Ca2+-induced permeabilization of rat liver mitochondria. *Biochemical Journal* **239**, 19-29.

51. Crompton, M., Costi, A., and Hayat, L. (1987) Evidence for the presence of a reversible Ca2+-dependent pore activated by oxidative stress in heart mitochondria. *Biochemical Journal* **245**, 915-918.

52. Ichas, F., and Mazat, J. P. (1998) From calcium signaling to cell death: two conformations for the mitochondrial permeability transition pore. Switching from low- to high-conductance state. *Biochimica et Biophysica Acta* **1366**, 33-50.

53. Ling, X., Zhou, Y., Li, S. W., Yan, B., and Wen, L. (2010) Modulation of mitochondrial permeability transition pore affects multidrug resistance in human hepatocellular carcinoma cells. *International Journal of Biological Sciences* **6**, 773-783.

54. Tanveer, A., Virji, S., Andreeva, L., Totty, N. F., Hsuan, J. J., Ward, J. M., and Crompton, M. (1996) Involvement of cyclophilin D in the activation of a mitochondrial pore by Ca2+ and oxidant stress. *European Journal of Biochemistry / FEBS* **238**, 166-172.

55. Schinzel, A. C., Takeuchi, O., Huang, Z., Fisher, J. K., Zhou, Z., Rubens, J., Hetz, C., Danial, N. N., Moskowitz, M. A., and Korsmeyer, S. J. (2005) Cyclophilin D is acomponent of mitochondrial permeability transition and mediates neuronal cell death after focal cerebral ischemia. *Proceedings of the National Academy of Sciences of the United States of America* **102**, 12005-12010.

56. Basso, E., Fante, L., Fowlkes, J., Petronilli, V., Forte, M. A., and Bernardi, P. (2005) Properties of the permeability transition pore in mitochondria devoid of Cyclophilin D. *Journal of Biological Chemistry* **280**, 18558-18561.

57. Baines, C. P., Kaiser, R. A., Purcell, N. H., Blair, N. S., Osinska, H., Hambleton, M. A., Brunskill, E. W., Sayen, M. R., Gottlieb, R. A., Dorn, G. W., Robbins, J., and Molkentin, J. D. (2005) Loss of cyclophilin D reveals a critical role for mitochondrial permeability transition in cell death. *Nature* **434**, 658-662.

58. Eliseev, R. A., Malecki, J., Lester, T., Zhang, Y., Humphrey, J., and Gunter, T. E. (2009) Cyclophilin D interacts with Bcl2 and exerts an anti-apoptotic effect. *Journal of Biological Chemistry* **284**, 9692-9699.

59. Machida, K., Ohta, Y., and Osada, H. (2006) Suppression of apoptosis by cyclophilin D via stabilization of hexokinase II mitochondrial binding in cancer cells. *Journal of Biological Chemistry* **281**, 14314-14320.

60. Ghosh, J. C., Siegelin, M. D., Dohi, T., and Altieri, D. C. (2010) Heat shock protein 60 regulation of the mitochondrial permeability transition pore in tumor cells. *Cancer Research* **70**, 8988-8993.

61. Kinnally, K. W., Zorov, D. B., Antonenko, Y. N., Snyder, S. H., McEnery, M. W., and Tedeschi, H. (1993) Mitochondrial benzodiazepine receptor linked to inner membrane ion channels by nanomolar actions of ligands. *Proceedings of the National Academy of Sciences of the United States of America* **90**, 1374-1378.

62. Sileikyte, J., Petronilli, V., Zulian, A., Dabbeni-Sala, F., Tognon, G., Nikolov, P., Bernardi, P., and Ricchelli, F. (2011) Regulation of the inner membrane mitochondrial permeability transition by the outer membrane translocator protein (peripheral benzodiazepine receptor). *Journal of Biological Chemistry* **286**, 1046-1053.

63. Mukherjee, S., and Das, S. K. (2012) Translocator protein (TSPO) in breast cancer. *Current Molecular Medicine* **12**, 443-457.

64. Hardwick, M., Fertikh, D., Culty, M., Li, H., Vidic, B., and Papadopoulos, V. (1999) Peripheral-type benzodiazepine receptor (PBR) in human breast cancer: correlation of breast cancer cell aggressive phenotype with PBR expression, nuclear localization, and PBR-mediated cell proliferation and nuclear transport of cholesterol. *Cancer Research* **59**, 831-842.

65. Wu, X., and Gallo, K. A. (2013) The 18-kDa Translocator Protein (TSPO) Disrupts Mammary Epithelial Morphogenesis and Promotes Breast Cancer Cell Migration. *PloS One* **8**, doi: 10.1371/journal.pone.0071258.

66. Galiegue, S., Casellas, P., Kramar, A., Tinel, N., and Simony-Lafontaine, J. (2004) Immunohistochemical assessment of the peripheral benzodiazepine receptor in breast cancer and its relationship with survival. *Clinical Cancer Research: An Official Journal of the American Association for Cancer Research* **10**, 2058-2064.

67. Crompton, M., Virji, S., and Ward, J. M. (1998) Cyclophilin-D binds strongly to complexes of the voltage-dependent anion channel and the adenine nucleotide translocase to form the permeability transition pore. *European Journal of Biochemistry / FEBS* **258**, 729-735.

68. Gincel, D., Zaid, H., and Shoshan-Barmatz, V. (2001) Calcium binding and translocation by the voltage-dependent anion channel: a possible regulatory mechanism in mitochondrial function. *Biochemical Journal* **358**, 147-155.

69. Szabo, I., and Zoratti, M. (1993) The mitochondrial permeability transition pore may comprise VDAC molecules. I. Binary structure and voltage dependence of the pore. *FEBS Letters* **330**, 201-205.

70. Baines, C. P., Kaiser, R. A., Sheiko, T., Craigen, W. J., and Molkentin, J. D. (2007) Voltage-dependent anion channels are dispensable for mitochondrial-dependent cell death. *Nature Cell Biology* **9**, 550-555.

71. Krauskopf, A., Eriksson, O., Craigen, W. J., Forte, M. A., and Bernardi, P. (2006) Properties of the permeability transition in VDAC1(-/-) mitochondria. *Biochimica et Biophysica Acta* **1757**, 590-595.

72. Abu-Hamad, S., Sivan, S., and Shoshan-Barmatz, V. (2006) The expression level of the voltage-dependent anion channel controls life and death of the cell. *Proceedings of the National Academy of Sciences of the United States of America* **103**, 5787-5792.

73. Koren, I., Raviv, Z., and Shoshan-Barmatz, V. (2010) Downregulation of voltage-dependent anion channel-1 expression by RNA interference prevents cancer cell growth in vivo. *Cancer Biology and Therapy* **9**, 1046-1052.

74. Azoulay-Zohar, H., Israelson, A., Abu-Hamad, S., and Shoshan-Barmatz, V. (2004) In self-defence: hexokinase promotes voltage-dependent anion channel closure and prevents mitochondria-mediated apoptotic cell death. *Biochemical Journal* **377**, 347-355.

75. Halestrap, A. P., and Brenner, C. (2003) The adenine nucleotide translocase: a central component of the mitochondrial permeability transition pore and key player in cell death. *Current Medicinal Chemistry* **10**, 1507-1525.

76. Klingenberg, M. (1975) Energetic aspects of transport of ADP and ATP through the mitochondrial membrane. *Ciba Foundation Symposium*, 105-124.

77. Kokoszka, J. E., Waymire, K. G., Levy, S. E., Sligh, J. E., Cai, J., Jones, D. P., MacGregor, G. R., and Wallace, D. C. (2004) The ADP/ATP translocator is not essential for the mitochondrial permeability transition pore. *Nature* **427**, 461-465.

78. Bauer, M. K., Schubert, A., Rocks, O., and Grimm, S. (1999) Adenine nucleotide translocase-1, a component of the permeability transition pore, can dominantly induce apoptosis. *Journal of Cell Biology* **147**, 1493-1502.

79. Zamora, M., Granell, M., Mampel, T., and Vinas, O. (2004) Adenine nucleotide translocase 3 (ANT3) overexpression induces apoptosis in cultured cells. *FEBS Letters* **563**, 155-160.

80. Chevrollier, A., Loiseau, D., Chabi, B., Renier, G., Douay, O., Malthiery, Y., and Stepien, G. (2005) ANT2 isoform required for cancer cell glycolysis. *Journal of Bioenergetics and Biomembranes* **37**, 307-316.

81. Gallerne, C., Touat, Z., Chen, Z. X., Martel, C., Mayola, E., Sharaf el dein, O., Buron, N., Le Bras, M., Jacotot, E., Borgne-Sanchez, A., Lemoine, A., Lemaire, C., Pervaiz, S., and Brenner, C. (2010) The fourth isoform of the adenine nucleotide translocator inhibits mitochondrial apoptosis in cancer cells. *International Journal of Biochemistry and Cell Biology* **42**, 623-629.

82. Chevrollier, A., Loiseau, D., Reynier, P., and Stepien, G. (2011) Adenine nucleotide translocase 2 is a key mitochondrial protein in cancer metabolism. *Biochimica et Biophysica Acta* **1807**, 562-567.

83. Schubert, A., and Grimm, S. (2004) Cyclophilin D, a component of the permeability transition-pore, is an apoptosis repressor. *Cancer Research* **64**, 85-93.

84. Tartaglia, L. A., Ayres, T. M., Wong, G. H., and Goeddel, D. V. (1993) A novel domain within the 55 kd TNF receptor signals cell death. *Cell* **74**, 845-853.

85. Fulda, S., Scaffidi, C., Susin, S. A., Krammer, P. H., Kroemer, G., Peter, M. E., and Debatin, K. M. (1998) Activation of mitochondria and release of mitochondrial apoptogenic factors by betulinic acid. *Journal of Biological Chemistry* **273**, 33942-33948.

86. Chen, M., and Wang, J. (2002) Initiator caspases in apoptosis signaling pathways. *Apoptosis: An International Journal on Programmed Cell Death* **7**, 313-319.

87. Slee, E. A., Adrain, C., and Martin, S. J. (2001) Executioner caspase-3, -6, and -7 perform distinct, non-redundant roles during the demolition phase of apoptosis. *Journal of Biological Chemistry* **276**, 7320-7326.

88. Cheng, E. H., Wei, M. C., Weiler, S., Flavell, R. A., Mak, T. W., Lindsten, T., and Korsmeyer, S. J. (2001) BCL-2, BCL-X(L) sequester BH3 domain-only molecules preventing BAX- and BAK-mediated mitochondrial apoptosis. *Molecular Cell* **8**, 705-711.

89. Wei, M. C., Zong, W. X., Cheng, E. H., Lindsten, T., Panoutsakopoulou, V., Ross, A. J., Roth, K. A., MacGregor, G. R., Thompson, C. B., and Korsmeyer, S. J. (2001) Proapoptotic BAX and BAK: a requisite gateway to mitochondrial dysfunction and death. *Science* **292**, 727-730.

90. Nagata, S., Hanayama, R., and Kawane, K. (2010) Autoimmunity and the clearance of dead cells. *Cell* **140**, 619-630.

91. Meijerink, J. P., Mensink, E. J., Wang, K., Sedlak, T. W., Sloetjes, A. W., de Witte, T., Waksman, G., and Korsmeyer, S. J. (1998) Hematopoietic malignancies demonstrate loss-of-function mutations of BAX. *Blood* **91**, 2991-2997.

92. Lee, J. W., Soung, Y. H., Kim, S. Y., Nam, S. W., Kim, C. J., Cho, Y. G., Lee, J. H., Kim, H. S., Park, W. S., Kim, S. H., Lee, J. Y., Yoo, N. J., and Lee, S. H. (2004) Inactivating mutations of proapoptotic Bad gene in human colon cancers. *Carcinogenesis* **25**, 1371-1376.

93. Placzek, W. J., Wei, J., Kitada, S., Zhai, D., Reed, J. C., and Pellecchia, M. (2010) A survey of the anti-apoptotic Bcl-2 subfamily expression in cancer types provides a platform to predict the efficacy of Bcl-2 antagonists in cancer therapy. *Cell Death and Disease* **1**, doi: 10.1038/cddis.2010.18.

94. Smith, A. J., Karpova, Y., D'Agostino, R., Jr., Willingham, M., and Kulik, G. (2009) Expression of the Bcl-2 protein BAD promotes prostate cancer growth. *PloS One* **4**, doi: 10.1371/journal.pone.0006224.

95. Dalafave, D. S., and Prisco, G. (2010) Inhibition of Antiapoptotic BCL-XL, BCL-2, and MCL-1 Proteins by Small Molecule Mimetics. *Cancer Informatics* **9**, 169-177.

96. Li, Y., Ahmed, F., Ali, S., Philip, P. A., Kucuk, O., and Sarkar, F. H. (2005) Inactivation of nuclear factor kappaB by soy isoflavone genistein contributes to increased apoptosis induced by chemotherapeutic agents in human cancer cells. *Cancer Research* **65**, 6934-6942.

97. Haldar, S., Negrini, M., Monne, M., Sabbioni, S., and Croce, C. M. (1994) Down-regulation of bcl-2 by p53 in breast cancer cells. *Cancer Research* **54**, 2095-2097.

98. Holler, N., Zaru, R., Micheau, O., Thome, M., Attinger, A., Valitutti, S., Bodmer, J. L., Schneider, P., Seed, B., and Tschopp, J. (2000) Fas triggers an alternative, caspase-8-independent cell death pathway using the kinase RIP as effector molecule. *Nature Immunology* **1**, 489-495.

99. Chan, F. K., Shisler, J., Bixby, J. G., Felices, M., Zheng, L., Appel, M., Orenstein, J., Moss, B., and Lenardo, M. J. (2003) A role for tumor necrosis factor receptor-2 and receptor-interacting protein in programmed necrosis and antiviral responses. *Journal of Biological Chemistry* **278**, 51613-51621.

100. Temkin, V., Huang, Q., Liu, H., Osada, H., and Pope, R. M. (2006) Inhibition of ADP/ATP exchange in receptor-interacting protein-mediated necrosis. *Molecular and Cellular Biology* **26**, 2215-2225.

101. Lemasters, J. J., Nieminen, A. L., Qian, T., Trost, L. C., Elmore, S. P., Nishimura, Y., Crowe, R. A., Cascio, W. E., Bradham, C. A., Brenner, D. A., and Herman, B. (1998) The mitochondrial permeability transition in cell death: a common mechanism in necrosis, apoptosis and autophagy. *Biochimica et Biophysica Acta* **1366**, 177-196.

102. Choi, K., Kim, J., Kim, G. W., and Choi, C. (2009) Oxidative stress-induced necrotic cell death via mitochondira-dependent burst of reactive oxygen species. *Current Neurovascular Research* **6**, 213-222.

103. Nieminen, A. L., Gores, G. J., Wray, B. E., Tanaka, Y., Herman, B., and Lemasters, J. J. (1988) Calcium dependence of bleb formation and cell death in hepatocytes. *Cell Calcium* **9**, 237-246.

104. Nakagawa, T., Shimizu, S., Watanabe, T., Yamaguchi, O., Otsu, K., Yamagata, H., Inohara, H., Kubo, T., and Tsujimoto, Y. (2005) Cyclophilin D-dependent mitochondrial permeability transition regulates some necrotic but not apoptotic cell death. *Nature* **434**, 652-658.

105. Piao, L., Li, Y., Kim, S. J., Byun, H. S., Huang, S. M., Hwang, S. K., Yang, K. J., Park, K. A., Won, M., Hong, J., Hur, G. M., Seok, J. H., Shong, M., Cho, M. H., Brazil, D. P., Hemmings, B. A., and Park, J. (2009) Association of LETM1 and MRPL36 contributes to the regulation of mitochondrial ATP production and necrotic cell death. *Cancer Research* **69**, 3397-3404.

106. Sato, A., Satake, A., Hiramoto, A., Miyazaki, E., Okamatsu, A., Nakama, K., Hiraoka, O., Miyake, T., Kim, H. S., and Wataya, Y. (2008) Molecular mechanisms in two cell death-types, necrosis and apoptosis, induced by 5-fluoro-2'-deoxyuridine. *Nucleic Acids Symposium Series*, 627-628.

107. Sun, X., Li, Y., Li, W., Zhang, B., Wang, A. J., Sun, J., Mikule, K., Jiang, Z., and Li, C. J. (2006) Selective induction of necrotic cell death in cancer cells by beta-lapachone through activation of DNA damage response pathway. *Cell Cycle* **5**, 2029-2035.

108. Zong, W. X., Ditsworth, D., Bauer, D. E., Wang, Z. Q., and Thompson, C. B. (2004) Alkylating DNA damage stimulates a regulated form of necrotic cell death. *Genes and Development* **18**, 1272-1282.

109. Yan, S. D., Fu, J., Soto, C., Chen, X., Zhu, H., Al-Mohanna, F., Collison, K., Zhu, A., Stern, E., Saido, T., Tohyama, M., Ogawa, S., Roher, A., and Stern, D. (1997) An intracellular protein that binds amyloid-beta peptide and mediates neurotoxicity in Alzheimer's disease. *Nature* **389**, 689-695.

110. Lustbader, J. W., Cirilli, M., Lin, C., Xu, H. W., Takuma, K., Wang, N., Caspersen, C., Chen, X., Pollak, S., Chaney, M., Trinchese, F., Liu, S., Gunn-Moore, F., Lue, L. F., Walker, D. G., Kuppusamy, P., Zewier, Z. L., Arancio, O., Stern, D., Yan, S. S., and Wu, H. (2004) ABAD directly links Abeta to mitochondrial toxicity in Alzheimer's disease. *Science* **304**, 448-452.

111. He, X. Y., Merz, G., Yang, Y. Z., Mehta, P., Schulz, H., and Yang, S. Y. (2001) Characterization and localization of human type10 17beta-hydroxysteroid dehydrogenase. *European Journal of Biochemistry / FEBS* **268**, 4899-4907.

112. Kobayashi, A., Jiang, L. L., and Hashimoto, T. (1996) Two mitochondrial 3-hydroxyacyl-CoA dehydrogenases in bovine liver. *Journal of Biochemistry* **119**, 775-782.

113. Zschocke, J., Ruiter, J. P., Brand, J., Lindner, M., Hoffmann, G. F., Wanders, R. J., and Mayatepek, E. (2000) Progressive infantile neurodegeneration caused by 2-methyl-3-hydroxybutyryl-CoA dehydrogenase deficiency: a novel inborn error of branched-chain fatty acid and isoleucine metabolism. *Pediatric Research* **48**, 852-855.

114. He, X. Y., Merz, G., Mehta, P., Schulz, H., and Yang, S. Y. (1999) Human brain short chain L-3-hydroxyacyl coenzyme A dehydrogenase is a single-domain multifunctional enzyme. Characterization of a novel 17beta-hydroxysteroid dehydrogenase. *Journal of Biological Chemistry* **274**, 15014-15019.

115. Luo, M. J., Mao, L. F., and Schulz, H. (1995) Short-chain 3-hydroxy-2-methylacyl-CoA dehydrogenase from rat liver: purification and characterization of a novel enzyme of isoleucine metabolism. *Archives of Biochemistry and Biophysics* **321**, 214-220.

116. Yang, S. Y., He, X. Y., and Schulz, H. (2005) 3-Hydroxyacyl-CoA dehydrogenase and short chain 3-hydroxyacyl-CoA dehydrogenase in human health and disease. *FEBS Journal* **272**, 4874-4883.

117. He, X. Y., Schulz, H., and Yang, S. Y. (1998) A human brain L-3-hydroxyacyl-coenzyme A dehydrogenase is identical to an amyloid beta-peptide-binding protein involved in Alzheimer's disease. *Journal of Biological Chemistry* **273**, 10741-10746.

118. He, X. Y., Yang, Y. Z., Peehl, D. M., Lauderdale, A., Schulz, H., and Yang, S. Y. (2003) Oxidative 3alpha-hydroxysteroid dehydrogenase activity of human type 10 17beta-hydroxysteroid dehydrogenase. *Journal of Steroid Biochemistry and Molecular Biology* **87**, 191-198.

119. Frackowiak, J., Mazur-Kolecka, B., Kaczmarski, W., and Dickson, D. (2001) Deposition of Alzheimer's vascular amyloid-beta is associated with decreased expression of brain L-3-hydroxyacyl-coenzyme A dehydrogenase (ERAB). *Brain Research* **907**, 44-53.

120. Sambamurti, K., and Lahiri, D. K. (1998) ERAB contains a putative noncleavable signal peptide. *Biochemical and Biophysical Research Communications* **249**, 546-549.

121. NIH. HSD17B10 Gene. *Genetics Home Reference*, http://ghr.nlm.nih.gov/gene/HSD17B10

122. Powell, A. J., Read, J. A., Banfield, M. J., Gunn-Moore, F., Yan, S. D., Lustbader, J., Stern, A. R., Stern, D. M., and Brady, R. L. (2000) Recognition of structurally diverse substrates by type II 3-hydroxyacyl-CoA dehydrogenase (HADH II)/amyloid-beta binding alcohol dehydrogenase (ABAD). *Journal of Molecular Biology* **303**, 311-327.

123. Labrie, F., Luu-The, V., Lin, S. X., Labrie, C., Simard, J., Breton, R., and Belanger, A. (1997) The key role of 17 beta-hydroxysteroid dehydrogenases in sex steroid biology. *Steroids* **62**, 148-158.

124. Furuta, S., Kobayashi, A., Miyazawa, S., and Hashimoto, T. (1997) Cloning and expression of cDNA for a newly identified isozyme of bovine liver 3-hydroxyacyl-CoA dehydrogenase and its import into mitochondria. *Biochimica et Biophysica Acta* **1350**, 317-324.

125. Yang, S. Y., He, X. Y., and Schulz, H. (2005) Multiple functions of type 10 17beta-hydroxysteroid dehydrogenase. *Trends in Endocrinology and Metabolism* **16**, 167-175.

126. Du Yan, S., Zhu, Y., Stern, E. D., Hwang, Y. C., Hori, O., Ogawa, S., Frosch, M. P., Connolly, E. S., Jr., McTaggert, R., Pinsky, D. J., Clarke, S., Stern, D. M., and Ramasamy, R. (2000) Amyloid beta -peptide-binding alcohol dehydrogenase is a component of the cellular response to nutritional stress. *Journal of Biological Chemistry* **275**, 27100-27109.

127. Yan, S. D., and Stern, D. M. (2005) Mitochondrial dysfunction and Alzheimer's disease: role of amyloid-beta peptide alcohol dehydrogenase (ABAD). *International Journal of Experimental Pathology* **86**, 161-171.

128. Yang, S. Y., He, X. Y., Isaacs, C., Dobkin, C., Miller, D., and Philipp, M. (2014) Roles of 17β-hydroxysteroid dehydrogenase type 10 in neurodegenerative disorders. *Journal of Steroid Biochemistry and Molecular Biology* **143**, 460-472.

129. Ensenauer, R., Niederhoff, H., Ruiter, J. P., Wanders, R. J., Schwab, K. O., Brandis, M., and Lehnert, W. (2002) Clinical variability in 3-hydroxy-2-methylbutyryl-CoA dehydrogenase deficiency. *Annals of Neurology* **51**, 656-659.

130. Olpin, S. E., Pollitt, R. J., McMenamin, J., Manning, N. J., Besley, G., Ruiter, J. P., and Wanders, R. J. (2002) 2-methyl-3-hydroxybutyryl-CoA dehydrogenase deficiency in a 23-year-old man. *Journal of Inherited Metabolic Disease* **25**, 477-482.

131. Poll-The, B. T., Wanders, R. J., Ruiter, J. P., Ofman, R., Majoie, C. B., Barth, P. G., and Duran, M. (2004) Spastic diplegia and periventricular white matter abnormalities in 2-methyl-3-hydroxybutyryl-CoA dehydrogenase deficiency, a defect of isoleucine metabolism: differential diagnosis with hypoxic-ischemic brain diseases. *Molecular Genetics and Metabolism* **81**, 295-299.

132. Sutton, V. R., O'Brien, W. E., Clark, G. D., Kim, J., and Wanders, R. J. (2003) 3-Hydroxy-2-methylbutyryl-CoA dehydrogenase deficiency. *Journal of Inherited Metabolic Disease* **26**, 69-71.

133. Sass, J. O., Forstner, R., and Sperl, W. (2004) 2-Methyl-3-hydroxybutyryl-CoA dehydrogenase deficiency: impaired catabolism of isoleucine presenting as neurodegenerative disease. *Brain and Development* **26**, 12-14.

134. Rauschenberger, K., Scholer, K., Sass, J. O., Sauer, S., Djuric, Z., Rumig, C., Wolf, N. I., Okun, J. G., Kolker, S., Schwarz, H., Fischer, C., Grziwa, B., Runz, H., Numann, A., Shafqat, N., Kavanagh, K. L., Hammerling, G., Wanders, R. J., Shield, J. P., Wendel, U., Stern, D., Nawroth, P., Hoffmann, G. F., Bartram, C. R., Arnold, B., Bierhaus, A., Oppermann, U., Steinbeisser, H., and Zschocke, J. (2010) A non-enzymatic function of 17beta-hydroxysteroid dehydrogenase type 10 is required for mitochondrial integrity and cell survival. *EMBO Molecular Medicine* **2**, 51-62.

135. Lenski, C., Kooy, R. F., Reyniers, E., Loessner, D., Wanders, R. J., Winnepenninckx, B., Hellebrand, H., Engert, S., Schwartz, C. E., Meindl, A., and Ramser, J. (2007) The reduced expression of the HADH2 protein causes X-linked mental retardation, choreoathetosis, and abnormal behavior. *American Journal of Human Genetics* **80**, 372-377.

136. Reyniers, E., Van Bogaert, P., Peeters, N., Vits, L., Pauly, F., Fransen, E., Van Regemorter, N., and Kooy, R. F. (1999) A new neurological syndrome with mental retardation, choreoathetosis, and abnormal behavior maps to chromosome Xp11. *American Journal of Human Genetics* **65**, 1406-1412.

137. Tieu, K., Perier, C., Vila, M., Caspersen, C., Zhang, H. P., Teismann, P., Jackson-Lewis, V., Stern, D. M., Yan, S. D., and Przedborski, S. (2004) L-3-hydroxyacyl-CoA dehydrogenase II protects in a model of Parkinson's disease. *Annals of Neurology* **56**, 51-60.

138. Oppermann, U. C., Salim, S., Tjernberg, L. O., Terenius, L., and Jornvall, H. (1999) Binding of amyloid beta-peptide to mitochondrial hydroxyacyl-CoA dehydrogenase (ERAB): regulation of an SDR enzyme activity with implications for apoptosis in Alzheimer's disease. *FEBS Letters* **451**, 238-242.

139. Kissinger, C. R., Rejto, P. A., Pelletier, L. A., Thomson, J. A., Showalter, R. E., Abreo, M. A., Agree, C. S., Margosiak, S., Meng, J. J., Aust, R. M., Vanderpool, D., Li, B., Tempczyk-Russell, A., and Villafranca, J. E. (2004) Crystal structure of human ABAD/HSD10 with a bound inhibitor: implications for design of Alzheimer's disease therapeutics. *Journal of Molecular Biology* **342**, 943-952.

140. Yang, S. Y., and He, X. Y. (2001) Role of type 10 17beta-hydroxysteroid dehydrogenase in the pathogenesis of Alzheimer's disease. *Advances in Experimental Medicine and Biology* **487**, 101-110.

141. Yan, S. D., Shi, Y., Zhu, A., Fu, J., Zhu, H., Zhu, Y., Gibson, L., Stern, E., Collison, K., Al-Mohanna, F., Ogawa, S., Roher, A., Clarke, S. G., and Stern, D. M. (1999) Role of ERAB/L-3-hydroxyacyl-coenzyme A dehydrogenase type II activity in Abeta-induced cytotoxicity. *Journal of Biological Chemistry* **274**, 2145-2156.

142. Takuma, K., Yan, S. S., Stern, D. M., and Yamada, K. (2005) Mitochondrial dysfunction, endoplasmic reticulum stress, and apoptosis in Alzheimer's disease. *Journal of Pharmacological Sciences* **97**, 312-316.

143. Gunnarsson, C., Ahnstrom, M., Kirschner, K., Olsson, B., Nordenskjold, B., Rutqvist, L. E., Skoog, L., and Stal, O. (2003) Amplification of HSD17B1 and ERBB2 in primary breast cancer. *Oncogene* **22**, 34-40.

144. Zhang, C. Y., Chen, J., Yin, D. C., and Lin, S. X. (2012) The contribution of 17beta-hydroxysteroid dehydrogenase type 1 to the estradiol-estrone ratio in estrogen-sensitive breast cancer cells. *PloS One* **7**, doi: 10.1371/journal.pone.0029835.

145. Jansson, A. K., Gunnarsson, C., Cohen, M., Sivik, T., and Stal, O. (2006) 17beta-hydroxysteroid dehydrogenase 14 affects estradiol levels in breast cancer cells and is a prognostic marker in estrogen receptor-positive breast cancer. *Cancer Research* **66**, 11471-11477.

146. Cornel, K. M., Kruitwagen, R. F., Delvoux, B., Visconti, L., Van de Vijver, K. K., Day, J. M., Van Gorp, T., Hermans, R. J., Dunselman, G. A., and Romano, A. (2012) Overexpression of 17beta-hydroxysteroid dehydrogenase type 1 increases the exposure of endometrial cancer to 17beta-estradiol. *Journal of Clinical Endocrinology and Metabolism* **97**, E591-601.

147. Rawluszko, A. A., Horbacka, K., Krokowicz, P., and Jagodzinski, P. P. (2011) Decreased expression of 17beta-hydroxysteroid dehydrogenase type 1 is associated with DNA hypermethylation in colorectal cancer located in the proximal colon. *BMC Cancer* **11**, 522.

148. Salas, S., Jezequel, P., Campion, L., Deville, J. L., Chibon, F., Bartoli, C., Gentet, J. C., Charbonnel, C., Gouraud, W., Voutsinos-Porche, B., Brouchet, A., Duffaud, F., Figarella-Branger, D., and Bouvier, C. (2009) Molecular characterization of the response to chemotherapy in conventional osteosarcomas: Predictive value of HSD17B10 and IFITM2. *International Journal of Cancer* **125**, 851-860.

149. Jernberg, E., Thysell, E., Bovinder Ylitalo, E., Rudolfsson, S., Crnalic, S., Widmark, A., Bergh, A., and Wikstrom, P. (2013) Characterization of prostate cancer bone metastases according to expression levels of steroidogenic enzymes and androgen receptor splice variants. *PloS One* **8**, doi: 10.1371/journal.pone.0077407.

150. Jazbutyte, V., Kehl, F., Neyses, L. and Pelzer, T. (2009) Estrogen receptor alpha interacts with 17β-hydroxysteroid dehydrogenase type 10 in mitochondria. *Biochemical and Biophysical Research Communications* **384**, 450-454.

151. Rauschenberger, K. (2011) Analysis of dehydrogenase-independent functions of HSD17B10 in humans and animal models. http://archiv.ub.uni-heidelberg.de/volltextserver/11826/

152. Carlson, E. A., Marquez, R. T., Du, F., Wang, Y., Xu, L., and Yan, S. S. (2015) Overexpression of 17beta-hydroxysteroid dehydrogenase type 10 increases pheochromocytoma cell growth and resistance to cell death. *BMC Cancer* **15**, doi: 10.1186/s12885-015-1173-5.

153. pcDNA3 (Invitrogen). http://www2.kumc.edu/soalab/LabLinks/vectors/pcdna3.htm.

154. Gan, X., Huang, S., Wu, L., Wang, Y., Hu, G., Li, G., Zhang, H., Yu, H., Swerdlow, R. H., Chen, J. X., and Yan, S. S. (2014) Inhibition of ERK-DLP1 signaling and mitochondrial division alleviates mitochondrial dysfunction in Alzheimer's disease cybrid cell. *Biochimica et Biophysica Acta* **1842**, 220-231.

155. Ji, Q., Hao, X., Zhang, M., Tang, W., Yang, M., Li, L., Xiang, D., Desano, J. T., Bommer, G. T., Fan, D., Fearon, E. R., Lawrence, T. S., and Xu, L. (2009) MicroRNA miR-34 inhibits human pancreatic cancer tumor-initiating cells. *PloS One* **4**, doi: 10.1371/journal.pone.0006816.

156. Wu, X., Li, M., Qu, Y., Tang, W., Zheng, Y., Lian, J., Ji, M., and Xu, L. (2010) Design and synthesis of novel Gefitinib analogues with improved anti-tumor activity. *Bioorganic and Medicinal Chemistry* **18**, 3812-3822.

157. Kovar, J. L., Volcheck, W., Sevick-Muraca, E., Simpson, M. A., and Olive, D. M. (2009) Characterization and performance of a near-infrared 2-deoxyglucose optical imaging agent for mouse cancer models. *Analytical Biochemistry* **384**, 254-262.

158. Freed, W. J., Patel-Vaidya, U., and Geller, H. M. (1986) Properties of PC12 pheochromocytoma cells transplanted to the adult rat brain. *Experimental Brain Research* **63**, 557-566.

159. Falchi, A. M., Isola, R., Diana, A., Putzolu, M., and Diaz, G. (2005) Characterization of depolarization and repolarization phases of mitochondrial membrane potential fluctuations induced by tetramethylrhodamine methyl ester photoactivation. *FEBS Journal* **272**, 1649-1659.

160. Lin, D. T. and Lechleiter, J. D. (2002) Mitochondrial targeted cyclophilin D protects cells from cell death by peptidyl prolyl isomerization. *Journal of Biological Chemistry* **277**, 31134-31141.

161. Berry, D. A., Cronin, K. A., Plevritis, S. K., Fryback, D. G., Clarke, L., Zelen, M., Mandelblatt, J. S., Yakovlev, A. Y., Habbema, J. D., Feuer, E. J., Cancer, I., and Surveillance Modeling Network, C. (2005) Effect of screening and adjuvant therapy on mortality from breast cancer. *New England Journal of Medicine* **353**, 1784-1792.

162. Jemal, A., Siegel, R., Xu, J., and Ward, E. (2010) Cancer statistics, 2010. *CA: A Cancer Journal for Clinicians* **60**, 277-300.

163. Subik, K., Lee, J. F., Baxter, L., Strzepek, T., Costello, D., Crowley, P., Xing, L., Hung, M. C., Bonfiglio, T., Hicks, D. G., and Tang, P. (2010) The Expression Patterns of ER, PR, HER2, CK5/6, EGFR, Ki-67 and AR by Immunohistochemical Analysis in Breast Cancer Cell Lines. *Breast Cancer: Basic and Clinical Research* **4**, 35-41.

164. Schafer, J. M., Lee, E. S., O'Regan, R. M., Yao, K., and Jordan, V. C. (2000) Rapid development of tamoxifen-stimulated mutant p53 breast tumors (T47D) in athymic mice. *Clinical Cancer Research* **6**, 4373-4380.

165. Harrell, J. C., Dye, W. W., Allred, D. C., Jedlicka, P., Spoelstra, N. S., Sartorius, C. A., and Horwitz, K. B. (2006). Estrogen receptor positive breast cancer metastasis: altered hormonal sensitivity and tumor aggressiveness in lymphatic vessels and lymph nodes. *Cancer Research* **66**, 9308-9315.

166. Bartlett, D. W. and Davis, M. E. (2006) Insights into the kinetics of siRNA-mediated gene silencing from live-cell and live-animal bioluminescent imaging. *Nucleic Acids Research* **34**, 322-333.

167. Moore, C. B., Guthrie, E. H., Huang, M. T. H., and Taxman, D. J. (2010) Short hairpin RNA (shRNA): design, delivery, and assessment of gene knockdown. *Methods in Molecular Biology* **629**, 141-158.

168. Valasani, K. R., Hu, G., Chaney, M. O., and Yan, S. S. (2013) Structure-based design and synthesis of benzothiazole phosphonate analogues with inhibitors of human ABAD-Abeta for treatment of Alzheimer's disease. *Chemical Biology and Drug Design* **81**, 238-249.

169. Valasani, K. R., Sun, Q., Hu, G., Li, J., Du, F., Guo, Y., Carlson, E. A., Gan, X., and Yan, S. S. (2014) Identification of human ABAD inhibitors for rescuing Aβ-mediated mitochondrial dysfunction. *Journal of Current Alzheimer's Research* **11**, 128-136.

170. Rinaldo, P., Matern, D., and Bennett, M. J. (2002) Fatty acid oxidation disorders. *Annual Review of Physiology* **64**, 477-502.

171. Eaton, S., Pourfarzam, M., and Bartlett, K. (1996) The effect of respiratory chain impairment of beta-oxidation in rat heart mitochondria. *Biochemistry Journal* **319**, 633-640.

172. Owen, O. E., Morgan, A. P., Kemp, H. G., Sullivan, J. M., Herrera, M. G., and Cahill, G. F., Jr. (1967) Brain metabolism during fasting. *Journal of Clinical Investigation* **46**, 1589-1595.

173. Stryer, L. (1995) *Biochemistry, Fourth ed*. New York: W. H. Freeman and Company, pp. 581-613.

174. Sheehan, P. M. and Yeh, Y. Y. (1984) Pathways of acetyl CoA production for lipogenesis from acetoacetate, bet-hydroxybutyrate, pyruvate and glucose in neonatal rat lung. *Lipids* **19**, 103-108.

175. Kallinowski, F., Vaupel, P., Runkel, S., Berg, G., Fortmeyer, H. P., Baessler, K. H., Wagner, K., Mueller-Klieser, W., and Walenta, S. (1988) Glucose uptake, lactate release, ketone body turnover, metabolic micromilieu, and pH distributions in human breast cancer xenografts in nude rats. *Cancer Research* **48**, 7264-7272.

176. Pavlides, S., Tsirigos, A., Migneco, G., Whitaker-Menezes, D., Chiavarina, B., Flomenberg, N., Frank, P. G., Casimiro, M. C., Wang, C., Pestell, R. G., Martinez-Outschoorn, U. E., Howell, A., Sotgia, F., and Lisanti, M. P. (2010) The autophagic tumor stroma model of cancer: Role of oxidative stress and ketone production in fueling tumor cell metabolism. *Cell Cycle* **9**, 3485-3505.

177. Li, Y., Park, J. S., Deng, J. H., and Bai, Y. (2006) Cytochrome c oxidase subunit IV is essential for assembly and respiratory function of the enzyme complex. *Journal of Bioenergetics and Biomembranes* **38**, 283-291.

178. Williams, R. S., Salmons, S., Newsholme, E., Kaufman, R.E., and Mellor, J. (1986) Regulation of nuclear and mitochondrial gene expression by contractile activity in skeletal muscle. *Journal of Biological Chemistry* **261**: 376-80.

179. Hood, D., Zak, R., and Pette, D. (1989) Chronic stimulation of rat skeletal muscle induces coordinate increases in mitochondrial and nuclear mRNAs of cytochrome c oxidase subunits. *European Journal of Biochemistry* **179**: 275-80.

180. Scaduto, R. C., Jr and Grotyohann, L. W. (1999) Measurement of mitochondrial membrane potential using fluorescent rhodamine derivatives. *Biophysical Journal* **76**, 469-477.

181. Ward, M. W., Huber, H. J., Weisova, P., Dussmann, H., Nicholls, D. G., and Prehn, J. H. (2007) Mitochondrial and plasma membrane potential of cultured cerebellar neurons during glutamate-induced necrosis, apoptosis, and tolerance. *Journal of Neuroscience* **27**, 8238-8249.

182. Perry, S. W., Norman, J. P., Barbieri, J., Brown, E. B., and Gelbard, H. A. (2011) Mitochondrial membrane potential probes and the proton gradient: a practical usage guide. *BioTechniques* **50**, 98-115.

183. Stockert, J. C., Blázquez-Castro, A., Cañete, M., Horobin, R. W., and Villanueva, Á. (2012) MTT assay for cell viability: intracellular localization of the formazan product is in lipid droplets. *Acta Histochemica* **114**, 785-796.

184. Van Meerloo, J., Kaspers, G. J., and Cloos, J. (2011) Cell sensitivity assays: the MTT assay. *Methods in Molecular Biology* **731**, 237-245.

185. Etxeberria, A., Mendarte, S., and Larregla, S. (2011) Determination of viability of *Phytophthora capsici* oospores with the tetrazolium bromide staining test versus a plasmolysis method. *Revista Iberoamericana de Micología* **28**, 43-49.

186. Lupu, A. R. and Popescu, T. (2013) The noncellular reduction of MTT tetrazolium salt by TiO_2 nanoparticles and its implications for cytotoxicity assays. *Toxicology in Vitro* **27**, 1445-1450.

187. Berridge, M. V., Herst, P. M., and Tan, A. S. (2005) Tetrazolium dyes as tools in cell biology: new insights into their cellular reduction. *Biotechnology Annual Review* **11**, 127-152.

188. Niles, A. L., Moravec, R. A., Hesselberth, P. E., Scurria, M. A., Daily, W. J., and Riss, T. L. (2007) A homogeneous assay to measure live and dead cells in the same sample by detecting different protease markers. *Analytical Biochemistry* **366**, 197-206.

189. Crouch, S. P., Kozlowski, R., Slater, K. J., and Fletcher, J. (1993) The use of ATP bioluminescence as a measure of cell proliferation and cytotoxicity. *Journal of Immunological Methods* **160**, 81–88.

190. Watanabe, M., Hitomi, M., Van der Wee, K., Rothenberg, F., Fisher, S. A., Zucker, R., Svoboda, K. K. H., Goldsmith, E. C., Heiskanen, K. M., and Nieminen, A. L. (2002) The pros and cons of apoptosis assays for use in the study of cells, tissues, and organs. *Microscopy and Microanalysis* **8**, 375-391.

191. Kockx, M. M., Muhring, J., Knaapen, M. W., and De Meyer, G. R. (1998) RNA synthesis and splicing interferes with DNA *in situ* end labeling techniques used to detect apoptosis. *American Journal of Pathology* **152**, 885-888.

192. Grasl-Kraupp, B., Ruttkay-Nedecky, B., Koudelka, H., Bukowska, K., Bursch, W., and Schulte-Hermann, R. (1995) *In situ* detection of fragmented DNA (TUNEL assay) fails to discriminate among apoptosis, necrosis, and autolytic cell death: a cautionary note. *Hepatology* **21**, 1465-1468.

193. Schaper, J., Elsasser, A., and Kostin, S. (1999) The role of cell death in heart failure. *Circulation Research* **85**, 867-869.

194. Nicholson, D. W. and Thornberry, N. A. (1997) Caspases: killer proteases. *Trends in Biochemical Science* **22**, 299-306.

195. Blankenberg, F. and Strauss, H. W. (1999) Non-invasive diagnosis of acute heart- or lung-transplant rejection using radiolabeled annexin V. *Pediatric Radiology* **29**, 299-305.

196. Chan, F. K., Moriwaki, K., and De Rosa, M. J. (2013) Detection of necrosis by release of lactate dehydrogenase activity. *Methods in Molecular Biology* **979**, 65-70.

197. Yang, Z. J., Chee, C. E., Huang, S., and Sinicrope, F. A. (2011) The role of autophagy in cancer: therapeutic implications. *Molecular Cancer Therapeutics* **10**, 1533-1541.

198. Barth, S., Glick, D., and Macleod, K. F. (2010) Autophagy: assays and artifacts. *Journal of Pathology* **221**, 117-124.

199. Zha, J., Harada, H., Yang, E., Jockel, J., and Korsmeyer, S. J. (1996) Serine phosphorylation of death agonist BAD in response to survival factor results in binding to 14-3-3 not BCL-X(L). *Cell* **87**, 619-628.

200. Masters, S. C., Yang, H., Datta, S. R., Greenberg, M. E., and Fu, H. (2001) 14-3-3 inhibits Bad-induced cell death through interaction with serine-136. *Molecular Pharmacology* **60**, 1325-1331.

201. Chen, J., Fujii, K., Zhang, L., Roberts, T., and Fu, H. (2001) Raf-1 promotes cell survival by antagonizing apoptosis signal-regulating kinase 1 through a MEK-ERK independent mechanism. *Proceedings of the National Academy of Sciences of the United States of America* **98**, 7783-7788.

202. Masters, S. C. (2004) Protein-protein interactions: co-immunoprecipitation from transfected cells. *Methods in Molecular Biology* **261**, 337-348.

203. Geva, G. and Sharan, R. (2011) Identification of protein complexes from co-immunoprecipitation data. *Bioinformatics* **27**, 111-117.

204. Devalaraja-Narashimha, K., Diener, A. M., and Padanilam, B. J. (2011) Cyclophilin D deficiency prevents diet-induced obesity in mice. *FEBS Letters* **585**, 677-682.

205. Tavecchio, M., Lisanti, S., Bennett, M. J., Languino, L. R., and Altieri, D. C. (2015) Deletion of cyclophilin D impairs β-oxidation and promotes glucose metabolism. *Scientific Reports* **5**, doi: 10.1038/srep15981.

206. Shulga, N., Wilson-Smith, R., and Pastorino, J. G. (2010) Sirtuin-3 deacetylation of cyclophilin D induces dissociation of hexokinase II from the mitochondria. *Journal of Cell Science* **123**, 894-902.

207. Chavez, K. J., Garimella, S. V., and Lipkowitz, S. (2010) Triple negative breast cancer cell lines: one tool in the search for better treatment of triple negative breast cancer. *Breast Disease* **32**, 35-48.

208. Labrie, F., Luu-The, V., Lin, S. X., Labrie, C., Simard, J., Breton, R., and Bélanger, A. (1997) The key role of 17β-hydroxysteroid dehydrogenases in sex steroid biology. *Steroids* **62**, 148-158.

209. Kasperk, C. H., Faehling, K., Börcsök, I., and Ziegler, R. (1996) Effects of androgens on subpopulations of the human osteosarcoma cell line SaOS2. *Calcified Tissue International* **58**, 376-382.

210. Chen, F. P., Hsu, T., Hu, C. H., Wang, W. D., Wang, K. C., and Teng, L. F. (2004) Expression of estrogen receptors α and β in human osteoblasts: identification of exon-2 deletion variant of estrogen receptor β in postmenopausal women. *Chang Gung Medical Journal* **27**, 107-115.

211. Saraiva, P. P., Teixeira, S. S., Conde, S. J., and Noqueira, C. R. (2008) The importance of hormone receptor analysis in osteosarcoma cells growth submitted to treatment with estrogen in association with thyroid hormone. *Cell Biochemistry and Function* **26**, 107-110.

212. Häggström, M. (2014) Diagram of the pathways of human steroidogenesis. *Wikiversity Journal of Medicine* **1**, doi: 10.15347/wjm/2014.005.

213. Ferriere, F., Habauzit, D., Pakdel, F., Saligaut, C., and Flouriot, G. (2013) Unliganded estrogen receptor alpha promotes PC-12 survival during serum starvation. *PLoS One* **8**, doi: 10.1371/journal.pone.0069081.

214. Wang, H., Si, L., Li, X., Deng, W., Yang, H., Yang, Y., and Fu, Y. (2012) Overexpression of estrogen receptor beta alleviates the toxic effects of beta-amyloid protein on PC-12 cells via non-hormonal ligands. *Neural Regeneration Research* **7**, 1095-1100.

215. Nilsen, J., Mor, G., and Naftolin, F. (1998) Raloxifene induces neurite outgrowth in estrogen receptor positive PC12 cells. *Menopause* **5**, 211-216.

216. Charalampopoulos, I., Alexaki, V. I., Lazaridis, I., Dermitzaki, E., Avlonitis, N., Tsatsanis, C., Calogeropoulou, T., Margioris, A. N., Castanas, E., and Gravanis, A. (2006) G protein-associated, specific membrane binding sites mediate the neuroprotective effect of dehydroepiandrosterone. *FASEB Journal* **20**, 577-589.

217. Barone, I., Brusco, L., and Fuqua, S. A. W. (2015) Estrogen receptor mutations and changes in downstream gene expression and signaling. *Clinical Cancer Research* **16**, 2702-2708.

218. Younes, M. and Honma, N. (2011) Estrogen receptor β. *Archives of Pathology and Laboratory Medicine* **135**, 63-66.

219. Lu, M., Mira-y-Lopez, R., Nakajo, S., Nakaya, K., and Jing, Y. (2005) Expression of estrogen receptor alpha, retinoic acid receptor alpha and cellular retinoic acid binding protein II genes is coordinately regulated in human breast cancer cells. *Oncogene* **24**, 4362-4369.

220. Subik, K., Lee, J. F., Baxter, L., Strzepek, T., Costello, D., Crowley, P., Xing, L., Hung, M. C., Bonfiglio, T., Hicks, D. G., and Tang, P. (2010) The expression patterns of ER, PR, HER2, CK5/6, EGFR, Ki-67 and AR by immunohistochemical analysis in breast cancer cell lines. *Breast Cancer: Basic and Clinical Research* **4**, 35-41.

221. Pike, M. C., Spicer, D. V., Dahmoush, L., and Press, M. F. (1993) Estrogens, progesterones, normal breast cell proliferation, and breast cancer risk. *Epidemiolic Reviews* **15**, 17-35.

222. Ciocca, D. R. and Fanelli, M. A. (1997) Estrogen receptors and cell proliferation in breast cancer. *Trends in Endocrinology and Metabolism* **8**, 313-321.

223. Russo, J., Ao, X., Grill, C., and Russo, I. H. (1999) Pattern of distribution of cells positive for estrogen receptor alpha and progesterone receptor in relation to proliferating cells in the mammary gland. *Breast Cancer Research Treatment* **53**, 217-227.

224. Russo, I. H. and Russo, J. (2005) The role of estrogen in breast cancer. *Russo, J. Russo, I. H. eds. Molecular Basis of Breast Cancer Prevention and Treatment*, pp. 89-136 Springer-Verlag Heidelberg.

225. Bocchinfuso, W. P. and Korach, K. S. (1997) Mammary gland development and tumorigenesis in estrogen receptor knockout mice. *Journal of Mammary Gland Biology Neoplasia* **2**, 323-334.

226. Bocchinfuso, W. P., Hively, W. P., Couse, J. F., Varmus, H. E., and Korach, K. S. (1999) A mouse mammary tumor virus-Wnt1 transgene induces mammary gland hyperplasia and tumorigenesis in mice lacking estrogen receptor-alpha. *Cancer Research* **59**, 1869-1876.

227. Russo, J. and Russo, I. H. (2006) The role of estrogen in the initiation of breast cancer. *Journal of Steroid Biochemistry and Molecular Biology* **102**, 89-96.

228. Russo, J., Fernandez, S. V., Russo, P. A., Fernbaugh, R., Sheriff, F. S., Lareef, H. M., Garber, J., and Russo, I. M. (2006) 17-beta-estradiol induces transformation and tumorigenesis in human breast epithelial cells. *FASEB Journal* **20**, 1622-1634.

229. Pruefer, F. G., Lizarraga, F., Maldonado, V., and Melendez-Zajgla, J. (2008) Participation of Omi Htra2 serine-protease activity in the apoptosis induced by cisplatin on SW480 colon cancer cells. *Journal of Chemotherapy* **20**, 348-54.

230. Gordaliza, M., García, P. A., Del Corral, J. M., Castro, M. A., and Gómez-Zurita, M. A. (2004) Podophyllotoxin: distribution, sources, applications and new cytotoxic derivatives. *Toxicon* **44**, 441-59.

231. Bharadwaj, R. and Yu, H. (2004). The spindle checkpoint, aneuploidy, and cancer. *Oncogene* **23**, 2016-27.

232. Nestal de Moraes, G., Vasconcelos, F. C., Delbue, D., Mognol, G. P., Sternberg, C., Viola, J. P. B., and Maia, R. C. (2013) Doxorubicin induces cell death in breast cancer cells regardless of survivin and XIAP expression levels. *European Journal of Cell Biology* **92**, 247-256.

233. Jansson, A., Gunnarsson, C., and Stål, O. (2006) Proliferative responses to altered 17beta-hydroxysteroid dehydrogenase (17HSD) type 2 expression in human breast cancer cells are dependent on endogenous expression of 17HSD type 1 and the oestradiol receptors. *Endocrine-Related Cancer* **13**, 875-884.

234. Day, J. M., Foster, P. A., Tutill, H. J., Parsons, M. F., Newman, S. P., Chander, S. K., Allan, G. M., Lawrence, H. R., Vicker, N., Potter, B. V., Reed, M. J., and Purohit, A. (2008) 17beta-hydroxysteroid dehydrogenase Type 1, and not Type 12, is a target for endocrine therapy of hormone-dependent breast cancer. *International Journal of Cancer* **122**, 1931-1940.

235. Aka, J. A., Zerradi, M., Houle, F., Huot, J., and Lin, S. X. (2012) 17beta-hydroxysteroid dehydrogenase type 1 modulates breast cancer protein profile and impacts cell migration. *Breast Cancer Research* **14**, doi: 10.1186/bcr3207.

APPENDICES

List of Abbreviations

Abbreviation	Full Name
ΔΨ	Mitochondrial transmembrane potential
2-DG	IRDye 800CW 2-deoxyglucose
Aβ	Amyloid-β
ABAD	Aβ-binding alcohol dehydrogenase
AD	Alzheimer's disease
ADP	Adenosine diphosphate
Amp	Ampicillin
Adiol	Androstanediol
ANT	Adenine nucleotide translocase
APP	Amyloid precursor protein
APS	Ammonium persulfate
ATP	Adenosine triphosphate
BCA	Bicinchoninic acid
BHB	β-hydroxybutyrate
BSA	Bovine serum albumin
Ca^{2+}	Calcium
Co-IP	Co-immunoprecipitation
Complex I	NADH-ubiquinone oxidoreductase
Complex II	Succinate-ubiquinone oxidoreductase
Complex III	Ubiquinol-cytochrome *c* oxidoreductase
Complex IV	Cytochrome *c* oxidase
CypD	Cyclophilin D
Cyto c	Cytochrome c
DAPI	4',6-diamidino-2-phenylindole
DCPIP	2,6-dichlorophenolindophenol
DHEA	Dehydroepiandrosterone
DHT	Dihydrotestosterone
DMEM	Dulbecco's modified eagle's medium
DMEM/F12	DMEM/nutrient mixture F-12
DMSO	Dimethyl sulfoxide
DTT	Dithiothreitol
E2	17β-estradiol
EDTA	Ethylenediaminetetraacetic acid
EGF	Epidermal growth factor
ER	Estrogen receptor
ERAB	Endoplasmic reticulum-associated Aβ-peptide binding protein
ETC	Electron transport chain

Abbreviation	Full Name
EtOH	Ethanol absolute
EV	Empty vector
FBS	Fetal bovine serum
GFP	Green fluorescent protein
H_2O_2	Hydrogen peroxide
HADH2	L-3-hydroxyacyl-CoA dehydrogenase type II
HBSS	Hank's balanced salt solution
HCl	Hydrochloric acid
HK	Hexokinase
HSD17B	17β-hydroxysteroid dehydrogenase
HSD10	HSD17B type 10
HSD10 ov	HSD10 overexpression
ILE	Isoleucine
IM	Inner membrane
K buffer	Potassium buffer
K_2HPO_4	Dipotassium phosphate
Kan	Kanomycin
KCl	Potassium chloride
KCN	Potassium cyanide
KH_2PO_4	Potassium dihydrogen phosphate
LDH	Lactate dehydrogenase
LETM1	Leucine zipper/EF hand-containing transmembrane-1
MeOH	Methanol absolute
$MgCl_2$	Magnesium Chloride
MHBD	2-methyl-3-hydroxybutyryl-CoA dehydrogenase
MPTP	Mitochondrial permeability transition pore
mtDNA	Mitochondrial DNA
MTT	3-(4,5-dimethylthiazol-2-yl)-2,5-diphenyltetrazolium bromide
Na_2HPO_4	Disodium phosphate
NaCl	Sodium chloride
NADH	β-nicotinamide adenine dinucleotide
OM	Outer membrane
OXPHOS	Oxidative phosphorylation
PAGE	Polyacrylamide-gel electrophoresis
PBS	Phosphate buffered saline
PD	Parkinson's disease
Pen/Strep	Penicillin/streptomycin
PFA	Paraformaldehyde
PMSF	Phenylmethylsulfonyl fluoride
PPIF	Peptidylprolyl isomerase F
qPCR	Quantitative polymerase chain reaction

Abbreviation	Full Name
ROS	Reactive oxygen species
RPMI-1640	Roswell park memorial institute 1640 medium
RT	Room temperature
RT-PCR	Reverse transcription polymerase chain reaction
SCHAD	Short chain 3-hydroxyacyl-CoA dehydrogenase
SCHMAD	Short chain L-3-hydroxy-2-methylacyl-CoA dehydrogenase
SCID	Severe combined immunodeficient
SDS	Sodium dodecyl sulfate
SOC	Super optimal broth with catabolite repression
SOD	Superoxide dismutase
SPR	Surface plasmon resonance
TBH	Tert-butyl hydroperoxide
TBS	Tris-buffered saline
TCA	Tricarboxylic acid
TEMED	N, N, N', N'-tetramethylethylenediamine
TMRM	Tetramethylrhodamine methyl ester
TNM	Tumor-node-metastasis
TSPO	Translocator protein
TUNEL	Terminal deoxynucleotidyl transferase dUTP nick end labeling
VDAC	Voltage dependent anion channel

Table 17: List of abbreviations used in this thesis

List of Tables

List of Schematics and Figures

List of Publications

The following publications originated specifically from this dissertation work:

Carlson, E.A., Marquez, R.T., Du, F., Wang, Y., Xu, L., and Yan, S.S. (2015) Overexpression of 17β-hydroxysteroid dehydrogenase type 10 increases pheochromocytoma cell growth and resistance to cell death. *BMC Cancer* **15**, doi: 10.1186/s12885-015-1173-5. PMID: 25879199.

Carlson, E.A., Du, F., Marquez, R.T., Xu, L., and Yan, S.S. Knockdown of 17β-hydroxysteroid dehydrogenase type 10 decreases T47D human breast cancer cell growth and induces cell death. *In preparation.*

The subsequent papers were published during Emily's graduate studies:

Rao, V.K., **Carlson, E.A.**, and Yan, S.S. (2013) Mitochondrial permeability transition pore is a potential drug target for neurodegeneration. *Biochimica et Biophysica Acta: Molecular Basis of Disease* **1842**, 1267-1272. PMID: 24055979.

Carlson, E.A., Rao, V.K., and Yan, S.S. (2013) From a cell's viewpoint: targeting mitochondria in Alzheimer's disease. *Drug Discovery Today: Therapeutic Strategies* **10**, doi: 10.1016/j.ddstr.2014.04.002. PMID: 25558270.

Valasani, K.R., Sun, Q., Hu, G., Li, J., Du, F., Guo, Y., **Carlson, E.A.**, Gan, X., and Yan, S.S. (2014) Identification of ABAD inhibitors for rescuing Aβ-mediated mitochondrial dysfunction. *Journal of Current Alzheimer's Research* **11**, 128-136. PMID: 24479630.

Valasani, K.R., **Carlson, E.A.**, Battaile, K.P., Bisson, A., Wang, C., Lovell, S., and Yan, S.S. (2014) High-resolution crystal structures of two crystal forms of human cyclophilin D in complex with PEG 400 molecules. *Acta Crystallographica Section F: Structural Biology and Crystallization Communications* **70**, 717-722. PMID: 24915078.

Carlson, E.A. and Yan, S.S. (2014) Disrupting cancer cell function by targeting mitochondria. *Integrative Cancer Science and Therapeutics* **1**, doi: 10.15761/ICST.1000105.

Valasani, K.R., **Carlson, E.**, Vangavaragu, J.R., and Yan, S.S. (2016) Mitochondria as a therapeutic target for the treatment of Alzheimer's disease. *Drug Discovery for Neurodegenerative Disorders: Alzheimer's Disease*. *Pending publication.*